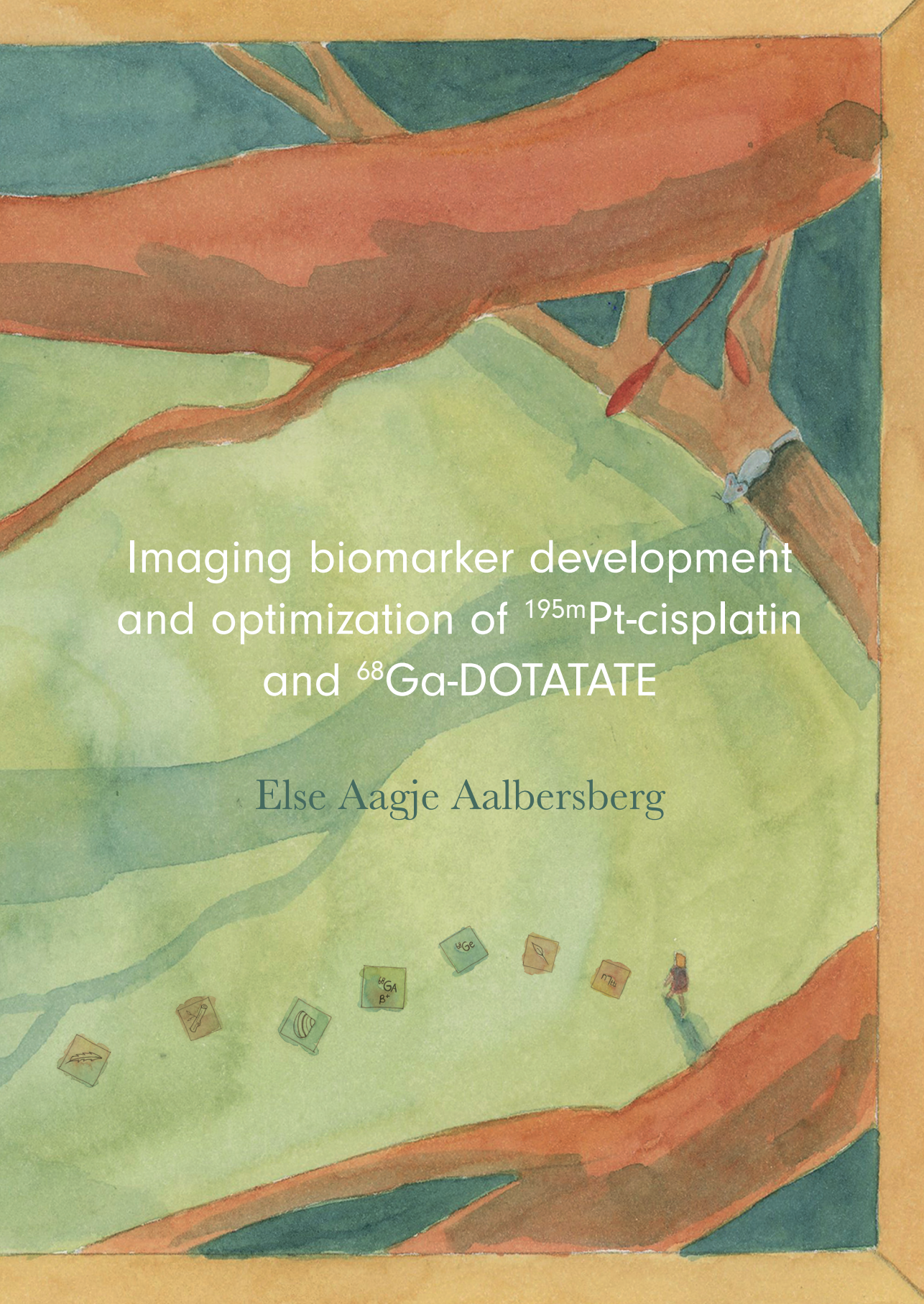

Imaging biomarker development and optimization of ^{195m}Pt-cisplatin and ^{68}Ga-DOTATATE

Else Aagje Aalbersberg

Imaging biomarker development and optimization of ^{195m}Pt-cisplatin and ^{68}Ga-DOTATATE

Else Aagje Aalbersberg

ISBN: 978-94-6323-813-7

Cover design and layout: © evelienjagtman.com
Printed by: Gildeprint

Imaging biomarker development and optimization of ^{195m}Pt-cisplatin and ^{68}Ga-DOTATATE

Ontwikkeling en optimalisatie van ^{195m}Pt-cisplatin en ^{68}Ga-DOTATATE als biomarker
(met een samenvatting in het Nederlands)

Proefschrift

ter verkrijging van de graad van doctor aan de
Universiteit Utrecht
op gezag van de
rector magnificus, prof.dr. H.R.B.M. Kummeling,
ingevolge het besluit van het college voor promoties
in het openbaar te verdedigen op

dinsdag 29 oktober 2019 des middags te 12.45 uur

door

Else Aagje Aalbersberg

geboren op 16 oktober 1987
te Waalre

Promotor:
Prof. dr. G.D. Valk

Copromotoren:
Dr. M.P.M. Stokkel
Dr. W.V. Vogel

This research was performed at the department of Nuclear Medicine at the Antoni van Leeuwenhoek hospital, Amsterdam, the Netherlands.

Printing of this thesis was financially supported by:

2Quart Medical BV

Advanced Accelerator Applications

ChipSoft

Ipsen

MILabs

NKI-AVL

NRG

Pfizer

CONTENTS


195mPt
IT
68GA
B+

Chapter 1

General introduction

GENERAL INTRODUCTION

Cancer affects people worldwide, causing approximately 9.6 million deaths in 2018 globally, making it the second leading cause of death after cardiovascular disease.[1] The socio-economic impact of cancer is enormous, and it was estimated that the worldwide cost of cancer was $1.16 trillion in 2010. Although cancer remains a deadly disease, the 10-year survival rate for all cancers has increased in the Netherlands from 32% in 1961-1970 to 54% in 2006-2010.[2] This increase in survival is due to both early detection and improved treatment strategies, in which new anti-cancer drugs play a pivotal role. However, with the increasing number of drugs and drug-classes (chemotherapy, targeted therapy, immunotherapy, etc.) either approved or in development, other challenges present itself.

The first challenge is selecting the most effective drug for a patient when many alternatives are available. Since ineffective treatment wastes valuable time and allows for disease progression, the most effective drug for an individual patient should be identified prior to the start of treatment based on patient- or tumor characteristics. This not only benefits individual patients, but also society as a whole since many modern therapies come at a high economic cost. The second challenge is choosing the drug with the least side-effects for a patient, without compromising treatment outcome. Side-effects can be severe, impact quality of life, and require dose adjustments, leading to sub-optimal treatment. The third challenge is performing response-assessment at the right time allowing for alterations of the treatment-regimen. Premature response-assessment can unjustly conclude that a drug is ineffective while late response-assessment risks disease progression under ineffective therapy. Nuclear medicine and quantitative imaging biomarkers could play a pivotal role in overcoming these challenges.

Nuclear medicine

Nuclear medicine employs radiopharmaceuticals for imaging of organ function or pathophysiology of disease. In contrast to anatomical imaging, nuclear molecular imaging provides information at the cellular or molecular level. These changes often present themselves on molecular imaging prior to anatomical changes which occur later in the course of a disease.[3] Due to the nano- to picomolar sensitivity of nuclear medicine imaging modalities, tracer amounts of radiopharmaceuticals provide accurate information without interfering with the biological process that is being studied.[4] Ideally, the half-life of the radioactive isotope that is used matches the duration of the biologically relevant distribution of the molecule being investigated. This ensures complete imaging of the desired physiological process without causing excess radiation dose.[4] Furthermore, data can be acquired over time through dynamic or serial imaging. With the increasing number of molecules, linkers, and isotopes becoming available, and the advances in imaging technology, the field of nuclear medicine is diversifying and gaining importance in healthcare.[3]

Imaging biomarkers

When a nuclear medicine examination is used to diagnose or stage cancer or to predict or monitor treatment efficacy or toxicity, this is known as an imaging biomarker. A biomarker is defined as 'a characteristic that is measured as an indicator of normal biological processes, or responses to an exposure or intervention, including therapeutic interventions.'[5] Biomarkers in nuclear medicine often fall in the category of diagnostic biomarker, but are also used as monitoring biomarker, response biomarker, predictive biomarker, prognostic biomarker, or safety biomarker.[5] Imaging biomarkers can provide non-invasive data for tumor detection, monitoring, and response assessment, and examine all pathological- and normal organ tissues in one non-invasive examination, even providing data on heterogeneity within a tissue.[6] In order for an imaging biomarker to be applicable in healthcare, it should measure a relevant (biological) feature, be measured quantitatively or categorically, be both repeatable and reliable, and should be validated both technically and clinically.[7] This requires standardized acquisition, reconstruction, and analysis protocols.

For patient selection in clinical oncological care, predictive and prognostic nuclear imaging biomarkers are gaining importance. A classic example in nuclear medicine is radioactive iodine, in which scintigraphic uptake of iodine is demonstrated with a low-dose of ^{123}I or ^{131}I prior to high-dose therapy with ^{131}I.[8] In the past decade imaging of radiolabeled drugs, peptides, and antibodies has increased tremendously for treatment selection, with ^{68}Ga-labeled peptides and ^{89}Zr-labeled antibodies as frontrunners. Uptake of ^{68}Ga-labeled peptides is a prerequisite for treatment with ^{177}Lu-labeled peptides in both neuroendocrine tumors and prostate cancer, while ^{89}Zr-labeled antibodies related to the immune system (immunoPET) are currently being explored for patient selection prior to immunotherapy.

Imaging biomarkers not only provide essential information in routine clinical care, but can also be instrumental in clinical trials. In an era where oncological treatment is shifting from traditional chemotherapies to molecular therapies or personalized medicine, patient selection, or patient enrichment, in clinical trials has become increasingly important.[9] Introducing (imaging) biomarkers as early as phase I trials could accelerate research and decrease the number of negative phase II and phase III trials and increase the a priori chance of success.[4,7,9,10] Up-front selection of patients with (imaging) biomarkers could prevent drugs from being effective only in a sub-group of a larger clinical trial.[11,12] When used appropriately, imaging biomarkers could enhance drug discovery, aid in smart clinical trial design to improve the clinical management of oncological patients.

The concept of imaging biomarkers is identical for each different type of cancer or different therapy, but each requires its own radiolabeled molecule, imaging protocol, and (pre-)clinical testing and validation. In this thesis, the described aspects of biomarker imaging are explored for two different radiolabeled molecules. **Part 1** of this thesis describes the first pre-clinical

steps for the introduction of ^{195m}Pt-cisplatin as an imaging biomarker for cisplatin treatment. Additionally, factors that influence the biodistribution of cisplatin are investigated. **Part 2** focusses on ^{68}Ga-somatostatin receptor imaging for neuroendocrine tumors, factors that influence the uptake of ^{68}Ga-somatostatin receptor imaging, and the subsequent treatment with ^{177}Lu-somatostatin analogues.

Part 1: Cisplatin

Cisplatin (cis-diamminedichloridoplatinum(II)) is a traditional chemotherapeutic drug that was first described by Rosenberg in 1965 and acquired FDA approval for the treatment of cancer in 1978.[13,14] More than four decades later, it still remains (part of) the first-line treatment for many malignancies such as lung cancer and head- and neck cancer and is classified by the WHO as an essential medicine.[15] Cisplatin acts by forming cisplatin-DNA adducts, which have to be removed by the cell prior to mitosis, however this process induces double strand breaks in the DNA. When only minor DNA damage exists, this can be repaired, however a multitude of DNA double strand breaks is lethal driving the cell into apoptosis.[14] Since cisplatin is not a targeted anti-tumor agent, the therapeutic window is narrow and dose-limiting toxicities are a serious and common occurrence.[16]

Nuclear medicine and cisplatin

Patient selection for cisplatin-based chemotherapy could aid in increasing effectiveness and decreasing toxicity. This might be possible with radiolabeled cisplatin, which makes use of ^{191}Pt, ^{193m}Pt, or ^{195m}Pt as the central platinum element in the drug.[17] Aside from becoming a predictive and/or risk biomarker, radiolabeled cisplatin could be used to gain further knowledge about the biodistribution and related aspects of cisplatin. A handful of pre-clinical and clinical studies have been performed throughout the years.[18–21] The number in these studies are low, undoubtedly due to the limited availability and high cost of the production of radiolabeled cisplatin, for which a nuclear reactor must be available. Furthermore, due to the era in which most studies were performed, planar gamma camera imaging was performed, limiting image quality. In the present, imaging systems have become more sensitive and three-dimensional imaging has become available with single photon emission tomography (SPECT).

This thesis

In this thesis, steps towards a new clinical trial with ^{195m}Pt-cisplatin are performed, as well as studies into the biodistribution of cisplatin. **Chapter 2** describes the imaging characteristics of ^{195m}Pt on a small animal scanner with both a high resolution and sensitivity. **Chapter 3** investigates the safety and efficacy of ^{195m}Pt-cisplatin compared to cisplatin, and explores the image quality of ^{195m}Pt-cisplatin in mice. **Chapter 4** studies the effect of pre-hydration on tumor concentration of cisplatin in mice and the impact of pre-hydration on survival after concurrent chemoradiotherapy with cisplatin in patients.

Part 2: Neuroendocrine neoplasms

Neuroendocrine neoplasms originate from neuroendocrine cells and form a heterogenous group of neoplasms divided into well-differentiated neuroendocrine tumors (NETs) and poorly differentiated neuroendocrine carcinomas (NECs).[22] The incidence of NETs increased steadily over the past three decades, rising faster than the incidence of all malignant neoplasms, and reached 6.98 per 100,000 persons in 2012 in the United States, therefore qualifying as an orphan disease.[23,24] NETs occur throughout the body, although the majority arise in the gastroenteropancreatic (GEP) tract or the lung. Based mainly on proliferation index, measured by Ki-67 staining, tumors are classified from low to high in grade I-III.[22] Together with tumor stage at diagnosis, primary tumor location and tumor grade largely determine the overall survival of patients, with a median overall survival of 9.3 years.[23,25] Although many different types of tumors are classified as a NET, most are characterized by (over)expression of the somatostatin receptor (SSTR). Over the years, SSTR has proved to be invaluable in the diagnosis and treatment of NETs; somatostatin analogues (SSAs) such as octreotide and lanreotide are first-line systemic treatment[26,27], and radiolabeled SSAs are utilized for imaging and radionuclide therapy.[27,28]

Nuclear medicine and NET

Radiolabeled somatostatin analogues have a central role in both imaging and treatment of NETs. For diagnostic purposes, ^{111}In-pentetreotide two-dimensional gamma camera imaging or three-dimensional SPECT imaging was standard of care in NET for many years, until it was replaced by ^{68}Ga-SSA PET (positron emission tomography) imaging in the 21st century.[28,29] For treatment of NETs, SSAs coupled to beta-emitting isotopes (^{90}Y or ^{177}Lu) were designed and peptide receptor radionuclide therapy (PRRT) with ^{177}Lu-DOTATATE was effective in a Phase III trial.[27] This led to both FDA and EMA approval of ^{177}Lu-DOTATATE for the treatment of unresectable and/or metastatic GEP-NET. Therapy selection for ^{177}Lu-DOTATATE therapy relies heavily on ^{68}Ga-SSA PET, as uptake of ^{68}Ga-SSA is a requirement for PRRT, making this a predictive biomarker.

This thesis

In this thesis, several aspects of imaging and treatment with radiolabeled SSAs are investigated. **Chapter 5** describes the production, quality control, and PET acquisition of ^{68}Ga-DOTATATE. It is shown that an automated production of ^{68}Ga-DOTATATE leads to a reliable production and a radiopharmaceutical product of high quality. Implementation of such protocols could aide in harmonization of multi-center research leading to more reproducible results. In **Chapter 6** two different radiolabeled SSAs (DOTATATE and HA-DOTATATE) are compared. Although initial reports describe similar properties, there can be differences in biodistribution. Not only does this affect image quantification, this might impact the detection rate of tumors in imaging or lead to different doses in treatment. **Chapter 7** describes the influence of treatment with non-radiolabeled SSAs on the biodistribution of ^{68}Ga-DOTATATE. In **Chapter 8** PRRT is investigated, and pre-existing parameters identified that impact treatment outcome.

REFERENCES

1. World Health Organization. Cancer. https://www.who.int/en/news-room/fact-sheets/detail/cancer. Accessed July 4, 2019.
2. Nederlandse Kankerregistratie. Cijfers over kanker. www.cijfersoverkanker.nl. Accessed July 4, 2019.
3. Kramer-Marek G, Capala J. The role of nuclear medicine in modern therapy of cancer. *Tumour Biol*. 2012;33:629-640.
4. Workman P, Aboagye EO, Chung YL, et al. Minimally invasive pharmacokinetic and pharmacodynamic technologies in hypothesis-testing clinical trials of innovative therapies. *J Natl Cancer Inst*. 2006;98:580-598.
5. FDG-NIH Biomarker Working Group. *BEST (Biomarkers, EndpointS, and Other Tools) Resource*. 2018.
6. Waterton JC, Pylkkanen L. Qualification of imaging biomarkers for oncology drug development. *Eur J Cancer*. 2012;48:409-415.
7. O'Connor J, Aboagye E, Adams J, et al. Imaging biomarker roadmap for cancer studies. *Nat Rev Clin Oncol*. 2016;14:169-186.
8. Luster M, Clarke SE, Dietlein M, et al. Guidelines for radioiodine therapy of differentiated thyroid cancer. *Eur J Nucl Med Mol Imaging*. 2008;35:1941-1959.
9. Yap TA, Sandhu SK, Workman P, De Bono JS. Envisioning the future of early anticancer drug development. *Nat Rev Cancer*. 2010;10:514-523.
10. Mandel JJ, Yust-Katz S, Patel AJ, et al. Inability of positive phase II clinical trials of investigational treatments to subsequently predict positive phase III clinical trials in glioblastoma. *Neuro Oncol*. 2018;20:113-122.
11. Amado RG, Wolf M, Peeters M, et al. Wild-type KRAS is required for panitumumab efficacy in patients with metastatic colorectal cancer. *J Clin Oncol*. 2008;26:1626-1634.
12. Takano T, Fukui T, Ohe Y, et al. EGFR mutations predict survival benefit from gefitinib in patients with advanced lung adenocarcinoma: a historical comparison of patients treated before and after gefitinib approval in Japan. *J Clin Oncol*. 2008;26:5589-5595.
13. Rosenberg B, Vancamp L, Krigas T. Inhibition of cell division in escherichia coli by electrolysis products from a platinum electrode. *Nature*. 1965;13:698-699.
14. Fennell DA, Summers Y, Cadranel J, et al. Cisplatin in the modern era: The backbone of first-line chemotherapy for non-small cell lung cancer. *Cancer Treat Rev*. 2016;44:42-50.
15. World Health Organization. *WHO Model List of Essential Medicines*. 2017.
16. Launay-Vacher V, Rey J-B, Isnard-Bagnis C, Deray G, Daouphars M. Prevention of cisplatin nephrotoxicity: state of the art and recommendations from the European Society of Clinical Pharmacy Special Interest Group on Cancer Care. *Cancer Chemother Pharmacol*. 2008;61:903-909.
17. Areberg J, Norrgren K, Mattsson È. Absorbed doses to patients from ^{191}Pt-, ^{193m}Pt- and ^{195m}Pt-cisplatin. *Appl Radiat Isot*. 1999;51:581-586.
18. Lange RC, Spencer RP, Harder HC. The antitumor agent cis-Pt(NH3)2Cl2: Distribution and dose calculations for ^{193m}Pt and ^{195m}Pt. *J Nucl Med*. 1972;14:191-195.
19. Areberg J, Björkman S, Einarsson L, et al. Gamma camera imaging of platinum in tumours and tissues of patients after administration of ^{191}Pt-cisplatin. *Acta Oncol*. 1999;38:221-228.
20. Buckley SE. A study of the distribution of ^{195m}Platinum-labelled cisplatin in tumours ssing single photon emission computed tomography (SPECT). 2005.
21. Sathekge M, Wagener J, Smith S, et al. Biodistribution and dosimetry of ^{195m}Pt-cisplatin in normal volunteers. *Nuklearmedizin*. 2013;52:222-227.

22. Rindi G, Klimstra D, Abedi-Ardekani B, et al. A common classification framework for neuroendocrine neoplasms: an International Agency for Research on Cancer (IARC) and World Health Organization (WHO) expert consensus proposal. *Mod Pathol*. 2018;31:1770-1786.
23. Dasari A, Shen C, Halperin D, et al. Trends in the incidence, prevalence, and survival outcomes in patients with neuroendocrine yumors in the United States. *JAMA Oncol*. 2017;77030:1335-1342.
24. Oronsky B, Ma PC, Morgensztern D, Carter CA. Nothing but NET: a review of neuroendocrine tumors and carcinomas. *Neoplasia*. 2017;19:991-1002.
25. Man D, Wu J, Shen Z, Zhu X. Prognosis of patients with neuroendocrine tumor: A SEER database analysis. *Cancer Manag Res*. 2018;10:5629-5638.
26. Rinke A, Müller HH, Schade-Brittinger C, et al. Placebo-controlled, double-blind, prospective, randomized study on the effect of octreotide LAR in the control of tumor growth in patients with metastatic neuroendocrine midgut tumors: A report from the PROMID study group. *J Clin Oncol*. 2009;27:4656-4663.
27. Strosberg J, El-Haddad G, Wolin E, et al. Phase 3 Trial of ^{177} Lu-DOTATATE for Midgut Neuroendocrine Tumors. *N Engl J Med*. 2017;376:125-135.
28. Bozkurt MF, Virgolini I, Balogova S, et al. Guideline for PET/CT imaging of neuroendocrine neoplasms with ^{68}Ga-DOTA-conjugated somatostatin receptor targeting peptides and ^{18}F–DOPA. *Eur J Nucl Med Mol Imaging*. 2017;44:1588-1601.
29. Balon H, Goldsmith S, Siegal B, Silberstein E, Krenning E, Donahoue K. Procedure guideline for somatostatin receptor scintigraphy with ^{111}In-pentetreotide. *J Nucl Med*. 2001;42:1134-1138.


195mPt
IT
68GA
B+

Chapter 2

Preclinical imaging characteristics and quantification of Platinum-195m SPECT

Else A. Aalbersberg
Linda J. de Wit-van der Veen
Oene Zwaagstra
Karlijn Codee-van der Schilden
Erik Vegt
Wouter V. Vogel

Eur J Nucl Med Mol Imaging. 2017;44(8):1347-1354.

ABSTRACT

Aims: In vivo biodistribution imaging of platinum-based compounds may allow better patient selection for treatment with chemo(radio)therapy. Radiolabeling with Platinum-195m (^{195m}Pt) allows SPECT imaging, without altering the chemical structure or biological activity of the compound. We have assessed the feasibility of ^{195m}Pt SPECT imaging in mice, with the aim to determine the image quality and accuracy of quantification for current preclinical imaging equipment.

Methods: Enriched (> 96%) ^{194}Pt was irradiated in the High Flux Reactor (HFR) in Petten, The Netherlands (NRG). A 0.05 M HCl ^{195m}Pt-solution with a specific activity of 33 MBq/mg was obtained. Image quality was assessed for the NanoSPECT/CT (Bioscan Inc., Washington DC, USA) and U-SPECT^{+}/CT (MILabs BV, Utrecht, the Netherlands) scanners. A radioactivity-filled rod phantom (rod diameter 0.85-1.7 mm) filled with 1 MBq ^{195m}Pt was scanned with different acquisition durations (10-120 min). Four healthy mice were injected intravenously with 3-4 MBq ^{195m}Pt. Mouse images were acquired with the NanoSPECT during 120 min at 0, 2, 4, or 24 h after injection. Organs were delineated to quantify ^{195m}Pt concentrations. Immediately after scanning the mice were sacrificed, and the platinum concentration was determined in organs using a gamma counter and graphite furnace – atomic absorption spectroscopy (GF-AAS) as reference standards.

Results: A 30-minute acquisition of the phantom provided visually adequate image quality for both scanners. The smallest visible rods were 0.95 mm in diameter on the NanoSPECT and 0.85 mm in diameter on the U-SPECT^{+}. The image quality in mice was visually adequate. Uptake was seen in the kidneys with excretion to the bladder, and in the liver, blood and intestine. No uptake was seen in the brain. The Spearman correlation between SPECT and gamma counter was 0.92, between SPECT and GF-AAS 0.84, and between GF-AAS and gamma counter 0.97 (all $p<0.0001$).

Conclusion: Preclinical ^{195m}Pt SPECT is feasible with acceptable tracer doses and acquisition times, and provides good image quality and accurate signal quantification.

INTRODUCTION

The anti-proliferative effects of platinum (Pt) complexes were observed in 1965 by Rosenberg *et al.* and led to the introduction of cisplatin in clinical oncology in the 1970's.[1] Forty years later cisplatin is still widely applied for the treatment of various cancers, most often combined with radiotherapy. Cisplatin-based concurrent chemoradiotherapy (CCRT) is considered a standard treatment option for stage II-III cancers of the lungs, head and neck, cervix, bladder, endometrium, and esophagus.[2-3] In the last decade, other platinum compounds including carboplatin and oxaliplatin have also found a place in clinical practice, with similar benefits for selected indications.[4]

Although cisplatin is widely used, it exhibits significant toxicity and resistance to treatment is a common problem. It has been estimated that only 8-11% of patients with head and neck cancer benefit from the addition of cisplatin to radiotherapy, suggesting that a major percentage of patients are unnecessarily exposed to cisplatin toxicity.[5-7] Optimization of treatment requires a better understanding of the behavior of platinum-based chemotherapeutics in vivo, but tools to assess the biodistribution of these pharmaceuticals are currently lacking. Presently, platinum concentrations in tissues can only be determined in biopsy material, which are obtained invasively and do not represent the whole tumor.[8] A non-invasive method for determination of platinum concentrations would enable in vivo studies of pharmacokinetics, dosing, and factors affecting the distribution of platinum compounds and their relation to tumor response and toxicity.

The incorporation of a radioactive platinum isotope in platinum-based chemotherapies allows evaluation of tissue concentrations using various techniques, including non-invasive gamma camera imaging.[9] Radiolabeling can be achieved by substitution of the platinum atom with the radioactive isotopes ^{191}Pt, ^{193m}Pt, or ^{195m}Pt, each with their own physical characteristics.[10-11] Based on its decay scheme with a favorable half-life and photon energy, ^{195m}Pt is considered the isotope most suitable for medical imaging.

Only a limited number of studies using radiolabeled cisplatin have been described in the literature. Some of these were limited to determining platinum concentrations in plasma or tissues using a well counter or autoradiography.[12-14] Scintigraphy has been attempted incidentally with various platinum isotopes, especially in the 1970's and 1980's and in one more recent publication.[9,11,15-20] The available imaging studies show that tumors and normal tissues (liver, kidney, brain, bowels) may vary significantly in accumulation of cisplatin, both in animals and in humans.[18] However, all published imaging studies employed planar scintigraphy, which suffers from superposition of the counts emitted from different internal structures and does not allow accurate quantification of uptake in tissues.

Over the last decades, gamma camera design has improved a great deal, especially in terms of sensitivity, spatial resolution and attenuation correction. The introduction of 3-dimensional (3D) imaging using single photon emission computed tomography (SPECT) combined with computed tomography (CT) has enabled anatomical correlation and quantitative imaging.[21] These developments have also benefited pre-clinical imaging equipment, sparking new interest for in vivo biodistribution imaging.

The purpose of the current study was to investigate the feasibility and characteristics of ^{195m}Pt SPECT in mice using state-of-the-art preclinical SPECT/CT systems. We especially focused on the accuracy of in vivo concentration measurements compared to ex vivo measurements.

MATERIALS AND METHODS

Production of ^{195m}Pt

Platinum-195m was produced by thermal neutron irradiation (n,γ) of enriched Platinum-194 contained in a quartz ampoule in the High Flux Reactor (HFR) in Petten, the Netherlands. After irradiation, a $H_2{}^{195m}PtCl_6$ solution of 52 MBq ^{195m}Pt/ml 0.05 M HCl was prepared with a specific activity of 33 MBq ^{195m}Pt/mg Pt at end of irradiation (EOI). Part of the ^{195m}Pt solution was analyzed for radioactivity and radionuclide purity (^{197}Pt, ^{191}Pt ^{192}Ir, ^{194}Ir, ^{198}Au, ^{199}Au) using a high purity Germanium detector (HPGe) coupled to a multi-channel analyzer system. The energy window ranged from 50 to 1640 keV. Data were processed using NEMO software version 2.4.7 (NRG, van Dijken and Oudshoorn 2011).

Phantom study

Two preclinical SPECT/CT systems were evaluated for image characteristics using ^{195m}Pt: the NanoSPECT/CT (Bioscan Inc., Washington DC, USA) and the U-SPECT$^+$/CT (MILabs BV, Utrecht, the Netherlands). The resolution of ^{195m}Pt-SPECT was assessed using a radioactivity-filled rod phantom containing six sections with capillaries respectively 0.85, 0.95, 1.1, 1.3, 1.5, or 1.7 mm in diameter. The distance between neighboring capillaries within each section equaled the diameter of the capillaries in that section. The phantom was filled with 1 MBq of ^{195m}Pt. Quantification of the NanoSPECT was determined with a dilution series of 1.5 ml Eppendorf tubes filled with 4, 2, 1, 0.5, 0.25, 0.125, 0.063, and 0.031 MBq of ^{195m}Pt in 1 ml.

Animal imaging study

The local animal ethics committee approved all animal studies. Mice were only scanned on the NanoSPECT, not on the U-SPECT$^+$ because this scanner was located in a different facility. Balb/c nude mice (n = 4), 13 weeks of age, received 133 MBq/kg $H_2{}^{195m}PtCl_6$ intravenously in the tail vein. SPECT/CT imaging of the four mice was performed under isoflurane anesthesia at 0, 2, 4, or 24 h after injection of ^{195m}Pt, respectively. Organs (kidneys, liver, blood pool over the heart, brain) were delineated manually on fused SPECT/CT images to quantify organ uptake (counts/mm^3). Immediately after imaging, the mice were sacrificed and the major organs were collected, weighed, and processed for ex vivo platinum measurement.

SPECT imaging

For the NanoSPECT, images were acquired over 10, 30, 60, and 120 minutes for the phantom and over 120 minutes for the animal experiment, using general-purpose pinhole mouse collimators (pinhole diameters 1.4 mm) in 24 projections. The two energy windows were set manually around the three major gamma peaks of ^{195m}Pt (65 keV and 67 keV peaks, range 59-75 keV and 99 keV peak, range 86-105 keV). Images were reconstructed using HiSPECT software (Scivis, Goettingen, Germany) with medium smoothing and resolution settings in 15 iterations,

in isotropic voxels of 0.3 mm in 3 directions. No corrections were performed for attenuation, decay, or scatter as this was not possible in the software version provided with this imaging system. A CT scan was acquired for image correlation purposes. SPECT and CT images were fused using InVivoScope.

For the U-SPECT^{+}, images of the phantom were acquired for 120 minutes in list-mode with both the general-purpose mouse collimator (GP-M, pinhole diameter 0.6 mm) and the extra-ultra high sensitivity mouse collimator (XUHS-M, pinhole diameter 2.0 mm). The energy windows were centered at 66 keV and 100 keV using a width of 15%. Image reconstruction was performed using the software provided by the manufacturer with an iterative reconstruction protocol, using the information from 10 min, 30 min, 60 min and 120 min counting, respectively, with a voxel size of 0.2 x 0.2 mm and slice thickness of 0.4 mm. Gaussian blur filters of 0.4, 0.8, and 1.2 mm full-width-half-maximum were applied to determine the optimum imaging quality. No corrections were performed for attenuation, decay, or scatter. No CT scan was acquired.

SPECT evaluation

All phantom SPECT images were evaluated visually for general image quality. The resolution was determined for both scanners by visual identification of the smallest separately visible rods. The sensitivity of the NanoSPECT scanner was determined from activity measurements with the Eppendorf tubes using a manually defined volume of interest (VOI), from which the count rate was related to the known activity concentration. The image quality of the animal SPECT images was assessed visually. The activity concentrations in different tissues / organs (kidneys, liver, blood pool and brain) were determined by manually drawing a VOI in these organs and recording the mean activity concentration. The accuracy and linearity of the measured activity concentrations on SPECT in vivo were determined by correlation with ex vivo measurement of different tissues, as described below.

Ex vivo platinum measurement

^{195m}Pt concentrations in collected tissues were measured using a well-type gamma counter (1480 Wizard, PerkinElmer) for 60 seconds with an energy window of 50 to 110 keV. In addition, total Pt concentrations (radioactive and non-radioactive combined) were measured using Graphite-furnace atomic absorption spectroscopy (GF-AAS). Tissue samples of approximately 100 mg were weighed and 1 ml of HNO_3 was added to the samples overnight. The samples were subsequently heated to 130°C until 100 µl remained. 0.5 ml of 1M HCl was added and the samples were reheated to 130°C until 100 µl remained; this process was repeated once with 0.1 M HCl. The samples were diluted 10-fold in volume in measuring buffer containing 0.15 M NaCl and 0.2 M HCl and stored at -20°C until analysis. Tissue analysis was performed using an atomic absorption spectrometer

(SOLAAR MQZ Zeeman, Thermo Optek) with a GF95 graphite furnace and FS95/97 autosampler (Thermo Elemental). Reference samples with known platinum concentrations were used for calibration.

Data analysis

Statistical analyses were performed in GraphPad Prism version 6.0b for Mac OS X (GraphPad Software). The Spearman correlation test was used to evaluate relations between quantitative SPECT, GF-AAS, and gamma counter values.

RESULTS

Production of ^{195m}Pt

Determination of the radionuclide purity in a sample of the analyzed solution showed 1.48E+07 Bq ^{195m}Pt, 4.53E+06 Bq of ^{197}Pt, 3.15E+04 Bq of ^{191}Pt, 6.18E+04 Bq of ^{192}Ir, 1.48E+06 Bq of ^{194}Ir, 2.60E+04 Bq of ^{198}Au, and 3.01E+06 Bq of ^{199}Au at EOI, indicating that ^{195m}Pt comprised 62% of the total radioactivity at EOI. ^{197}Pt and ^{194}Ir have relatively short half-lives in comparison to that of ^{195m}Pt; that is 19.89 and 19.16 hours, respectively, versus 4.02 days. As a result, 77% of the total radioactivity was from ^{195m}Pt at 2 days after EOI, compared to 6% and 2% from ^{197}Pt and ^{194}Ir, respectively. ^{199}Au ($T_{1/2}$: 3.14 days) remained present for 14 % of the total radioactivity at 2 days after EOI. Table 1 shows the radionuclide purity at each step during production and the experiment. Figure 1 shows an acquired spectrum on the NanoSPECT.

	^{195m}Pt	^{197}Pt	^{191}Pt	^{192}Ir	^{194}Ir	^{198}Au	^{199}Au
$T_{1/2}$ (days)	4.02	0.83	2.86	73.8	0.80	2.7	3.14
End of Irradiation	61.82	18.92	0.13	0.26	6.18	0.11	12.57
Injection in mice	79.61	4.15	0.14	0.51	1.24	0.11	14.23
24 hours p.i. in mice	90.32	0.26	0.08	0.67	0.07	0.06	8.54
Phantom NanoSPECT	95.33	0.00	0.03	1.34	0.00	0.02	3.29
Phantom USPECT^{+}	98.51	0.00	0.00	0.77	0.00	0.00	0.71

Table 1. Radionuclidic composition in percentage of the total activity at each step of the production and experiment. p.i. = post-injection.

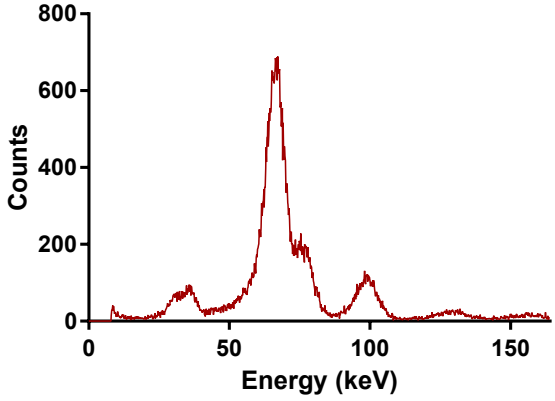

Figure 1. Energy spectrum of $H_2{}^{195m}PtCl_6$ acquired on the NanoSPECT.

Phantom study

For the NanoSPECT, the resolution was visually determined at 0.95 mm (Figure 2). The 0.95 mm rods were visible as separate rods at an acquisition time of 30 min. At 10 min duration the smallest visible rods were 1.1 mm. Extension of the scan time beyond 30 minutes did not improve the resolution further.

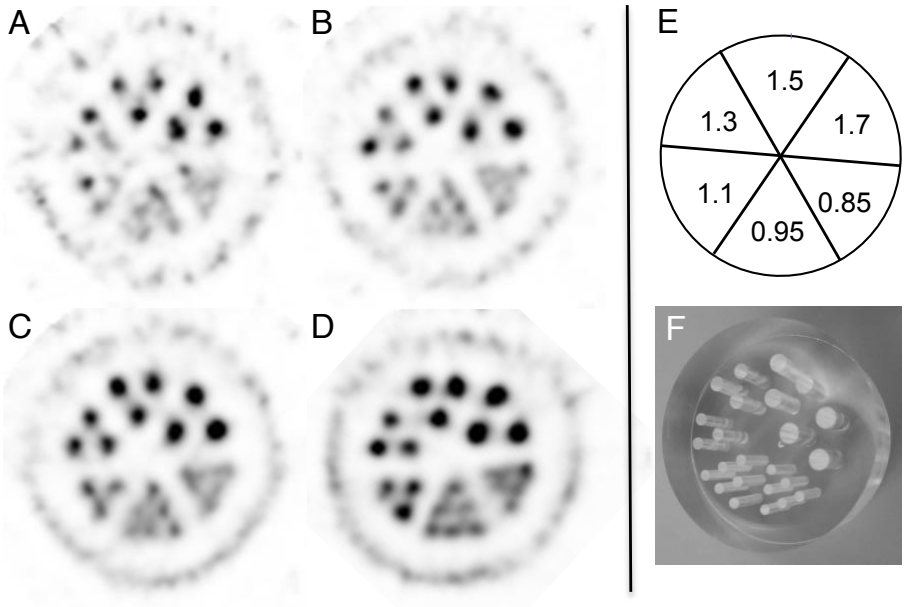

Figure 2. Images of the radioactivity-filled rod phantom filled with 1 MBq of ^{195m}Pt acquired on the NanoSPECT in (A) 10 minutes, (B) 30 minutes, (C) 60 minutes, and (D) 120 minutes. (E) Diagram of the rod sizes in the phantom in millimeters. (F) Photograph of the radioactivity-filled rod phantom.

For the U-SPECT$^+$, the image quality was found to be optimal using the GP-M collimator and 0.8 mm FWHM Gaussian blurring. This resulted in good visibility of the 0.85 mm rods (the smallest rods present in the phantom, Figure 3) at a scanning time of 30 minutes. Scanning longer than 30 minutes did not improve image quality significantly. However, with a coarser acquisition time of 10 minutes, use of the XUHS collimator (with larger pinholes and a lower specified spatial resolution) and 0.4 mm Gaussian blurring yielded better image quality compared to the GP collimator. With these settings, the 1.1 mm rods were separately visible.

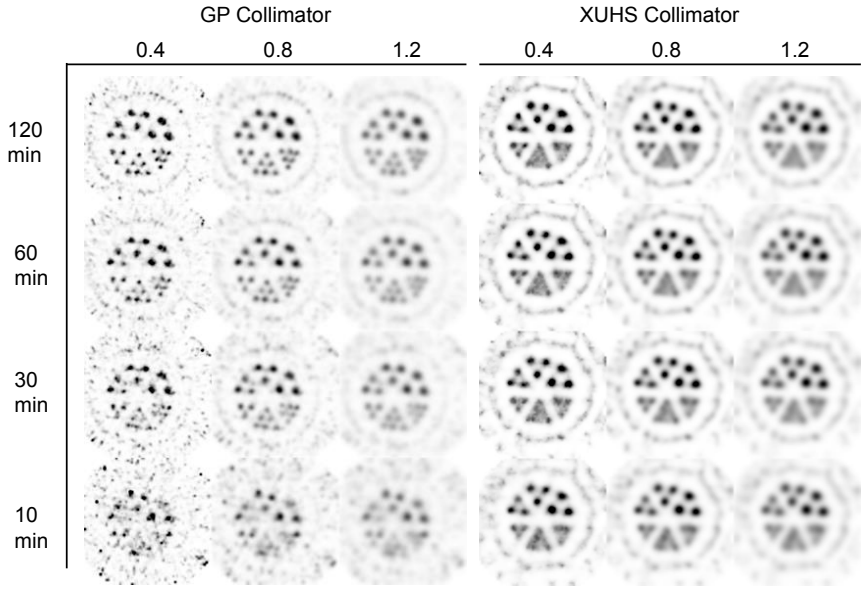

Figure 3. Images of the radioactivity-filled rod phantom filled with 1 MBq of ^{195m}Pt acquired on the U-SPECT^{+} with the GP and XUHS collimator, increasing acquisition times, and 0.4-1.2 mm Gaussian blur filtering. GP = general purpose, XUHS = extra ultra high sensitivity

Mouse imaging

Figure 4 shows SPECT images of four mice at different time points after intravenous injection of ^{195m}Pt. Imaging was performed for two hours, as this was considered the maximum time to keep the animals under anesthesia. The general image quality was considered adequate, especially giving the relative low dosage and intense accumulation in the tail. The kidneys and the bladder are clearly visualized, indicating high platinum uptake and excretion. Lower uptake, retention, and/or excretion are visible in the liver, blood pool and intestine. This strongly suggests a dominant renal clearance of $H_2{}^{195m}PtCl_6$. After 24 hours the bladder was hardly visible anymore, whereas the kidney and liver uptake remained similar. This may indicate renal retention of platinum. The high activity concentrations in the tail of the mice are probably due to extravasation, probably due to the highly acidic platinum solution (pH 1-2). Figure 5 shows the distribution of ^{195m}Pt.

Quantification and ex vivo correlation

Quantification was based on the calibration curve determined with the dilution series of ^{195m}Pt and is shown in Figure 6. The activity concentrations in the liver, kidneys, blood pool, and brain, as quantified on the SPECT images, correlated well with ex vivo measurements (Figure 7). The correlation coefficient between SPECT and gamma counter was 0.92 ($p<0.0001$), between GF-AAS and gamma counter 0.97 ($p<0.0001$) and between SPECT and GF-AAS 0.84 ($p<0.0001$).

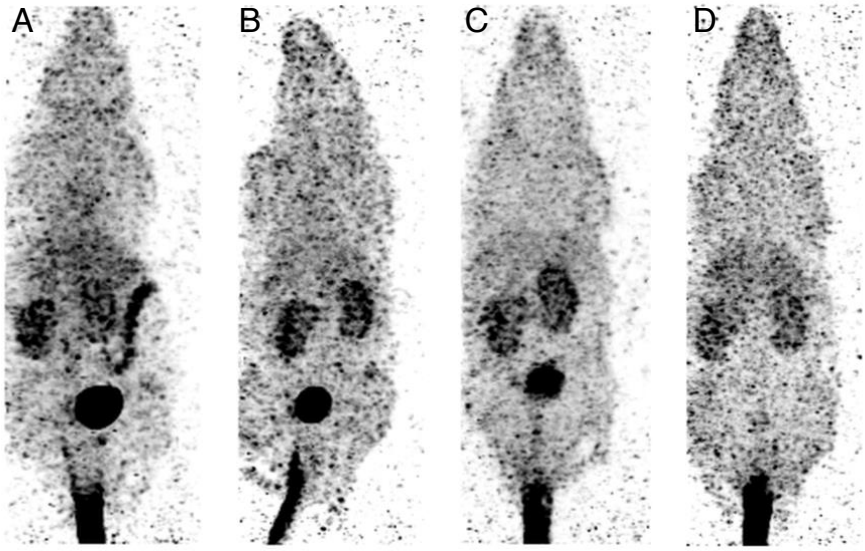

Figure 4. Maximum intensity projection images of the four mice injected with 133 MBq/kg ^{195m}Pt. All images were acquired on the NanoSPECT in 120 minutes. The mice were scanned either (A) immediately post injection, (B) 2 hours post injection, (C) 4 hours post injection, or (D) 24 hours post injection.

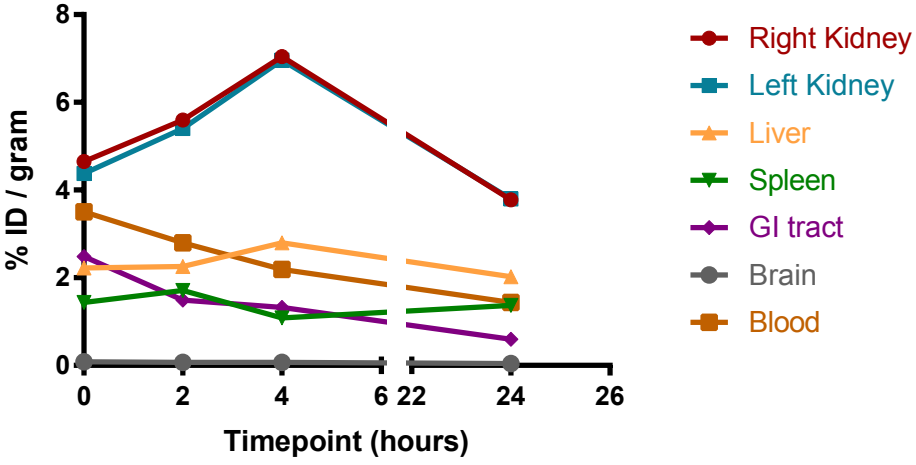

Figure 5. The amount of ^{195m}Pt in different organs measured in a gamma counter expressed in %ID/gram over time. ID = injected dose

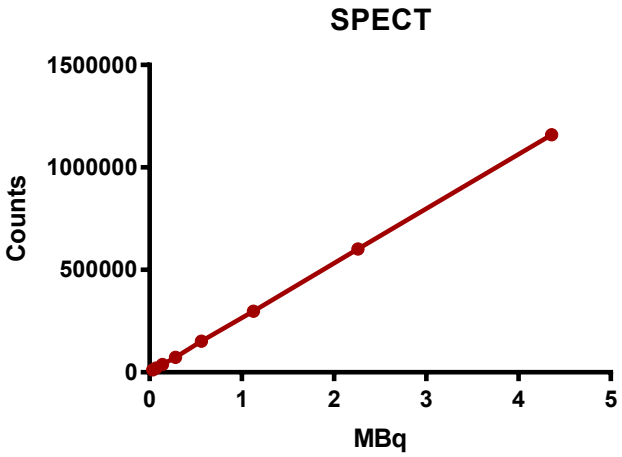

Figure 6. Linearity of the NanoSPECT demonstrated with phantom measurements

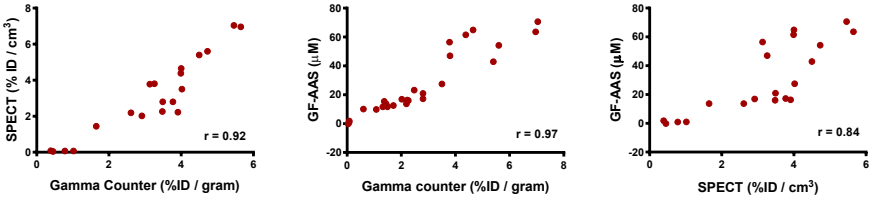

Figure 7. Correlation between the three methods used to measure organ platinum uptake: SPECT, gamma counting, and GF-AAS. The Spearman correlation and a linear regression line are shown. GF-AAS = graphite furnace atomic absorption spectroscopy, ID = injected dose, SPECT = single photon emission computed tomography

DISCUSSION

In this study we present the first preclinical SPECT images of ^{195m}Pt, showing its potential as a tracer to image the distribution of platinum-based compounds in vivo. The results indicate that quantitative ^{195m}Pt SPECT at sub-millimetric resolution is feasible in mice, and this characterizes the procedure for future applications. The isotope ^{195m}Pt can be incorporated into platinum based compounds, thus enabling in vivo prediction of compound effectiveness and toxicity in individuals, and could be used for personalizing medicine with platinum based chemotherapy.

To our knowledge, this is the first study to report high-resolution SPECT imaging of the isotope ^{195m}Pt in mice. Prior studies with clinical SPECT cameras have reported resolutions of approximately 12 mm at best. The gamma spectrum of ^{195m}Pt has three main photon peaks suitable for imaging, 65 keV, 67 keV, and 99 keV, which are of slightly lower energy than the photon peak of ^{99m}Tc (141 keV). Accordingly, imaging characteristics of ^{195m}Pt are theoretically expected to be somewhat sub-optimal compared to the mainstream isotope ^{99m}Tc, with higher photon scatter and attenuation especially in clinical imaging.

An important finding of this study is that ^{195m}Pt accumulation can be accurately quantified in mice using both SPECT systems. The data demonstrate a high correlation between the measured activity of ^{195m}Pt on SPECT and the tissue concentration of platinum measured ex vivo. Accurate quantification of ^{195m}Pt activity in vivo by SPECT is possible, with a linear response over a wide activity range (0.035-4.36 MBq), suggesting that succeeding preclinical studies with radioactive cisplatin are possible.

For radiolabeling cisplatin, either ^{191}Pt, ^{193m}Pt, or ^{195m}Pt can be applied. The isotope ^{195m}Pt decays to ^{195}Pt with a half-life of 4.02 days, keeping the platinum compound and its biological behavior unaltered, and emitting 60-100 keV photons suitable for imaging. ^{191}Pt decays to ^{191}Ir and thus becomes a different molecule, which leads to regulatory challenges in human imaging studies because the chemical structure is no longer the same. ^{193m}Pt decays with a half-life of 4.33 days to the radioactive isotope ^{193}Pt, which has a relatively long half-life of 50 years. Moreover, the yield of suitable photons for imaging is much lower than for ^{195m}Pt.[11] Therefore, ^{195m}Pt is considered the isotope most suitable for medical imaging.

This feasibility study has several limitations. Firstly, a relatively low activity dose of ^{195m}Pt was administered to the mice. This was due to the relatively low specific activity of ^{195m}Pt and extravasation in the tail due to the highly acidic solution, but was compensated for by an scanning time up to a maximum of two hours. However, the phantom images demonstrated

that 30 min acquisition time is sufficient to obtain images of sufficient quality. Secondly, only 4 animals were scanned. Nevertheless, we found a good and statistically significant correlation among the three quantification methods SPECT, ex vivo gamma counting, and GF-AAS.

Thirdly, this study was performed with platinum-chloride and not cisplatin; with only 80% ^{195m}Pt present when injected in mice. The $H_2{}^{195m}PtCl_6$ solution was used for the preclinical imaging studies using the low energy gammas of ^{195m}Pt of 65 keV (22.4%), 67 keV (38.3%), and 99 keV (11.4%). The high energy gammas from the radionuclidic impurities ^{192}Ir (316 keV (82.8%), 296 keV (29.0%), 308 keV (29.7%) and 468 keV (47.8%)) and ^{199}Au (158 keV (40.0%) and 208 keV (8.7%)) were not supposed to interfere with the data acquisition. The same is reasoned for the high energy gamma of 191 keV (3.7%) of ^{197}Pt. The contribution of its 77 keV (17.0%) gamma will be minimal at the time of the data acquisition, about 2 days after EOI, because of the relatively fast decay of ^{197}Pt, but could be reduced further by letting the solution decay for 1 more day. However, when platinum-chloride is used as a starting product for the synthesis of radioactive cisplatin, the iridium and gold impurities are removed, leading to a much higher radionuclide purity of ^{195m}Pt, which of course will be necessary when further (pre-)clinical studies are performed.

Fourthly, with the current specific activity, only 3-4 MBq of ^{195m}Pt could be injected in each mice, leading to relatively high noise levels in the images. Experiments to increase specific activity are being performed at the moment, which are expected to improve image quality.

Despite these limitations, this study demonstrates that ^{195m}Pt SPECT is feasible in small animals and produces high-resolution quantifiable images. In the future, we plan to use ^{195m}Pt with higher specific activity for the labeling of cisplatin and other platinum containing drugs, and subsequently perform imaging studies in both small animal models and cancer patients. The ultimate aim will be personalized selection of those patients that are likely to benefit from cisplatin treatment or that might be susceptible to toxicities.

CONCLUSION

Preclinical ^{195m}Pt SPECT is feasible with acceptable tracer activities and acquisition times, and provides good image quality and accurate signal quantification. This makes biodistribution imaging of platinum compounds with ^{195m}Pt-SPECT a realistic possibility.

REFERENCES

1. Rosenberg B, Vancamp L, Krigas T. Inhibition of cell division in escherichia coli by electrolysis products from a platinum electrode. *Nature.* 1965;13:698–699.
2. O'Rourke N, Roqué i Figuls M, Farré Bernadó N, Macbeth F. Concurrent chemoradiotherapy in non-small cell lung cancer (Review). *Cochrane Database Syst Rev.* 2010;16:CD002140.
3. Green JA, Kirwan JJ, Tierney J, et al. Concomitant chemotherapy and radiation therapy for cancer of the uterine cervix. *Cochrane Database Syst. Rev.* 2005;3:CD002225.
4. Lokich J, Anderson N. Carboplatin versus cisplatin in solid tumors: an analysis of the literature. *Ann. Oncol.* 1998;9:13-21.
5. Browman G, Hodson D, Mackenzie R, Bestic N, Zuraw L. Choosing a concomitant chemotherapy and radiotherapy regimen for squamous cell head and neck cancer: a systematic review of the published literature with subgroup analysis. *Head Neck*. 2001;23:579-589.
6. Pignon JP, Bourhis J, Domenge C, Designé L. Chemotherapy added to locoregional treatment for head and neck squamous-cell carcinoma: three meta-analyses of updated individual data. *Lancet*. 2000;355:949-955.
7. Schaake-Koning C, van den Bogaert W, Dalesio O, et al. Effects of concomitant cisplatin and radiotherapy on inoperable non-small-cell lung cancer. *N Engl J Med.* 1992;326:524-530.
8. Bosch ME, Sánchez AJR, Rojas FS, Ojeda CB. Analytical methodologies for the determination of cisplatin. *J Pharm Biomed Anal.* 2008;47:451-459.
9. Lange RC, Spencer RP, Harder HC. Synthesis and distribution of a radiolabeled antitumor agent: cis-diamminedichloroplatinum (II). *J Nucl Med.* 1971;13:328-330.
10. Areberg J, Norrgren K, Mattsson È. Absorbed doses to patients from ^{191}Pt-, ^{193m}Pt- and ^{195m}Pt-cisplatin. *Appl Radiat Isot.* 1999;51:581-586.
11. Lange RC, Spencer RP, Harder HC. The antitumor agent cis-Pt(NH3)2Cl2: Distribution and dose calculations for ^{193m}Pt and ^{195m}Pt. *J Nucl Med.* 1972;14:191-195.
12. Lagasse L, Pretorius G, Petrilli E, Ford LC, Hoeschele J, Kean C. The metabolism of cis-dichlorociammineplatinum (II): distribution, clearance, and toxicity. *Am J Obstet Gynecol.* 1981;139:791-798.
13. Ewen C, Perera A, Hendry JH, McAuliffe CA, Sharma H, Fox BW. An autoradiographic study of the intrarenal localisation and retention of cisplatin, iproplatin and paraplatin. *Cancer Chemother Pharmacol.* 1988;22:241-245.
14. Los G, Mutsaers P, Lenglet W, Baldew G, McVie J. Platinum distribution in intraperitoneal tumors after intraperitoneal cisplatin treatment. *Cancer Chemother Pharmacol.* 1990;25:389-394.
15. Smith PS, Taylor DM. Distribution and retention of the antitumor agent ^{195m}Pt-cis-dichlorodiammine platinum (II) in man. *J Nucl Med.* 1974;15:349-351.
16. Iosilevsky G, Israel O, Frenkel A, et al. A practical SPECT technique for quantitation of drug delivery to human tumors and organ absorbed radiation dose. *Semin Nucl Med.* 1989;19:33-46.
17. Shani J, Bertram J, Russell C, et al. Noninvasive monitoring of drug biodistribution and metabolism: studies with intraarterial Pt-195m-cisplatin in humans. *Cancer Res.* 1989;49:1877-1881.
18. Areberg J, Bjorkman S, Einarsson L, et al. Gamma camera imaging of platinum in tumours and tissues of patients after administration of ^{191}Pt-cisplatin. *Acta Oncol.* 1999;38:221-228.
19. Zamboni WC, Gervais AC, Egorin MJ, et al. Inter- and intratumoral disposition of platinum in solid tumors after administration of cisplatin. *Clin Cancer Res.* 2002;8:2992-2999.

20. Sathekge M, Wagener J, Smith SV, et al. Biodistribution and dosimetry of ^{195m}Pt-cisplatin in normal volunteers. *Nuklearmedizin.* 2013;52:222-227.
21. Bailey DL, Willowson KP. An evidence-based review of quantitative SPECT imaging and potential clinical applications. *J Nucl Med.* 2013;54:83-89.


195mPt
IT
68GA
B+

Chapter 3

Toxicity, efficacy and tumour imaging of ^{195m}Pt-cisplatin in mice

Else A. Aalbersberg
Linda J. de Wit-van der Veen
Karlijn Codee-van der Schilden
Oene Zwaagstra
Sjoerd Klarenbeek
Erik Vegt
Wouter V. Vogel

Manuscript in preparation.

ABSTRACT

Purpose: Radiolabeled cisplatin imaging may enable image-based personalisation of cisplatin-based chemotherapy treatment. Cisplatin labelled with ^{195m}Pt is theoretically suitable for molecular imaging, but it is currently unknown if the emitted radiation influences the effects of cisplatin on tumour or normal tissues. The purpose of this study was to determine the toxicity and efficacy of ^{195m}Pt-cisplatin compared to regular cisplatin, and to investigate ^{195m}Pt-cisplatin tumour imaging in mice.

Methods: ^{195m}Pt-cisplatin (CISSPECT®) was produced at- and obtained from NRG. Toxicity was evaluated in 69 mice that received various activity doses of ^{195m}Pt-cisplatin at a constant total dose of cisplatin. Toxicity was assessed using weight loss, renal function measured with ^{99m}Tc-MAG3 renography, and renal histopathology. The anti-tumour effect of ^{195m}Pt-cisplatin was compared to (non-radioactive) cisplatin in 20 mice by determining progression-free and overall survival. To investigate the possibility of tumour imaging and quantification of uptake, five mice were administered with ^{195m}Pt-cisplatin and SPECT/CT images were acquired.

Results: At the end of irradiation, specific activity was 91 MBq/g ^{195m}Pt, and radionuclide purity of ^{195m}Pt-cisplatin was 96.1% at start of experiments. Radiolabeled cisplatin did not lead to weight loss >10% on average, but individual animals did have a delayed excretion of ^{99m}Tc-MAG3 one month after administration. Histopathology of the kidneys demonstrated only a small number of mild lesions after one month, comparable to administration of cisplatin only. Survival of tumour-bearing mice treated with ^{195m}Pt-cisplatin was similar to mice treated with non-radioactive cisplatin in this mouse model. Tumour uptake on SPECT/CT was mild to moderate. Background uptake in normal tissues was relatively high, probably due to the binding of cisplatin to plasma proteins.

Conclusion: In the applied mouse model, ^{195m}Pt-cisplatin did not prove more toxic or effective than regular non-radiolabeled cisplatin. SPECT/CT imaging and quantification of ^{195m}Pt-cisplatin uptake in tumour is feasible with adequate image quality in mice.

INTRODUCTION

Cisplatin is a cytotoxic drug that acts by generating platinum-DNA adducts. These damages to the DNA need to be removed prior to mitosis, in order to prevent abnormal cell division. When there is limited damage, cell cycle arrest occurs and the damage is repaired. However, if the damage to the DNA is beyond repair, the cell goes into apoptosis.[1] The cytotoxic action of cisplatin was described in 1965 and it was approved as a chemotherapeutic drug by the FDA in 1978.[2] Cisplatin-based chemo- and/or radiotherapy is still the backbone for the treatment of many cancers, such as lung cancer and head-and-neck cancer, and therefore it is on the list of essential medicines of the World Health Organization.[3] Despite the long experience with cisplatin in clinical care, there is still room for improvement of cisplatin chemotherapy, for example through better understanding and prediction of tumour resistance or sensitivity to cisplatin therapy as well as toxicity to normal tissues, enabling selection of patients who are likely going to benefit from cisplatin.[4]

One of the methods to gain a better understanding of cisplatin is through the use of molecular imaging. This would allow non-invasive whole-body evaluation of its biodistribution, including in tumour and in normal tissues that are at risk for toxicity. When a molecular compound that can be imaged also has therapeutic effects, it can be applied for image-guided treatment known as theranostics. In nuclear medicine, theranostics is applied by labelling a molecule or drug with a diagnostic isotope prior to treatment with a therapeutic isotope to the same molecule or drug.[5] Well-known examples are the use of Iodine-123 prior to treatment with Iodine-131 in thyroid disease and Gallium-68 somatostatin receptor PET/CT prior to treatment with somatostatin analogues coupled with Lutetium-177.[6-7] The development of radioactive cisplatin would allow for theranostics of cisplatin to predict therapeutic efficacy or toxicity.

Since cisplatin is a small molecule, it is assumed that coupling it to an isotope that is not naturally present in cisplatin would significantly alter the biodistribution of cisplatin. This can be solved by substituting platinum, which is both the central and pharmacologically active element of cisplatin. Of the different platinum isotopes, Platinum-195m (^{195m}Pt) is suitable for medical imaging due to its half-life of 4.02 days and emission of 66 and 99 keV photons.[8-9] However, ^{195m}Pt is not a pure gamma emitter, as 36 auger electrons are also emitted per disintegration.[10] These auger electrons deposit large amounts of energy within a very short distance.[11] This could lead to an additive therapeutic effect, but also to additive toxicity. Therefore, the aim of this study was to determine the toxicity and efficacy of ^{195m}Pt-cisplatin compared to regular cisplatin, and to investigate the feasibility of ^{195m}Pt-cisplatin tumour imaging in mice.

MATERIALS AND METHODS

^{195m}Pt-cisplatin and cisplatin

Platinum-195m was produced by irradiation in the High Flux Reactor (HFR) in Petten, the Netherlands. After irradiation, CISSPECT®, or [195mPt]Cisplatin, or cis-[195mPt][Pt(NH3)2Cl2], or ^{195m}Pt-cisplatin was synthesized according to known procedures as a 1 mg/ml solution in 0.9 % NaCl with a pH of 5 to 5.5.[12-13] Part of the ^{195m}Pt-cisplatin solution, containing 0.064 mg Pt, was analyzed for radioactivity and radionuclide purity (^{197}Pt, ^{191}Pt, ^{192}Ir, ^{194}Ir, ^{198}Au, ^{199}Au) using a high purity Germanium detector (HPGe) coupled to a multi-channel analyzer system. The energy window ranged from 50 to 1640 keV. Data were processed using NEMO software version 2.4.7 (NRG, van Dijken and Oudshoorn 2011). Ultraviolet-visible spectrophotometry (UV-VIS) (Perkin Elmer double-beam Lambda 365 UV-VIS spectrophotometer) was used to identify cisplatin by its characteristic absorbance at 301 and 365 nm. The absorbance at 301 nm was measured to determine the concentration of the ^{195m}Pt-cisplatin solution according to a calibration graph, which was plotted from the absorbance at 301 nm of solutions with concentrations of cisplatin ranging from 0.2 to 1 mg/ml cisplatin in 0.9% NaCl. The chemical and radiochemical purity were determined using High Performance Liquid Chromatography (HPLC) (Waters Acquity-arc HPLC system, XBridge C8 colomn (3.5 µm) of 4.6 x 250 mm, UV-detection at 210 nm, Berthold Flowstar LB513 radiodetector) following procedures as described in the European Pharmacopeia (edition 7.0) with slight modifications. An aqueous solution of 1.08 g sodium octanesulfonate, 1.70 g tetrabutylammonium hydrogensulfate and 2.72 g potassium dihydrogenphosphate per liter, of which the pH was adjusted to pH 5.9 with 1 M sodium hydroxide, was filtered (0.2 µm Whatman RC58) and used as the mobile phase. A flow rate of 1 ml/min. was used and a run time of 10 min. European Pharmacopoeia reference standard cisplatin CRS, cisplatin impurity A CRS and cisplatin impurity B CRS, were used to determine retention peaks of cisplatin and of hydrolyzed cisplatin (aquo complex), as well as of Transplatin (impurity A) en ammonium trichloroplatinate(—) (impurity B).

Non-radioactive cisplatin (1 mg/ml concentrate for solution for infusion) was purchased from Accord (Accord Healthcare Ltd., United Kingdom).

Toxicity

The toxicity of ^{195m}Pt-cisplatin was compared to cisplatin in different groups of mice in which the chemical dose of cisplatin was identical, but the percentage of radioactive cisplatin varied from 0-100%. Toxicity was assessed through weight loss, renography and histopathology.

Mouse model

Sixty-nine female FVB mice 12-13 weeks of age were obtained (Janvier Labs, France). The mice were divided into 4 groups, all receiving 6 mg/kg cisplatin with a different percentage of ^{195m}Pt-cisplatin: 100% ^{195m}Pt-cisplatin (n=15), 50% ^{195m}Pt-cisplatin (n=15), 25% ^{195m}Pt-cisplatin (n=15), and 0% ^{195m}Pt-cisplatin. The remaining 9 mice were a control group. All cisplatin administrations were given intravenously in the tail vein. Weight loss was monitored 3-4 times per week. The minimum weight was calculated as a percentage of the start weight ($Weight_{min}$).

After 24 hours, 7 days and 28 days, one-third of the animals in each group received a renal scan to measure nephrotoxicity. These mice were subsequently sacrificed and the organs were harvested for histological examination.

Renal scans

For renal scans, mice were anaesthetized with 1.5-2.5% isoflurane. A catheter was placed in the tail vein and the animal placed on the animal SPECT/CT scanner (USPECT/CT, MILabs, the Netherlands). Immediately after injection of 20-30 MBq of ^{99m}Tc-MAG3, a dynamic scan was started (1 bed position, acquisition time 30 minutes, 10 seconds per frame, Rat collimator with 1.5mm pinhole). Reconstruction was done in U-SPECT-Rec (MILabs, the Netherlands) with 4 iterations and 8 subsets. Time-activity curves were generated in PMOD (version 3.610, PMOD Technologies LLC, Switzerland), and time to maximum uptake (T_{max}) and excretion time to half maximum (T_{half}) were measured.

Pathology

Immediately after sacrifice of an animal, its organs (colon, small intestine, stomach, pancreas, spleen, kidneys, liver and brain) were harvested and placed in ethanol-acetic acid-formaldehyde fixative for three months, ensuring that all samples were no longer radioactive. After paraffin embedding, 2 µm slices were cut and stained with haematoxylin and eosin. All slides were examined by a dedicated experimental animal pathologist blinded to the treatment groups. The following abnormalities were noted: intratubular protein casts (proteinuria), and degeneration, cell death and sloughing of renal tubular epithelium.

Statistics

Normality of $Weight_{min}$, T_{max}, and T_{half} was tested with the Kolmogorov-Smirnov test. In case of non-normality, the Kruskal-Wallis test was used to compare medians between the groups. If a significant difference was found between the groups, the significantly different groups were determined with correction for multiple comparisons. $P \leq 0.05$ was considered significant. Data are shown as mean ± SD or median [95% confidence interval] in case of non-normal distribution. Statistics were performed in SPSS (v22, IBM, United States) and figures made in Graphpad Prism (v7.03, GraphPad Software, Inc., United States).

Anti-tumour effect

Efficacy of ^{195m}Pt-cisplatin was compared to non-radioactive cisplatin in a cisplatin-sensitive mouse model.

Mouse model

Twenty female FVB mice were obtained (Janvier Labs, France) and transplanted with a p53$^{-/-}$ tumour in the mammary gland under anaesthesia with 2-2.5% isoflurane. Rimadyl was given for pain relief immediately and 24 hours after tumour transplantation. Tumour growth was measured at least three times a week using a calliper. When the tumours reached at least 7 mm in diameter, the animals were divided into four treatment groups, n=5 each: (1) 6 mg/kg cisplatin, (2) 3 mg/kg cisplatin, (3) 6 mg/kg ^{195m}Pt-cisplatin and (4) 3 mg/kg ^{195m}Pt-cisplatin. All injections were given in the tail vein.

Statistics

Kaplan-Meier curves of progression free survival (PFS) and overall survival (OS) were created in Graphpad Prism.

Tumour imaging

Tumour uptake of ^{195m}Pt-cisplatin was visualized and quantified with SPECT/CT.

Mouse model

Five female NRMI nude mice were obtained (Janvier Labs, France). A BRCA$^{-/-}$ p53$^{-/-}$ tumour was transplanted in the mammary gland under anaesthesia with 2-2.5% isoflurane. Rimadyl was given for pain relief immediately and 24 hours after tumour transplantation. Tumour growth was measured at least three times a week through calliper measurements. When a tumour reached at least 5 mm in the smallest diameter, 6 mg/kg ^{195m}Pt-cisplatin was injected in the tail vein. A SPECT/CT scan was acquired 1 and 24 hours after cisplatin administration.

Imaging

SPECT/CT imaging was performed on a USPECT/CT small animal scanner (MILabs, the Netherlands). Animals were anaesthetised with 1.5-2.5% isoflurane and placed on the mouse total body bed. A 60 minute acquisition of one bed position located around the tumour was performed using the rat collimator with 1.5 mm pinholes for increased sensitivity. Afterwards a CT scan of the whole mouse was acquired for anatomical correlation.

Reconstruction and quantification

Two energy windows were selected for detecting the photon peaks of ^{195m}Pt: 55-85 keV and 95-110 keV, with background windows from 45-55 keV and 85-95 keV. Reconstruction was performed with a voxel size of 0.8 mm, 6 iterations, 16 subsets and 1 mm full width half maximum Gaussian blurring. Volumes of interest (VOIs) were manually drawn around the tumour on CT images, and total activity within each VOI was calculated. Uptake was calculated as percentage of injected activity (%IA). Reconstruction was performed in the U-SPECT-Rec (MILabs, the Netherlands) and quantification was performed in PMOD (v3.610, PMOD Technologies LLC, Switzerland).

RESULTS

^{195m}Pt-cisplatin

Specific activity at the end of irradiation was 91 MBq ^{195m}Pt/mg platinum. At the end of point of synthesis (activity reference time of ^{195m}Pt-cisplatin), the specific activity was 67 MBq ^{195m}Pt/mg platinum or 44 MBq ^{195m}Pt/mg ^{195m}Pt-cisplatin, and the radionuclide purity was 94.5% with ^{197}Pt being the main impurity (5.4%, t½ = 19.9 h). Radionuclide purity increased to 96.5% at the start of experiments due to decay of ^{197}Pt. Table 1 shows the radionuclide purity of the sample. Radiolabeled cisplatin was dissolved in 0.9% NaCl and diluted to a concentration of 0.99 mg cisplatin/ml.

Radionuclide	Half-life (hrs)	Activity at ART (kBq)	% of total activity at ART	Activity at SoE	% of total activity at SoE
^{195m}Pt	96.5	4310	94.5	3810	96.5
^{197}Pt	19.9	246	5.40	136	3.44
^{191}Pt	67.92	0.773	0.017	0.653	0.017
^{198}Au	64.56	0.175	0.004	0.146	0.004
^{199}Au	75.36	0.305	0.007	0.261	0.007

Table 1. Radionuclide purity of ^{195m}Pt-cisplatin at activity reference time (ART) and start of experiments (SoE). Activities of ^{192}Ir, ^{194}Ir, and ^{193m}Pt were below detection limits.

The UV-VIS spectrum (Figure 1) of ^{195m}Pt-cisplatin showed the characteristic absorbances of cisplatin at 301 and 365 nm, thereby confirming the *cis* geometry of the synthesized complex. In contrast, transplatin shows maximum absorbance at 270 and 315 nm, and displays a minimum absorbance at 295 nm (data not shown).

HPLC-UV runs of European Pharmacopoeia reference standards showed retention times for cisplatin and hydrolyzed cisplatin (aquo complex) of 4.1 and 5.3 min., respectively. Retention times of 2.8 and 3.0 minutes were shown for transplatin (impurity A) and ammonium trichloroplatinate(—) (impurity B), respectively. The HPLC-UV run of synthesized ^{195m}Pt-cisplatin (Figure 2A) shows retention peaks at 4.09 and 5.30 minutes only, with the peak at 2.42 min. being the injection peak. This indicates a chemical purity of > 99.9% if, in line with the European Pharmacoepoeia regulations for cisplatin, the peak due to the aquo complex is disregarded. Retention peaks of ^{195m}Pt-cisplatin and its aquo complex in the HPLC radiochromatogram (Figure 2B) show a small time delay with respect to the UV chromatogram, due to the covered path length of the test sample from UV detection to radiodetection. The radiochromatogram confirms a radiochemical purity of > 99.9% as well.

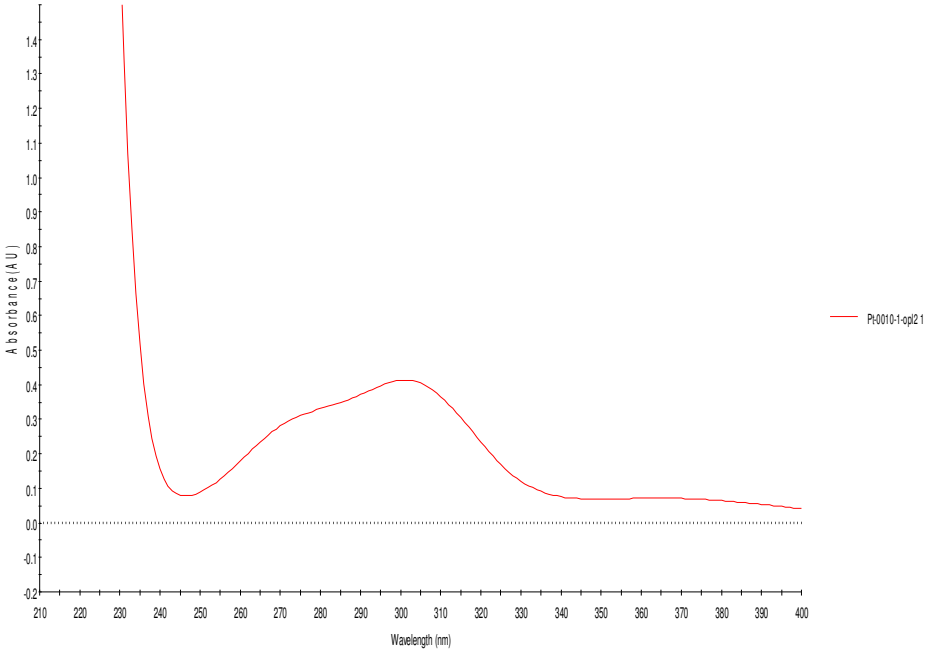

Figure 1. UV-vis spectrum of the 0.99 mg ^{195m}Pt-cisplatin 0.9 % NaCl aqueous solution.

Toxicity

Injected activity of ^{195m}Pt-cisplatin (mean ± standard deviation [SD]) was 9.3±0.7 MBq in the 100% activity group, 4.7±0.2 in the 50% activity group and 2.3±0.2 in the 25% activity group. In the 100% activity group, 2 mice died after 1 week of unknown cause (histopathological examination not possible), but probably related to the injection of ^{195m}Pt-cisplatin. In the 50% group 1 mouse died after 4 weeks, most likely due to fighting (visible wounds on the head and tail) and therefore unrelated to ^{195m}Pt-cisplatin administration.

Weight loss was not observed in the 0% activity group, the 50% activity group and the 100% activity group, as shown in Figure 3A. Only 50% activity led to a significant decrease in weight (to 93% [92-94] of baseline) compared to the 0% activity group (p=0.018).

Figure 3B and 3C show the results of quantification of the renal scans. At 1 week, there were no differences between any of the groups in both T_{max} and T_{half}. At 1 month, the median T_{max} of the dose group receiving 25% activity (165 s [134-231]) was significantly different from the control group (70 s [64-80]), 0% activity group (80s [75-91]), and 50% activity group (78s [69-96]). The median T_{half} at the time of the 25% activity group (600s [489-696]) also differed significantly from the control group (195s [183-214]) and 50% activity group (205s [490-696]).

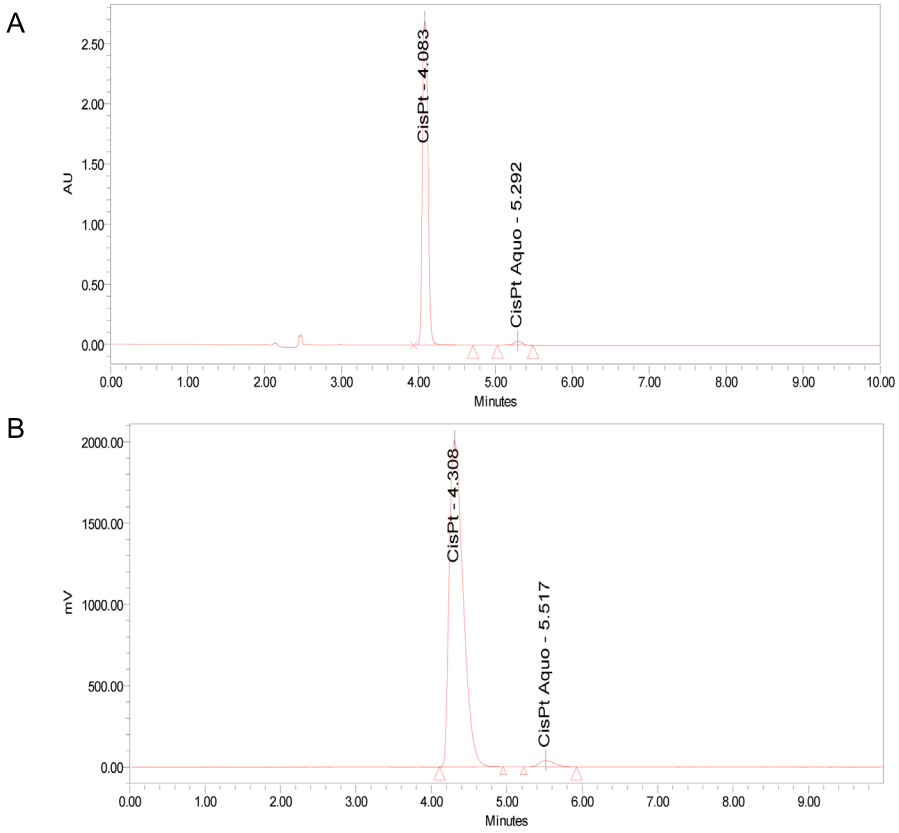

Figure 2. (A) HPLC-UV chromatogram of ^{195m}Pt-cisplatin, (B) HPLC radiochromatogram of ^{195m}Pt-cisplatin.

Histological examination revealed no renal toxicity one day post cisplatin administration. At one week, almost no lesions were seen. One month after cisplatin administration, mild lesions were found in the 25% activity group and very mild lesions in the group receiving 0% activity. Figure 3D shows an image with mild lesions.

Efficacy

Injected activity of ^{195m}Pt-cisplatin was 9.85±0.83 MBq in the 6 mg/kg ^{195m}Pt-cisplatin group, and 5.63±0.35 MBq in the 3 mg/kg ^{195m}Pt-cisplatin group. Median PFS was 14 days in the group receiving 3 mg/kg cisplatin, 13 days in the group receiving 3 mg/kg ^{195m}Pt-cisplatin, 14 days in the group receiving 6 mg/kg cisplatin, and 16 days in the group receiving 6 mg/kg ^{195m}Pt-cisplatin. Median OS was 19 days in the group receiving 3 mg/kg cisplatin, 19 days in the group receiving 3 mg/kg ^{195m}Pt-cisplatin, 21 days in the group receiving 6 mg/kg cisplatin, and 21 days in the group receiving 6 mg/kg ^{195m}Pt-cisplatin. Kaplan-Meier curves of survival data are shown in Figure 4.

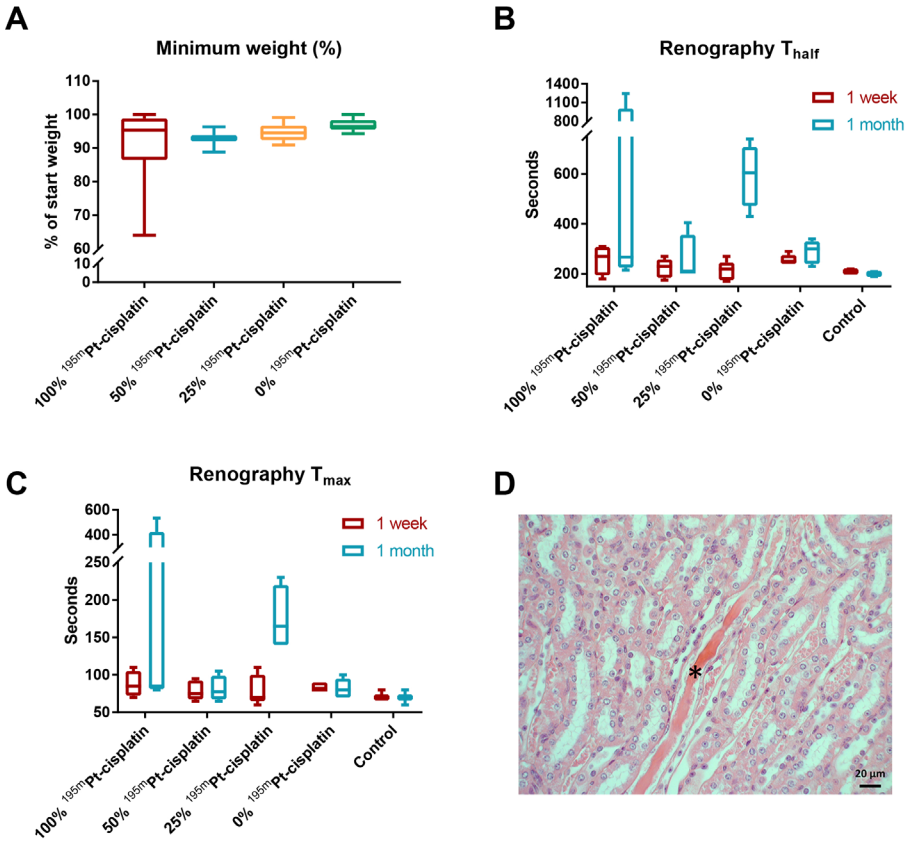

Figure 3. Toxicity analysis of radiolabelled cisplatin. (A) Minimum weight (% of baseline). (B) Time to maximum uptake (T_{max}) on renal scans. (C) Excretion time to half of the maximum uptake on renal scans (T_{half}). (D) Kidney pathology slide, haematoxylin and eosin staining, showing an intratubular protein cast (*).

Tumour imaging

Injected activity of ^{195m}Pt-cisplatin was 8.55±3.03 MBq. Tumour uptake on SPECT images was mild to moderate, as shown in an example in Figure 5. Moderate uptake was seen in the background, probably due to the known binding of cisplatin to plasma proteins such as albumin. Uptake in the tumours was quantified in 3 animals; in the other 2 animals an accurate VOI could not be drawn due to lack of contrast between the tumour and soft tissue on both the SPECT and CT images. In two mice, the uptake of ^{195m}Pt-cisplatin decreased between 1h and 24h post injection, from 0.44% to 0.18% IA and from 0.39% to 0.18% IA, respectively. In the third animal, the uptake of ^{195m}Pt-cisplatin increased from 0.19% IA at 1h post injection to 0.27% IA at 24h post injection.

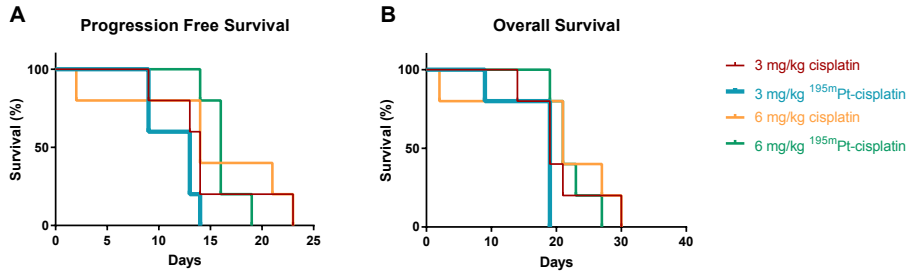

Figure 4. Survival after injection of either cisplatin or ^{195m}Pt-cisplatin. (A) Progression free survival and (B) overall survival.

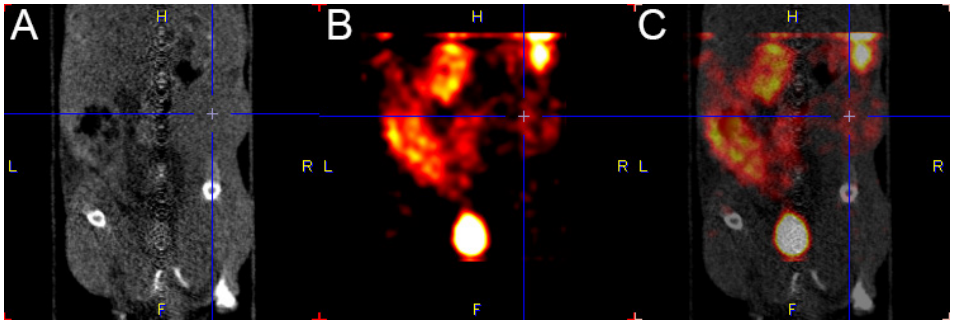

Figure 5. (A) CT, (B) SPECT, (C) SPECT/CT coronal slice of a tumour-bearing mouse 1 hour after administration of ^{195m}Pt-cisplatin. The tumour is indicated by the cross-hairs.

DISCUSSION

Imaging of ^{195m}Pt-cisplatin would provide an invaluable tool for further research into personalised medicine with cisplatin. With the rising amount of available anti-cancer drugs, treatment personalisation becomes increasingly important and image-based treatment decisions are becoming a valuable tool. ^{195m}Pt-cisplatin imaging for predicting treatment outcome and toxicity could assist patients and their physicians in the choice for cisplatin treatment. Patients with no or very low tumour cisplatin uptake will most likely not benefit from cisplatin treatment. Preventing these patients from receiving an ineffective, yet highly toxic treatment, would be of great clinical importance. Similarly, patients with high cisplatin retention in the kidneys could be spared cisplatin-related side effects by using alternative treatments. Furthermore, tumour cisplatin uptake imaging could simplify studies into the biodistribution of cisplatin, by reducing the need of surrogate endpoints such as blood pharmacokinetics

The synthesis of radioactive ^{195m}Pt-cisplatin has been reported before, and a specific activity of 14 MBq/mg cisplatin at the end of synthesis was stated.[13] Herein, we report a three-fold increase in specific activity at end of synthesis, i.e. 44 MBq/mg ^{195m}Pt-cisplatin. Zeevaart et. al. reported a shortened synthesis procedure due to irradiation of ^{195m}Pt-$PtCl_2$ instead of ^{195m}Pt-Pt, which was used as the starting material in our case. The increase in specific activity may be the result of the markedly narrowed cooling time after irradiation, as well as of different reactor characteristics. Radionuclide purity and radiochemical purity are approximately similar to what was reported earlier.[13]

Tumour imaging with ^{195m}Pt-cisplatin in this study shows moderate uptake of cisplatin in most tissues healthy organs. This immediately identifies a major challenge that cisplatin imaging faces, namely binding of cisplatin to plasma proteins. The irreversible binding of cisplatin to plasma proteins, which lies around 90% of the injected dose, leads to a long circulation time of protein-bound cisplatin. In our study, the uptake of radiolabelled cisplatin in cisplatin-sensitive tumours was comparable to background uptake in the muscle. Therefore, the tumours needed to be delineated on CT to enable quantification of uptake on SPECT. Cisplatin imaging might therefore be best feasible in lung cancer and head-and-neck cancer. Lung tumour imaging has the advantage of low background uptake and high tumour contrast on CT, both due to the presence of air in the lungs. Head-and-neck tumours are relatively superficial, leading to only moderate attenuation whilst lymph node metastases can be large and easily identifiable on CT. Other common indications for cisplatin treatment are testicular, bladder, ovarian and cervical cancer. Cisplatin imaging might be especially challenging for bladder cancer due to renal excretion and subsequent concentration of ^{195m}Pt-cisplatin in the bladder.

^{195m}Pt-cisplatin imaging showed a favourable toxicity profile in mice. As with cisplatin, the dose-limiting organ for ^{195m}Pt-cisplatin remains the kidneys. This study showed a spread in decrease of renal function in the animals receiving ^{195m}Pt-cisplatin. Furthermore, in the highest dosage group, two animals died, possibly due to administration of ^{195m}Pt-cisplatin. However, these studies in mice were performed with both a higher cisplatin dose / body weight and a higher activity / body weight compared to human studies: a therapeutic dose of cisplatin (6 mg/kg), which lies close to the maximal tolerated dose for the drug, was given. This was necessary to inject sufficient activity for imaging given the specific activity of ^{195m}Pt-cisplatin. The injected activity of 2-10 MBq of ^{195m}Pt-cisplatin (~65-330 MBq/kg) is higher than the 100 MBq previously administered in human subjects (~1.4 MBq/kg).[14] Previous studies in rats and humans did not note any renal toxicity due to radiolabeled cisplatin administration.[14-15]

Anti-tumour activity of ^{195m}Pt-cisplatin was compared to non-radioactive cisplatin in this study. The rationale behind this is the emission of auger electrons in near proximity of DNA, which causes DNA damage. Previous studies have shown an additive cytotoxic effect of radiolabeled cisplatin and other platinum compounds in cell lines.[16-17] The tumour mouse model utilized in this study did not show a difference in response between ^{195m}Pt-cisplatin and cisplatin. Since the tumour model lacked p53, an essential protein for DNA damage repair, these tumours are inherently sensitive to cisplatin treatment. Therefore, the additional effect of ^{195m}Pt-cisplatin might not be visible.

This study examined safety, efficacy, and tumour imaging of ^{195m}Pt-cisplatin. However, the scope of platinum imaging is much wider. Cisplatin is not the only platinum-based chemotherapeutic drug, other examples include carboplatin and oxaliplatin. Meanwhile, new platinum compounds and formulations of existing compounds are being developed and have entered the preclinical testing or clinical trials phase.[18] Platinum imaging is not limited to cisplatin and could be of value to research of both these traditional and novel platinum-based anti-cancer drugs.

CONCLUSION

^{195m}Pt-cisplatin imaging could provide a valuable tool for cisplatin treatment selection, especially for predicting treatment response or nephrotoxicity. This study shows that ^{195m}Pt-cisplatin SPECT imaging is feasible in mice with adequate image quality and a favourable toxicity profile. In the studied mouse model, ^{195m}Pt-cisplatin did not show improved efficacy over non-radioactive cisplatin for the treatment of cancer.

REFERENCES

1. Galluzzi L, Senovilla L, Vitale I, et al. Molecular mechanisms of cisplatin resistance. *Oncogene.* 2012;31:1869–83.
2. Rosenberg B, Vancamp L, Krigas T. Inhibition of cell division in escherichia coli by electrolysis products from a platinum electrode. *Nature.* 1965;13:698–9.
3. World Health Organization. WHO Model List of Essential Medicines. 2017.
4. Fennell DA, Summers Y, Cadranel J, et al. Cisplatin in the modern era: the backbone of first-line chemotherapy for non-small cell lung cancer. *Cancer Treat Rev.* 2016;44:42–50.
5. Yordanova A, Eppard E, Kürpig S, et al. Theranostics in nuclear medicine practice. *Onco Targets Ther.* 2017;10:4821–8.
6. Luster M, Clarke SE, Dietlein M, et al. Guidelines for radioiodine therapy of differentiated thyroid cancer. *Eur J Nucl Med Mol Imaging.* 2008;35:1941–59.
7. Zaknun JJ, Bodei L, Mueller-Brand J, et al. The joint IAEA, EANM, and SNMMI practical guidance on peptide receptor radionuclide therapy (PRRNT) in neuroendocrine tumours. *Eur J Nucl Med Mol Imaging.* 2013;40:800–16.
8. Buckley SE, Ali PA, Evans CJ, El-Sharkawi AM. Gamma camera scintigraphy of tumours using (195m) Pt-cisplatin. *Phys Med Biol.* 2006;51:1325–32.
9. Aalbersberg EA, de Wit-van der Veen BJ, Zwaagstra O, Codee-van der Schilden K, Vegt E, Vogel WV. Preclinical imaging characteristics and quantification of Platinum-195m SPECT. *Eur J Nucl Med Mol Imaging.* 2017;44:1347–54.
10. Knapp F, Dash A. Radiopharmaceuticals for therapy. 2016.
11. Areberg J, Norrgren K, Mattsson È. Absorbed doses to patients from ^{191}Pt-, ^{193m}Pt- and ^{195m}Pt-cisplatin. *Appl Radiat Isot.* 1999;51:581–6.
12. Hoeschele J, Butler T, Roberts J, Guyer C. Analysis and refinement of the microscale synthesis of the ^{195m}Pt-labeled antitumor drug, cis-Dichlorodiammineplatinum(II), cis-DDP. *Radiochim Acta.* 1982;31:27–36.
13. Zeevaart JR, Wagener J, Marjanovic-Painter B, et al. Production of high specific activity (195m)Pt-cisplatinum at South African Nuclear Energy Corporation for Phase 0 clinical trials in healthy individual subjects. *J Labelled Comp Radiopharm.* 2013;56:495–503.
14. Sathekge M, Wagener J, Smith S, et al. Biodistribution and dosimetry of ^{195m}Pt-cisplatin in normal volunteers. *Nuklearmedizin.* 2013;52:222–7.
15. Norrgren K, Sjölin M, Björkman S, et al. Comparative renal, hepatic, and bone marrow toxicity of Cisplatin and radioactive Cisplatin (^{191}Pt) in Wistar rats. *Cancer Biother Radiopharm.* 2006;21:528–34.
16. Areberg J, Johnsson A, Wennerberg J. In vitro toxicity of (191)Pt-labeled cisplatin to a human cervical carcinoma cell line (ME-180). *Int J Radiat Oncol Biol Phys.* 2000;46:1275–80.
17. Howell R, Kassis A, Adelstein S, et al. Radiotoxicity of platinum-195m-labeled trans-platinum (II) in mammalian cells. *Radiat Res.*1994;140:55–62.
18. Apps MG, Choi EHY, Wheate NJ. The state-of-play and future of platinum drugs. *Endocr Relat Cancer.* 2015;22:R219–33.


195mPt
IT
68GA
B+

Chapter 4

Pre-hydration in cisplatin-based CCRT: effects on tumour concentrations and treatment outcome

Else A. Aalbersberg
Maddalena M. Rossi
Linda J. de Wit-van der Veen
Iris Walraven
Michel M. van den Heuvel
Jan-Jakob Sonke
Jose S. Belderbos
Wouter V. Vogel

Radiother Oncol. 2019;134:30-36.

ABSTRACT

Aims: Pre-hydration is routinely applied to reduce nephrotoxicity in concurrent cisplatin-based chemo-radiotherapy (CCRT). However, pre-hydration may also have systemic effects, potentially leading to lower tumour cisplatin concentrations. We investigated the impact of pre-hydration on tumour cisplatin concentrations in mice, and on treatment outcomes in a clinical cohort study.

Materials and Methods: Four groups of 20 mice received either no pre-hydration prior to full-dose (6 mg/kg) or half-dose cisplatin, overnight dehydration prior to full-dose cisplatin (dehydration), or NaCl intraperitoneally prior to full-dose cisplatin (pre-hydration). Kidney function and tumour platinum concentration were measured. In patients, a retrospective study compared 2 historical NSCLC cohorts which received CCRT with daily cisplatin, with and without standard pre-hydration. Overall survival (OS) and progression free survival (PFS) were compared using Kaplan-Meier and cox-regression.

Results: Pre-hydration significantly decreased cisplatin tumour concentrations in mice, comparable to mice receiving half the dose. In 419 patients (211 without and 208 with pre-hydration) with median follow-up 22 months, there were no significant differences in PFS (18 vs. 15 months) or OS (23 vs. 23 months).

Conclusion: Pre-hydration reduces cisplatin tumour concentrations in mice, but it does not compromise treatment outcomes in NSCLC patients treated with daily cisplatin and radiotherapy.

INTRODUCTION

Concurrent chemo-radiotherapy (CCRT) is the current standard of care for patients with locally advanced non-small cell lung cancer (NSCLC). When compared to sequential chemoradiation, CCRT has been shown to lead to an OS of 5.7% after 3 years and 4.5% after 5 years, and to increase loco-regional control.[1] The type of chemotherapy used during CCRT does matter. In a recently published phase 3 trial in 200 patients two types of chemotherapy regimens were compared. It seemed that Carboplatin Taxol had a lower OS, and higher pulmonary toxicity compared to Cisplatin-Etoposide.[2]

The main drawback of adding cisplatin concurrent to radiotherapy is the increase of toxicities, such as radiation oesophagitis, nausea, and bone marrow depression.[1,3-4] In addition, the use of platinum-based chemotherapeutic drugs comes with significant risk of temporary or persistent renal toxicity, which is considered an important dose-limiting factor.[5] This toxicity is primarily caused by accumulation of cisplatin in the proximal tubules.[6]

One strategy to reduce the risk on cisplatin-induced renal toxicity is the application of hydration regimens, which has become standard of care for high-dose cisplatin administrations.[7] Other strategies are to reduce the dose of cisplatin per administration, while increasing the frequency of administrations to weekly or daily to achieve an adequate total dose or to use Carboplatin instead of Cisplatin.[8-9] Concurrent chemo-radiotherapy with daily low-dose cisplatin is generally well-tolerated, but about 20% of patients do not complete all of the 24 administrations due to toxicity.[10] Subsequently, efforts were made to mitigate renal toxicity by combining daily low-dose cisplatin with daily pre-hydration as standard practice for all chemoradiation NSCLC patients. This not only resulted in fewer patients being unable to complete the cisplatin administrations due to renal toxicity, but unexpectedly also reduced the grade ≥2 acute oesophageal toxicity from 62% to 34%.[11] This suggests that hydration not only has a local effect on the kidneys, but also a systemic effect. This led us to question whether pre-hydration could affect the kinetics of the cisplatin, with respect to normal tissues as well as in the tumour, and with potential consequences for treatment efficacy.

The aim of this study was to evaluate the impact of pre-hydration on tumour cisplatin concentrations and on treatment outcomes, by investigating its effects in (1) a pre-clinical in-vivo setting in mice and (2) in retrospective cohorts of NSCLC patients.

MATERIALS AND METHODS

Pre-clinical evaluation

Eighty female seven-week old FVB mice were transplanted with a BRCA1- and p53-deficient tumour in the fourth right mammary fat pad under isoflurane anaesthesia.[12] Rimadyl was given for pain relief during surgery and repeated after 24 hours. Tumour growth was evaluated 3x per week by calliper measurements. When the tumour diameter reached 10 mm, the mice were divided equally into 4 treatment groups (n=20): (1) free access to water followed by high-dose 6 mg/kg cisplatin iv (full-dose), (2) free access to water followed by 3 mg/kg cisplatin iv (half-dose), (3) overnight fasting from water followed by 6 mg/kg cisplatin iv (dehydration), and (4) free access to water followed by 1ml 0.9% NaCl intraperitoneally 1 hour prior to 6 mg/kg cisplatin iv (pre-hydration).

Renography

To evaluate renal toxicity scintigraphic renography was performed using ^{99m}Tc-MAG3, reflecting tubular function.[13] Five mice in each group underwent renography at 1, 24, 72, and 168 hours after cisplatin administration to determine the effect of cisplatin on kidney function at different time points. Mice were placed under anaesthesia with 1.5-2.5% isofluorane on the NanoSPECT (Mediso, Hungary). 30 MBq of ^{99m}Tc-MAG3 was injected in the tail vein. A dynamic scan was made for 30 minutes with 10 second time-frames using a parallel-hole collimator. Immediately after scanning the mice were sacrificed and the tumour was resected. The time to reach maximum tracer uptake in the kidney (T_{max}) and the time to reach clearance to 50% of the maximum tracer uptake ($T_{halfmax}$) were determined as measures for renal function.

Cisplatin tissue concentrations

Tumour platinum concentrations were determined through the nitric acid digestion method, as described by Siddik et al.[14] In short, 100 mg of tissue was dried overnight and dissolved in pure nitric acid (HNO_3). The nitric acid was subsequently evaporated through heating and the sample was diluted in 1M hydrochloric acid (HCl). Heating and evaporation were repeated and the sample was diluted in 0.1M HCl. Finally the samples were heated and evaporated and dissolved in a buffer solution containing 0.15M NaCl and 0.2M HCl. Platinum concentrations were measured with graphite furnace - atomic absorption spectrometry (SOLAAR MQZ Zeeman from Thermo Optek), GF95 graphite furnace and FS95/97 autosampler (Thermo Elemental).

Statistics for pre-clinical evaluations

Differences between groups in tumour concentrations and renal function were determined using median tests. Bonferroni correction was used to determine which groups differed significantly from each other. Analyses were performed in SPSS (v22.0.0.0, IBM Corporation). Graphs were plotted in GraphPad Prism (v7.03, GraphPad Software Inc.). $P<0.05$ was considered significant.

Clinical evaluation

Since tumour cisplatin concentrations are difficult to determine invasively in patients, a retrospective study was performed comparing 2 patient cohorts treated with and without standard pre-hydration. All patients with cytologically or histologically proven locally advanced NSCLC treated between 2007 to 2013 with concurrent daily-low dose cisplatin only and radiotherapy in our institute were included in this retrospective study. Patients treated between 2007-2010 did not receive standard pre-hydration (PH-); patients treated between 2011-2013 received daily 1 litre pre-hydration (PH+) before each Cisplatin administration. Approval from the ethics committee was not required for this retrospective study.

Cisplatin and saline administration

All patients were prescribed daily low-dose cisplatin (6mg/m^2 with a maximum of 12mg total) intravenously, administered 1-2 hours prior to radiotherapy as a bolus injection of 10ml. Patients in the PH- group only received pre-hydration when they demonstrated a ≥20% increase in serum creatinine during treatment. Patients in the PH+ group received standard pre-hydration from fraction 1 onwards. Serum creatinine (SC), urea (U) and glomerular filtration rate (GFR) were assessed prior to treatment and twice weekly during treatment in order to monitor dehydration and renal problems according to standard clinical protocol. Serum thrombocytes, leucocytes, Hb, sodium, potassium and magnesium were evaluated with the same frequency. Pre-hydration consisted of 1.0 litre of saline (0.9%) administered prior to cisplatin, with the exception of patients with a history of cardiac failure or the occurrence of the syndrome of anti-diuretic hormone secretion (SIADH), these patients received 0.5 litre of saline. For all patients, cisplatin was discontinued if SC increased by ≥30% from baseline or the GFR decreased to ≤60ml/min.[11]

Radiotherapy

All patients were prescribed a dose of 66Gy in 24 daily fractions (2.75Gy per fraction) with an overall treatment time of 32-34 days. Patients received contrast-enhanced planning 4DCT from which a mid-position 3D planning CT was derived with the tumour in its time-averaged position.[15] A recently acquired ^{18}F-FDG PET/CT scan was registered to the planning 3DCT to assist with tumour delineation. Gross tumour volume and pathological lymph nodes were delineated (GTV) and subsequently expanded with a margin of 12mm + ¼ tumour peak-to-peak amplitude for the tumour, and with 12mm for the lymph nodes, to provide the planning target volume (PTV). The planning CT was then also used to delineate the organs at risk and for dose calculation. A 7-8 field IMRT plan was generated using 6 or 10 MV photons (Pinnacle Radiation Oncology Systems, Milpitas, USA). All plans were generated with a physical dose constraint on the oesophagus of V35 <65%.[16] Patient setup correction was based on Cone beam CT (CBCT) for the first 3 fractions and then weekly thereafter until January 2012 then daily thereafter. Post treatment follow-up was performed according to standard clinical

protocol by either the radiation oncologist or the (referring) pulmonologist at 1, 3 and 6 weeks, then at 3 monthly intervals up to 2 years, twice a year in the following year, and then yearly. This involved toxicity scoring, chest X-ray and/or CT scans and blood tests. Survival was measured up to August 2016.

Statistics for clinical evaluations

Normal distribution of the data was tested, and in case of non-normality, data was categorized in quartiles. All data is presented as a percentage of the total; in case of normal distributed data as mean (± standard deviation), otherwise as median (interquartile range; IQR). Differences between the two groups were evaluated with either a t-test or chi-square test (for categorical variables). OS was calculated in months from the start of therapy to the date of the last follow-up (censored) or death from any cause. PFS was calculated from the start of treatment to the first recurrence or death from any cause, or last follow-up date (censored). Both PFS and OS were cut-off at 60 months to better compare the historical cohorts. Kaplan-Meier curves were plotted and differences in OS and PFS between the PH+ and PH- groups were assessed with cox regression analysis. Consequently, we tested the potential influencing effect of clinical characteristics that showed to be significantly different between the two groups at baseline, by adding them to the univariate model. When the variable changed the association between PH+ and OS/PFS >10% in hazard ratio (HR), the variable was kept in the model. All analyses were performed in SPSS (v22.0.0.0, IBM Corporation). Graphs were plotted in GraphPad Prism (v7.03, GraphPad Software Inc.). $P<0.05$ was considered significant.

RESULTS

Preclinical evaluation

Renal function in mice

The results of renal function evaluations are shown in Figure 1. The dehydration group showed highly variable but significant function loss at one hour after cisplatin administration: T_{max} was delayed to a median of 3.8 minutes (range up to 8.0 minutes) as compared to the other groups (full-dose 1.3, half-dose 1.3, pre-hydration 1.5 minutes). $T_{halfmax}$ was delayed to a median of 6.4 minutes (range up to 30 minutes) as compared to the other groups (full-dose 4.1, half-dose 5.0, pre-hydration 4.5 minutes), see figure 1b and 1c. Similar patterns were seen for dehydrated mice at evaluations up to 168 hours after administration of cisplatin, see figures 1d and e. This illustrates the ability of renography to detect renal toxicity, as expected to occur in dehydrated mice receiving 6 mg/kg cisplatin. This also shows that this animal model mimics the clinical situation in which renal failure after cisplatin can be prevented with hydration and that there is inter-individual variation.

In normal hydrated mice, renal toxicity occurred depending on the administered cisplatin dose and was variable among individual mice, and this was best detectable at 168 hours after administration: For 3 mg/kg cisplatin both median T_{max} and median $T_{halfmax}$ remained unaffected up to 168 hours. For 6 mg/kg cisplatin median T_{max} was 1.3 minutes at 1 hour (range up to 2.0 minutes) but increased in some of the animals leading to a median of 1.4 minutes after 168 hours but with a much higher range up to 9.2 minutes. Median $T_{halfmax}$ was 4.1 minutes at 1 hour (range up to 5.9 minutes) and increased to a median of 8.0 minutes after 168 hours (range up to 30.0 minutes). This confirms that cisplatin-induced nephrotoxicity is dose-dependent and develops in the course of days.

Pre-hydrated mice receiving 6 mg/kg cisplatin showed limited renal toxicity: T_{max} remained within normal range with a median of 1.5 minutes at 1 hour (range up to 2.0 minutes) and a median of 1.4 minutes after 168 hours (range up to 2.2 minutes). $T_{halfmax}$ remained within normal range with median 4.5 minutes at 1 hour (range up to 5.4 minutes), and showed a slight increase above the median of 6.0 minutes after 168 hours (range up to 12.5 minutes) but this is significantly less than the median 8.0 minutes (range up to 30 minutes) as reported in normally hydrated mice. This confirms that pre-hydration can protect against cisplatin-induced nephrotoxicity.

Tumour cisplatin concentrations in mice

Figure 2 shows the cisplatin concentrations in harvested tumour as measured at 1, 24, 72 and 168 hours after administration. Compared to normally hydrated mice (6 mg/kg), pre-hydrated mice demonstrated a significantly lower median cisplatin concentration in tumours at 1, 24, and 72 hours, but this difference was no longer present after 168 hours. Given the known renal function loss in this group, this illustrates that lower renal clearance of cisplatin leads to a higher accumulated dose in tumour in the clinically relevant window of the first hours after administration.

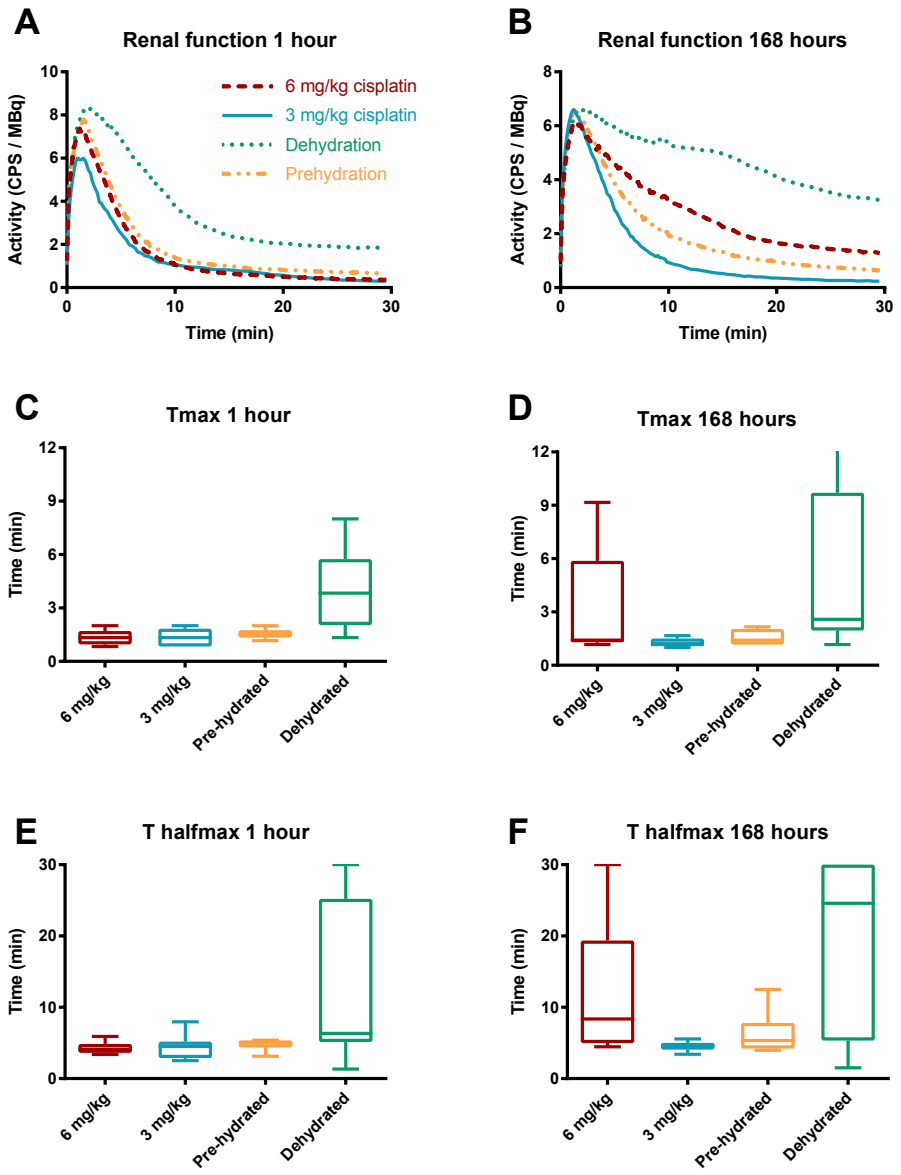

Figure 1. Renography results after administration of cisplatin. The first row (A and B) shows averaged renography for 5 mice at 1 and 168 hours post-injection of cisplatin. The time to reach the maximum uptake (Tmax) is quantified and shown in C and D. The time to reach the half of the maximum uptake (Thalfmax) is quantified and shown in E and F. 6 mg/kg = mice receiving a full-dose of 6 mg/kg cisplatin. 3 mg/kg = mice receiving a half-dose 3mg/kg of cisplatin. Pre-hydrated = mice pre-hydrated with 1ml of saline prior to a full dose of 6 mg/kg cisplatin. Dehydrated = mice dehydrated overnight prior to a full-dose 6 mg/kg cisplatin.

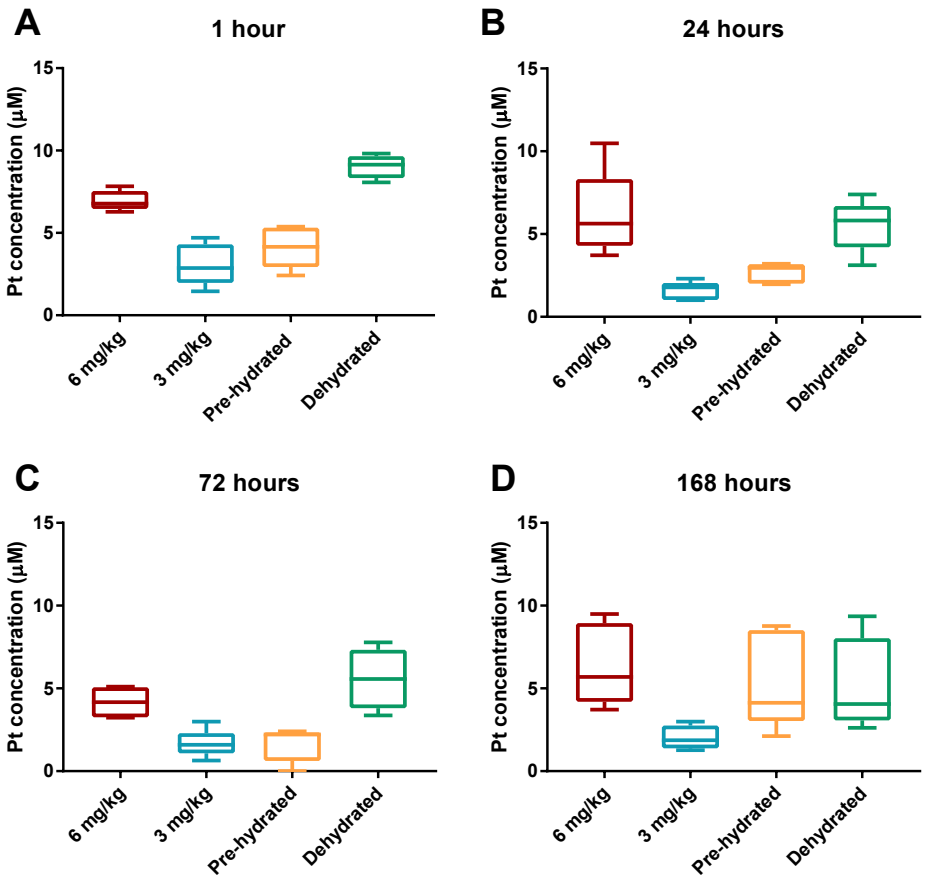

Figure 2. Tumour cisplatin concentrations 1 (A), 24 (B), 72 (C), and 168 (D) hours post-injection of cisplatin. 6 mg/kg = mice receiving a full-dose of 6 mg/kg cisplatin. 3 mg/kg = mice receiving a half-dose 3mg/kg of cisplatin. Pre-hydrated = mice pre-hydrated with 1ml of saline prior to a full dose of 6 mg/kg cisplatin. Dehydrated = mice dehydrated overnight prior to a full-dose 6 mg/kg cisplatin.

Normally hydrated mice showed cisplatin concentrations in tumour according to administered dose: Median 6.8 µM in the 6 mg/kg group versus 2.9 µM in the 3 mg/kg group, at one hour after administration. This difference remained significant 24 and 72 hours after administration. This illustrates the ability of the performed analysis to quantify tumour concentrations over time.

Pre-hydrated mice receiving 6 mg/kg cisplatin consistently showed significantly lower tumour concentrations as compared to normally hydrated mice receiving the same dose: 4.2 µM versus 6.8 µM at the clinically relevant time point of 1h after administration. The tumour concentrations of 4.2 µM achieved in the full-dose (6 mg/kg) normally hydrated group approached the 2.9 µM

achieved in the half-dose (3 mg/kg) normally hydrated group (difference not significant). This pattern remained similar until 168 hours after administration, although differences diminished over time and lost significance. This indicates that pre-hydration has systemic effects, and results in significantly lower cisplatin concentrations in tumour in the clinically relevant window of the first hours after administration.

Clinical evaluation

Patient cohort study

419 patients were included in the analysis, 211 in the PH- group and 208 in the PH+ group. The median follow-up for the whole cohort was 22 months, and for the PH- and PH+ groups 23 and 22 months respectively. Baseline and treatment characteristics are shown in Table 1. Patients treated in the PH- group had a poorer performance status (WHO 1-2 in 67.0% vs. 53.6%, p=0.006) compared to patients treated in the PH+ group. Furthermore, there was a difference in histological subtypes between the two groups (p=0.001). There was a higher percentage of patients in the PH- group who were unable to complete their cisplatin regimen, 30.4% vs. 12.6% in the PH+ group leading to a difference in number of cycles of cisplatin received (p<0.003). No other significant differences were found between the two groups.

Renal function in patients

Mean baseline GFR (94.78±23.02 vs. 97.77±23.30, p=0.22) and U (6.50±9.22 vs. 5.04±1.61, p=0.056) were similar in the PH- and PH+ groups, while baseline SC (73.60±16.03 vs. 69.51±15.94, p=0.006) was slightly increased in the PH- group. The maximum absolute decrease in GFR was significantly more in the PH- group (-22.96±20.67 vs. -11.97±13.21, p<0.001), and the maximum absolute increase in SC (25.74±70.41 vs. 9.17±10.57, p=0.001) and U (6.31±14.88 vs. 2.25±1.69, p<0.001) were significantly higher in the PH- group.

Survival analysis in patients

No significant differences were found in OS and PFS between the PH- and PH+ groups. Figure 3 shows the Kaplan-Meier curves for overall- and progression free survival, which were similar for PH- versus PH+ patients (23 vs. 23 months and 18 vs. 15 months, respectively). In univariate analysis, no association was found between pre-hydration and PFS (HR 1.021 CI 0.806-1.293) or OS (HR 0.935 0.741-1.180). Correction for potentially influencing factors performance status and histology did not significantly influence the association between pre-hydration and PFS and OS, whilst the number of cisplatin cycles changed the hazard ratio by 12%. However, the association between pre-hydration and PFS and OS remained insignificant (Table 2).

	Total Population	Group PH- 2007-2010	Group PH+ 2011-2013	p value
Number of patients	419	211	208	-
Mean age in years (IQR)	62.0 (54-70)	62.1 (55-70)	61.8 (54-69)	0.780
Gender (%)				0.902
Male	245 (58.5)	124 (58.8)	121 (58.2)	
Female	174 (41.5)	87 (41.2)	87 (41.8)	
Performance status[a] (%)				0.006 *
WHO 0	159 (39.5)	69 (33.0)	90 (46.4)	
WHO 1-2	244 (60.5)	140 (67.0)	104 (53.6)	
TNM (%)				0.203
1a – 2b	25 (6.0)	16 (7.6)	9 (4.4)	
3a	227 (54.6)	112 (53.3)	115 (55.8)	
3b	164 (39.4)	82 (39.1)	82 (39.8)	
Histology[b] (%)				0.001 *
AC	123 (31.5)	44 (23.3)	79 (39.3)	
SCC	123 (31.5)	65 (34.4)	58 (28.9)	
NSCLC NOS	112 (28.8)	68 (36.0)	44 (21.9)	
Other	32 (8.2)	12 (6.3)	20 (9.9)	
Metformin use (%)	32 (7.7)	17 (8.1)	15 (7.2)	0.734
Median GTV[c] in cc (IQR)	111 (65-207)	121 (74-204)	104 (57-212)	0.130
Median PTV[d] in cc (IQR)	566 (365-805)	576 (373-805)	526 (334-787)	0.776
FEV1[e] (IQR)	78 (64-93)	77 (60-91)	80 (66-93)	0.265
Median number of cisplatin cycles (IQR)	24 (24-24)	24 (20-24)	24 (24-24)	0.003 *
GFR baseline[f] (IQR)	97 (81-111)	95 (81-105)	98 (81-112)	0.203

Table 1. Patient characteristics of the total population and the groups receiving either no standard pre-hydration (PH-) or standard pre-hydration (PH+). Missing values (if N>10); [a]16, [b]29, [c]22, [d]185, [e]105, [f]87, TNM = TNM Classification of Malignant Tumours - 7th edition, AC = adenocarcinoma, SCC = squamous cell carcinoma, NSCLC NOS = non-small cell lung cancer not otherwise specified , GTV = gross tumour volume including lymph nodes, PTV = planning target volume, FEV1 = forced expiratory volume in 1 s, IQR = interquartile range. * indicates significant.

	PFS			OS		
	HR	CI	P value	HR	CI	P value
Pre-hydration	1.021	0.806-1.293	0.87	0.935	0.741-1.180	0.57
Pre-hydration + PS	1.020	0.800-1.299	0.88	0.925	0.728-1.177	0.53
Pre-hydration + histology	0.978	0.762-1.256	0.85	0.970	0.758-1.241	0.97
Pre-hydration + cisplatin cycles	1.071	0.836-1.371	0.59	1.044	0.819-1.331	0.73

Table 2. Hazard ratio and confidence interval for patients treated with standard pre-hydration (PH+) compared to patients without standard pre-hydration (PH-, reference). PS = performance status.

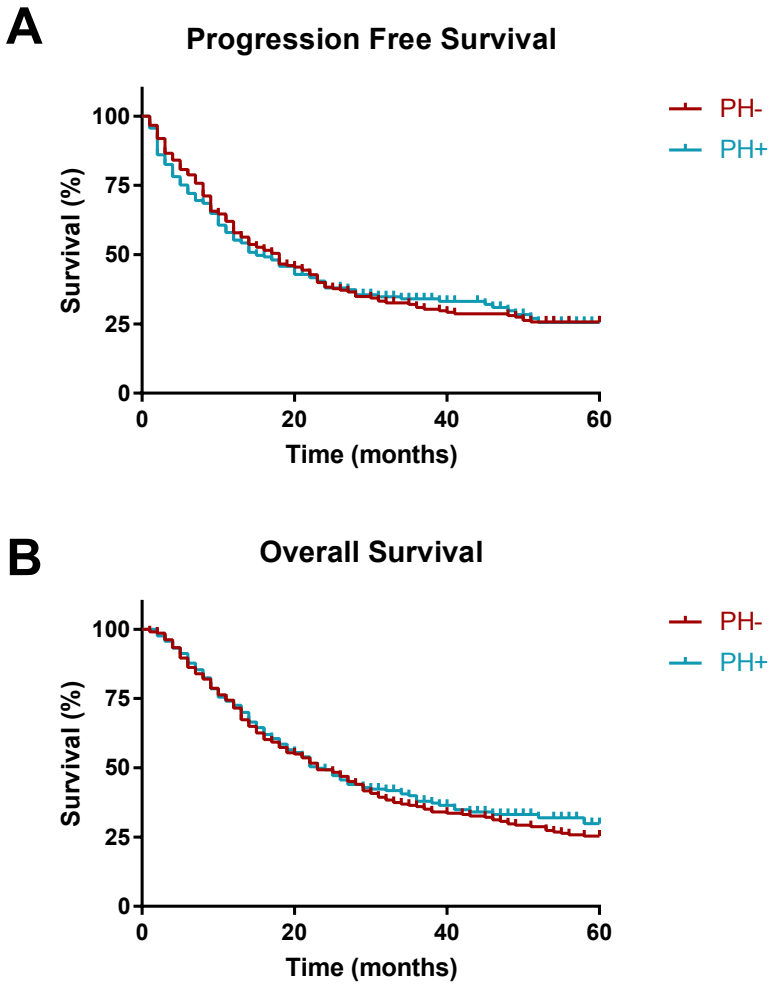

Figure 3. Kaplan-Meier curves for (A) progression free survival and (B) overall survival. PH- group receiving no standard pre-hydration (red line). PH+ group receiving standard pre-hydration (blue line).

DISCUSSION

We demonstrated for the first time that hydration prior to cisplatin administration in mice leads to significantly lower cisplatin concentrations in tumour up to 72 hours post administration, comparable to giving only half the cisplatin dose without pre-hydration. While the relationship between pre-hydration and the consequently altered plasma pharmacokinetics of cisplatin have been described previously in rats, to our knowledge no other studies have investigated the relationship between pre-hydration and tumour cisplatin concentrations or between pre-hydration and survival, either in pre-clinical or clinical research.[18-19]

Furthermore, we demonstrated for the first time in a clinical retrospective patient cohort that the administration of standard pre-hydration prior to daily cisplatin is not associated with reduced progression free or overall survival. There are several factors that can contribute to interpretation of these seemingly contradictory findings.

Pre-hydration

The results from the pre-clinical mouse study cannot be extrapolated directly to the patient cohort. In the animal study the maximum pre-hydration possible was given intraperitoneally prior to administration of one relatively high dose of cisplatin, whilst patients received rather modest pre-hydration with 1L of saline intravenously over 1 hour prior to daily low-dose cisplatin. Nonetheless, pre-clinical results should be considered indicative of a potential effect of pre-hydration on cisplatin concentrations in human tumours.

Many different hydration administration protocols exist, depending (amongst others) on tumour type, cisplatin dosing schedule, patient comorbidities, and logistics.[20] Stronger pre-hydration, e.g. 3-4L saline intravenous per 24 hours, is usually applied when renal function loss develops after high-dose cisplatin, or when limited pre-hydration provides insufficient protective effect.[7] It currently remains unknown whether such schemes can induce more extensive reductions in tumour cisplatin concentrations or can lead to measurable effects on treatment outcome parameters. The benefits of pre-hydration, however should not be disregarded. Pre-hydration is an effective strategy to prevent renal toxicity, as again demonstrated in this study with a reduced decrease in GFR and reduced increase in serum creatinine and urea. Patients in the cohort without standard pre-hydration would initiate the same pre-hydration scheme upon development of renal function loss. This will have diminished differences between the two groups.

Cisplatin concentrations

The animal model chosen in this study utilizes a one-time high dose of cisplatin. This model was chosen since this high-dose leads to measurable tumour cisplatin concentrations. The drawback is that this cannot be administered daily, comparable to the clinical situation. Although there are no indications that the pharmacokinetics of low-dose and high-dose cisplatin are different, the use of cumulative doses was not studied.

The question remains whether or not pre-hydration leads to altered cisplatin concentrations in tumour in patients. The pre-clinical study demonstrated that the pre-hydrated mice had lower tumour concentrations compared to dehydrated and normally hydrated mice receiving the same dose even up to a period of 168 hours, whereas the normal and dehydrated groups had renal function loss and therefore less cisplatin clearance resulting in a higher concentration in the tumour. Assuming these same processes occur in humans, this indicates that pre-hydration does have a systemic effect and that the concentration in the tumour is clinically relevant in the first hours after administration. This can only be evaluated directly in patients using invasive evaluations. Still, there are indirect indications that pre-hydration does lower cisplatin concentrations in tissues. With the addition of cisplatin to radiotherapy, many studies have demonstrated an increase in acute normal tissue toxicity.[21] We observed reductions in these toxicities with the introduction of standard-pre-hydration, most notably of oesophageal toxicity, which supports the concept of reduced accumulation of cisplatin in normal tissues.[11] Whether this will go together with similar reductions in tumour concentrations remains hypothetical.

Survival outcomes

The benefit of concurrent chemoradiotherapy (CCRT) over sequential chemoradiotherapy alone in overall survival has been estimated at 10% at two years in patients with NSCLC.[3] If pre-hydration would have a negative effect on this overall survival benefit, it would probably be small. In this study we did not see an effect on overall survival. In general, the patients evaluated in our cohorts demonstrated good treatment outcome (23 months), comparable to those receiving standard dose CCRT without cetuximab in the RTOG 0617 trial (24 months) and other trials.[17,22]

There were some significant differences between the 2 patient groups that may have diminished differences in treatment outcomes. The group treated without standard pre-hydration had a lower average performance score which is associated with poorer local control and OS.[23] Tumour histology and number of received cisplatin cycles were also significantly different. Although these factors by themselves did not affect the hazard ratio of hydration >10%, and were therefore not corrected for, together they could have compensated for a potential negative effect of pre-hydration on tumour cisplatin concentrations and treatment outcomes.

Since 2012, we have changed our image guidance protocol from weekly to daily cone beam CT based corrections. This may have allowed a slightly better tumour coverage in the second half of the group receiving standard pre-hydration, potentially also diminishing differences in treatment outcome.[24]

In summary, the presented pre-clinical evidence and clinical toxicity data support the hypothesis that pre-hydration reduces cisplatin concentrations in humans. This did not result in a detrimental effect on clinical outcome parameters of a detectable magnitude in the available retrospective cohorts treated with daily low-dose cisplatin and radiotherapy. It can however not be excluded that implementations of strong pre-hydration as performed in high-dose cisplatin may influence achieved tumour concentrations or treatment outcomes. This would need to be evaluated in prospective randomised clinical trials. However, as pre-hydration with daily low-dose cisplatin does not affect OS or PFS in this retrospective clinical study, we are continuing to use pre-hydration in our standard protocol due to its benefits for renal protection and patient treatment adherence.

CONCLUSION

Pre-hydration significantly decreases cisplatin tumour concentration in mice, comparable to administration of half a dose of cisplatin without pre-hydration. In a large cohort of patients with NSCLC treated with concurrent low-dose cisplatin and radiotherapy, pre-hydration appeared to have no detrimental effect on progression free- and overall survival.

REFERENCES

1. Auperin A, Le Pechoux C, Rolland E, et al. Meta-analysis of concomitant versus sequential radiochemotherapy in locally advanced non-small-cell lung cancer. *J Clin Oncol.* 2010;28:2181–90.
2. Liang J, Bi N, Wu S, et al. Etoposide and cisplatin versus paclitaxel and carboplatin with concurrent thoracic radiotherapy in unresectable stage III non-small cell lung cancer: a multicenter randomized phase III trial. *Ann Oncol.* 2017;28:777-783.
3. O'Rourke N, Roqué i Figuls M, Farré Bernadó N, Macbeth F. Concurrent chemoradiotherapy in non-small cell lung cancer. *Cochrane Database Syst Rev.* 2010;6:CD002140.
4. Koning CC, Wouterse SJ, Daams JG, Uitterhoeve LL, van den Heuvel MM, Belderbos JS. Toxicity of concurrent radiochemotherapy for locally advanced non-small-cell lung cancer: a systematic review of the literature. *Clin Lung Cacner.* 2013;14:481-7.
5. Dahal A, Bellows BK, Sonpavde G, et al. Incidence of severe nephrotoxicity with cisplatin based on renal function eligibility criteria: indirect comparison meta-analysis. *Am J Clin Oncol.* 2016;39:497-506.
6. Miller RP, Tadagavadi RK, Ramesh G, Reeves WB. Mechanisms of cisplatin nephrotoxicity. *Toxins (Basel).* 2010;2:2490-518.
7. Crona DJ, Faso A, Nishijima TF, McGraw KA, Galsky MD, Milowsky MI. A xystematic review of strategies to prevent cisplatin-induced nephrotoxicity. *Oncologist.* 2017;22:609-19.
8. Biedermann B, Landmann C, Kann R, et al. Combined chemoradiotherapy with daily low-dose cisplatin in locally advanced inoperable non-small cell lung cancer. *Radiother Oncol.* 2000;56:169-73.
9. Hazuka MB, Crowley JJ, Bunn PA Jr, O'Rourke M, Braun TJ, Livingston RB. Daily low-dose cisplatin plus concurrent high-dose thoracic irradiation in locally advanced unresectable non-small-cell lung cancer: results of a phase II Southwest Oncology Group study. *J Clin Oncol.* 1994;12:1814-20.
10. Uyterlinde W, Belderbos J, Baas C, et al. Prediction of acute toxicity grade ≥ 3 in patients with locally advanced non-small-cell lung cancer receiving intensity modulated radiotherapy and concurrent low-dose Cisplatin. *Clin Lung Cancer.* 2013;14:541-8.
11. Uyterlinde W, Chen C, Nijkamp J, et al. Treatment adherence in concurrent chemoradiation in patients with locally advanced non-small cell lung carcinoma: results of daily intravenous prehydration. *Radiother Oncol.* 2014;110:488-92.
12. Rottenberg S, Nygren AO, Pajic M, et al. Selective induction of chemotherapy resistance of mammary tumors in a conditional mouse model for hereditary breast cancer. *Proc Natl Acad Sci USA.* 2007;104;12117-22.
13. Szabo Z, Alachkar N, Xia J, Mathews W, Rabb H. Molecular imaging of the kidneys. *Semin Nucl Med.* 2011;41:20–8.
14. Siddik ZH, Boxall FE, Harrap KR. Flameless atomic absorption spectrophotometric determination of platinum in tissues solubilized in hyamine hydroxide. *Anal Biochem.* 1987;163:21–6.
15. Wolthaus JW, Schneider C, Sonke JJ, et al. Mid-ventilation CT scan construction from four-dimensional respiration-correlated CT scans for radiotherapy planning of lung cancer patients. *Int J Radiat Oncol Biol Phys.* 2006;65:1560-71.
16. Belderbos J, Heemsbergen W, Hoogeman M, Pengel K, Rossi M, Lebesque J. Acute esophageal toxicity in non-small cell lung cancer patients after high dose conformal radiotherapy. *Radiother Oncol.* 2005;75:157-64.

17. Walraven I, van den Heuvel M, van Diessen J, et al. Long-term follow-up of patients with locally advanced non-small cell lung cancer receiving concurrent hypofractionated chemoradiotherapy with or without cetuximab. *Radiother Oncol.* 2016;118:442-6.
18. Muggia FM, Rozencweig M, Penta J. Clinical implications of cisplatin pharmacology. *Recent Results Cancer Res.* 1980;74:132–8.
19. Litterst CL, LeRoy AF, Guarino AM. Disposition and distribution of platinum following parenteral administration of cis-dichlorodiammineplatinum(II) to animals. *Cancer Treat Rep.* 1979;63:1485–92.
20. Greystoke AP, Jodrell DI, Cheung M, Rivans I, Mackean MJ. How many cisplatin administration protocols does your department use? *Eur J Cancer Care.* 2010;19:80–90.
21. Uyterlinde W, Chen C, Kwint M, et al. Prognostic parameters for acute esophagus toxicity in intensity modulated radiotherapy and concurrent chemotherapy for locally advanced non-small cell lung cancer. Radiother Oncol. 2013;107:392-7.
22. Bradley JD, Paulus R, Komaki R, et al. Standard-dose versus high-dose conformal radiotherapy with concurrent and consolidation carboplatin plus paclitaxel with or without cetuximab for patients with stage IIIA or IIIB non-small-cell lung cancer (RTOG 0617): a randomised, two-by-two factorial phase 3 study. *Lancet Oncol.* 2015;16:187-99.
23. Werner-Wasik M, Swann RS, Bradley J, et al. Increasing tumor volume is predictive of poor overall and progression-free survival: secondary analysis of the Radiation Therapy Oncology Group 93-11 phase I-II radiation dose-escalation study in patients with inoperable non-small-cell lung cancer. *Int J Radiat Oncol Biol Phys.* 2008;70:385-90.
24. Kwint M, Conijn S, Schaake E, et al. Intra thoracic anatomical changes in lung cancer patients during the course of radiotherapy. *Radiother Oncol.* 2014;113:392-7.


195mPt
IT
68GA
B+

Chapter 5

A practical guide to production and PET/CT imaging of ^{68}Ga-DOTATATE for neuroendocrine tumors in daily clinical practice

Else A. Aalbersberg
Martine M. Geluk-Jonker
Chelvi Young-Mylvaganan
Linda J. de Wit-van der Veen
Marcel P.M. Stokkel

J Vis Exp. 2019 Apr 17;(146).

ABSTRACT

Neuroendocrine tumors are a rare form of cancer that arise from neuroendocrine cells and can present at almost any location throughout the body. Although heterogeneous in presentation, a common denominator among these tumors is the overexpression of somatostatin receptors. ^{68}Ga-DOTATATE is a somatostatin analogue labeled with the positron emitter gallium-68. For well-differentiated neuroendocrine tumors, ^{68}Ga-DOTATATE PET/CT imaging is used for diagnosis, determination of disease burden, and therapy selection.

This protocol details the radiolabeling of ^{68}Ga-DOTATATE, quality control, patient preparation, and subsequent PET/CT imaging. Radiolabeling of ^{68}Ga-DOTATATE is performed with a fully automated labeling module coupled to a ^{68}Ge/^{68}Ga generator. Quality control of the final product evaluates radiochemical purity with instant thin-layer chromatography and solid phase chromatography, and pH prior to patient injection. Periodical quality control is performed to determine ^{68}Ge breakthrough, sterility, and HEPES content. Patient preparation includes patient instructions, protocol for ^{68}Ga-DOTATATE during treatment with somatostatin analogues, and intravenous administration of the radiopharmaceutical. For PET/CT imaging the acquisition and reconstruction settings are described. For each step radiation safety will be highlighted, as well as time constrictions due to the short half-life of ^{68}Ga.

Fully automated in-house production and quality control of ^{68}Ga-DOTATATE leads to very high success rates (95%) and produces 2-4 patient dosages per batch depending on the yield of the generator.

In conclusion, ^{68}Ga-DOTATATE PET/CT imaging is a non-invasive and fast method providing information on tumor burden of NET while also assisting in diagnosis and therapy selection.

INTRODUCTION

Neuroendocrine tumors (NETs) are a heterogeneous group of tumors that arise from neuroendocrine cells. They can occur at almost any location in the body, but are most common in the gastro-intestinal tract, pancreas, and lung.[1] Although NET is a rare disease, the incidence in the United States is rising from 1.09 per 100000 persons in 1973 to 6.98 per 100000 persons in 2012.[2] For accurate diagnosis and staging of NET, ^{68}Ga-DOTATATE PET/CT is standard of care. This protocol describes the production and quality control of ^{68}Ga-DOTATATE as well as patient preparation and acquisition of PET/CT images.

Well-differentiated neuroendocrine tumors are characterized by an overexpression of somatostatin receptors. Somatostatin analogues that bind to this receptor can be labeled with a radioactive isotope to allow for nuclear medicine imaging. At first Iodine-123 was used with gamma camera imaging which was soon replaced by Indium-111 (^{111}In).[3-4] ^{111}In-octreotide scintigraphy was the golden standard for nuclear medicine NET imaging for over a decade.[5] Meanwhile, technical advances were made in positron emission tomography (PET), which has a higher sensitivity and resolution than gamma camera imaging. For NET, somatostatin analogues coupled to the positron emitter Gallium-68 (^{68}Ga) such as ^{68}Ga-DOTATATE were developed.[6]

^{68}Ga-somatostatin receptor (^{68}Ga-SRS) PET/CT is the current modality of choice in nuclear medicine imaging of well-differentiated neuroendocrine tumors. The superiority of ^{68}Ga-SRS PET/CT over ^{111}In-octreotide has been demonstrated in several studies.[7-8] The reported sensitivity and specificity lies around 90-95% and 85-100% respectively.[9-10] A meta-analysis has shown that ^{68}Ga-SRS PET/CT leads to a change is management in 44% of cases, even if preceded by ^{111}In-octreotide scintigraphy.[11] ^{68}Ga-SRS PET/CT is now recommended over ^{111}In-octreotide scintigraphy for NET imaging in guidelines and approved by the FDA and EMA.[12] A guideline for tumor imaging with ^{68}Ga-conjugated peptides is also available.[13]

This protocol details the radiolabeling of ^{68}Ga-DOTATATE, quality control conform the European Pharmacopoeia[14], patient preparation, and subsequent PET/CT imaging. Radiation safety and time constrictions due to the short half-life of ^{68}Ga are taken into account.

PROTOCOL

1. General radiation and radiopharmaceutical safety

1.1. Working with- and handling of radioactive materials should only be performed by trained personnel. The dose to hospital staff, patients and accompany persons should always be kept as low as reasonably achievable (ALARA).

1.2. Adhere to national laws, regulations, and guidelines regarding the preparation of radiopharmaceuticals such as Good Manufacturing Practice (GMP).

1.3. The following protocol is for ^{68}Ga-DOTATATE PET/CT imaging of adults only and is not suitable for children or pregnant women.

2. Preparations required prior to Labeling of ^{68}Ga-DOTATATE

2.1. Elute the ^{68}Germanium/^{68}Gallium (^{68}Ge/^{68}Ga) generator between 4 and 24 hours prior to the start of labeling of ^{68}Ga-DOTATATE according to the manufacturers specifications with hydrochloric acid (HCl).

3. Labeling of ^{68}Ga-DOTATATE

Note: The preparation for- and labeling of ^{68}Ga-DOTATATE takes 1½ hours, and should be started 2 hours prior to patient administration to allow for quality control.

Note: The labeling module should be placed in a lead shielding that can be closed during the labeling process to ensure radiation protection of personnel.

Note: If a registered kit is used, then the summary of product characteristics (SMPC) must be followed or cross-validated locally with the presented protocol.

3.1. Place the ^{68}Ga labeling kit on the labeling module according to the manufacturers specifications. Place the three manifolds on the corresponding module units. Attach the solutions provided in the ^{68}Ga labeling kit to the manifolds.

3.2. Prepare the final vial in a sterile environment such as a down flow unit or laminar flow cabinet.

3.2.1. Place a non-vented 0.22 µm filter underneath a vented 0.22 µm filter and attach the non-vented filter to a sterile needle (20G). Place the needle with the two filters attached in a 30 mL sterile vial.

3.2.2. Place a vented 0.2 µm bent filter with a needle (22G) in the same sterile vial as 3.2.1 to allow venting.

3.3. Attach the sterile vial with the non-vented filter to the output of the labeling module and place the vial in lead shielding sufficient for positron emitters.

3.4. Attach the output of the ^{68}Ga/^{68}Ge generator to the input of the labeling module.

3.5. Dissolve 50 µg of HA-DOTATATE (DOTA-3-iodo-Tyr3-octreotate) or 20 µg DOTATATE (DOTA-0-Tyr3-octreotate) peptide in 1.5 mL 1.5 M HEPES buffer solution provided in the kit and place in the reaction vial.

3.6. Close the lead shielding around the labeling module and start the production of ^{68}Ga-DOTATATE via the tablet attached to the labeling module.
3.7. Wait until the synthesis of ^{68}Ga-DOTATATE is finished (~36 minutes).
3.8. After labeling, remove the needles with filters from the glass vial and close the lead shielding around the vial.
3.9. Test the integrity of the non-vented 0.22 µm filter.
  3.9.1. Fill a syringe (10 mL) with air and place the syringe on top of the filter. Place the needle attached to the filter in a tube filled with water.
  3.9.2. Force the air through the filter and needle and determine when bubbles begin to form. The air should be compressed to <20% of the original volume.
3.10. Measure the activity of ^{68}Ga-DOTATATE produced by placing the vial in a dose calibrator and note the activity reference time (ART).
3.11. In a sterile environment such as a laminar flow cabinet remove 0.5 mL of ^{68}Ga-DOTATATE from the vial for quality control and prepare syringes for patient administration.

4. Quality control of ^{68}Ga-DOTATATE prior to patient administration

Note: The quality control of ^{68}Ga-DOTATATE takes 30 minutes, and should be started half an hour prior to patient administration.

Note: The described dilutions for stock solutions lead to <5% dead time in the measurement equipment. This can vary between different equipment and should be tested prior to performing quality control of ^{68}Ga-DOTATATE.

Note: Place the solution with ^{68}Ga-DOTATATE in lead shielding. In this protocol, the diluted solution do not have to be shielded due to the low levels of activity and short exposure time. However, a radiation risk assessment should be performed prior to performing quality control of ^{68}Ga-DOTATATE.

Note: The European Pharmacopoeia describes quality control of gallium edotreotide injection based on the following release criteria: appearance clear and colorless, pH 4.0-8.0, sterility, endotoxins < 175 IU per administered volume, ethanol < 10% v/v, radionuclide purity > 99.9% of total activity, radiochemical purity > 91% of total activity, absence of other impurities, HEPES < 200 µg per administered volume.[14] All tests have been evaluated during validation of the preparation method. For routine quality control a selected subset of tests (based on trend monitoring) is performed and described below. The solid phase extraction in this protocol has been cross-validated with- and obtains the same results as the high performance liquid chromatography method described in the European Pharmacopoeia. This was performed based on GMP (good manufacturing practice).

4.1. The following solutions can be prepared in advance:
  4.1.1. 1M ammonium acetate solution. Dissolve 3.9 g of ammonium acetate in 50 mL of water. The solution can be stored at room temperature up to 2 weeks.

4.1.2. 5 mM EDTA. Dissolve 0.1 g of EDTA in 50 mL of water. The solution can be stored at room temperature up to 1 year.

4.1.3. 50:50 Methanol / 1 M ammonium acetate. The solution can be stored at room temperature up to 24 hours.

4.2. Visual inspection

4.2.1. Inspect the final product to ensure that it is a colorless liquid without any particles.

4.3. pH

4.3.1. Measure the pH of the ^{68}Ga-DOTATATE solution with a pH indicator strip. The pH should lie between 6.5 and 7.5.

4.4. ^{68}Ga Colloids are measured through instant thin layer chromatography (ITLC)

4.4.1. Add 500 µl of water and 20 µl of ^{68}Ga-DOTATATE to prepare a stock solution and homogenize (GC) by carefully shaking the vial.

4.4.2. Cut a strip of ITLC-SG glass fiber paper at least 7 cm long and 1 cm wide.

Note: Only use clean ITLC-SG paper without damages. If the paper is damaged, the components traveling with the solvent can be hindered and the results will be inaccurate.

4.4.3. Add 5 µl of GC 1.5 cm from the bottom of the ITLC-SG paper and place in a tube containing 2 mL 50:50 Methanol / 1 M ammonium acetate. Ensure that the ^{68}Ga-DOTATATE does not come into contact with the liquid. Close the tubes to prevent evaporation.

4.4.4. Wait several minutes until the solvent has travelled at least 5 cm above where the ^{68}Ga-DOTATATE was applied. Cut the paper in half and place the bottom and upper halves in a separate tube (BH and UH).

4.4.5. Place UH and BH in a well counter and determine the number of counts in 30 seconds in each vial in the 400-600 keV energy window.

4.4.6. Perform 4.4.2 – 4.4.5 in *duplo*.

4.4.7. Perform a background measurement of the well counter and determine the number of counts in 30 seconds in the 400-600 keV energy window

4.4.8. Correct the counts in UH and BH to determine UH' and BH' for decay and background (determined in 4.4.7) to determine the number of counts at ART with the following formula, in which Δt is the time difference between the measured sample and ART in minutes.

$$Counts\ measured - counts\ background = Counts\ at\ ART * 0.5\text{^}(\frac{\Delta t}{68})$$

4.4.9. Calculate the amount of ^{68}Ga-colloids with the following formula, which should be less than 3%.

$$Colloids = \frac{\left(\frac{UH'1}{UH'1 + BH'1}\right) + \left(\frac{UH'2}{UH'2 + BH'2}\right)}{2} * 100\%$$

4.5. ^{68}Ga Ions are determined through column separation.

4.5.1. Make a stock solution by diluting 20 µL of ^{68}Ga-DOTATATE in 1 mL 5 mM EDTA.

4.5.2. Prepare a C-18 cartridge by slowly flushing it with 1 mL of 100% ethanol followed by 1 mL aqua.

4.5.3. Create a sample (S) by diluting 10 µL of the stock solution in 1 mL water and place in a well counter and determine the number of counts in 30 seconds in the 400-600 keV energy window.

4.5.4. Flush the sample slowly (5-10 mL/min) through the C-18 cartridge with a syringe, collect the remaining solution (C). Rinse the sample tube with 1 mL of water and flush this through the column in the collection tube.

4.5.5. Place the collecting tube, the empty sample tube (E), and the syringe (Sy) in a well counter and determine the number of counts in 30 seconds in each in the 400-600 keV energy window.

4.5.6. Perform 4.5.2 – 4.5.5 in *duplo*.

4.5.7. Correct the counts in C, S, E, and Sy to determine C', S', E' and Sy' for decay and background (determined in 4.4.7) to determine the number of counts at ART with the following formula, in which Δt is the time difference between the measured sample and ART in minutes.

$$Counts\ measured - counts\ background = Counts\ at\ ART * 0.5\text{^}(\frac{\Delta t}{68})$$

4.5.8. Calculate the ^{68}Ga ions with the following formula, which should be less than 2%.

$$Ions = \frac{\left(\frac{C'1}{S'1 - E'1 - Sy'1}\right) + \left(\frac{C'2}{S'2 - E'2 - Sy'2}\right)}{2} * 100\%$$

4.6. Radiopharmaceutical purity

4.6.1. Calculate the total amount of ^{68}Ga-DOTATATE with the following formula, which should be at least 91%.

$$Purity = (100 - colloids) * (\frac{100 - ions}{100})$$

5. Periodical quality control of ^{68}Ga-DOTATATE after patient administration.

Note: this should be performed > 48 hours after preparation of ^{68}Ga-DOTATATE to allow for the decay of ^{68}Ga.

5.1. The following solutions can be prepared in advance:

5.1.1. HEPES reference solution. Dissolve 20 mg HEPES in 50 mL aqua. The solution can be stored at room temperature up to 6 months. This is based on the maximum recommended HEPES dose of 200 µg per administered volume.

5.1.2. Water:Acetonitrile 25:75 v/v.

5.2. HEPES (weekly)

5.2.1. Transfer 3 µl of ^{68}Ga-DOTATATE solution in steps of 1 µl onto an ITLC-SG F_{254} paper of at least 8 cm. Use a blow dryer to dry the paper in between 1 µl applications.

5.2.2. Repeat 5.2.1 with the HEPES reference solution.

5.2.3. Place the strips in Water:Acetonitrile 25:75 solvent. Ensure that the applied solutions do not come into contact with the liquid.

5.2.4. Wait several minutes until the solvent has travelled at least 2/3 of the paper.

5.2.5. Develop the paper for at least 4 minutes in a closed chamber with iodine crystals.

5.2.6. Visually assess the outcome, a yellow spot should appear. The spot on the paper with ^{68}Ga-DOTATATE should be less intense than that of the reference solution.

5.3. ^{68}Ge breakthrough in the final product (monthly)

5.3.1. Prepare a sample with 200 µL of ^{68}Ga-DOTATATE solution (G). Place in a well counter and determine the number of counts in 30 seconds in each in the 400-600 keV energy window.

5.3.2. Repeat 5.3.1

5.3.3. Correct the counts in G to determine G' for decay to determine the number of counts at ART with the following formula, in which Δt is the time difference between the measured sample and ART in minutes.

$$Counts\ measured = Counts\ at\ ART * 0.5\text{^}(\frac{\Delta t}{68})$$

5.3.4. Calculate the ^{68}Ge breakthrough (MBq/MBq) with the following formula, which should be less than 0.001%.

$$Germanium\ breakthrough = \frac{G'1 + G'2}{S'1 + S'2} * 100\%$$

5.4. Sterility (monthly)

5.4.1. Add the remaining ^{68}Ga-DOTATATE solution to a tryptic soy broth (TSB) medium. Incubate for 14 days at 30-35 °C.

5.4.2. The TSB medium should be a clear liquid after the incubation period.

6. Patient preparation and administration of ^{68}Ga-DOTATATE

Note: The injected activity in this protocol provides good quality images with the PET/CT system available and the imaging protocol as described in part 7. With other imaging systems and protocols, the injected activity should be optimized.

6.1. The appointment and patient folder with information about ^{68}Ga-DOTATATE PET/CT is sent by mail to each patient. Every appointment is confirmed by telephone 1 day in advance.

6.2. Food and drinks are not restricted prior to ^{68}Ga-DOTATATE PET/CT imaging. Patients are advised to drink an extra 1 L of water in the two hours prior to imaging. It is also recommended to not bring children or pregnant women with them to the nuclear medicine department.

6.3. On the day of the ^{68}Ga-DOTATATE PET/CT, patients check in at the department of nuclear medicine 60 minutes prior the imaging. Take a short medical history.

6.4. Inquire about the date of the last somatostatin analogue administration. This is not a contraindication for ^{68}Ga-DOTATATE PET/CT, but should be noted.

6.5. Place an intravenous cannula in the arm and flush with saline to verify placement of the cannula.

6.6. Inject 100 MBq of ^{68}Ga-DOTATATE 45 minutes prior to PET/CT imaging.

7. PET/CT imaging

Note: acquisition and reconstruction parameters are vendor specific and should be adjusted and optimized for other PET/CT systems.

7.1. Place patient with the arms above the head on PET/CT. Instruct the patient to remain still throughout the exam.

7.2. Acquire a survey image and select the scan area from the pituitary gland to mid-thigh, unless otherwise specified due to clinical indications.

7.3. Perform a low-dose CT scan with 40 mAs, 140 keV, and 5 mm slices for attenuation correction and anatomical correlation.

7.4. Perform a PET scan with 2.5 minutes per bed position starting at the head of the patient.

7.5. Reconstruct the CT images with filtered back projection and 5 mm slices.

7.6. Reconstruct the PET images with BLOB-OS-TF with 3 iterations and 33 subsets with a voxel size of 4x4x4 mm.

7.7. Send all images to PACS.

REPRESENTATIVE RESULTS

Making use of an automated labeling system, 357 batches of ^{68}Ga-DOTATATE were produced between December 2014 and October 2018. Of the 357 produced, 17 batches failed and 340 batches were released, leading to an overall success rate of 95.2 %. Of the failed batches, 11 were caused by a technical failure whilst in 6 cases the produced ^{68}Ga-DOTATATE did not meet specifications. Figure 1 shows a flow chart of produced batches and the number of patient dosages produced. The average amount of ^{68}Ga-DOTATATE produced was 610±180 MBq. ^{68}Ga ions are on average 0.6±0.57 % and ^{68}Ga colloid are on average 1.37±0.69 % of the produced product. The radiopharmaceutical purity was on average 98.02±1.05 %.

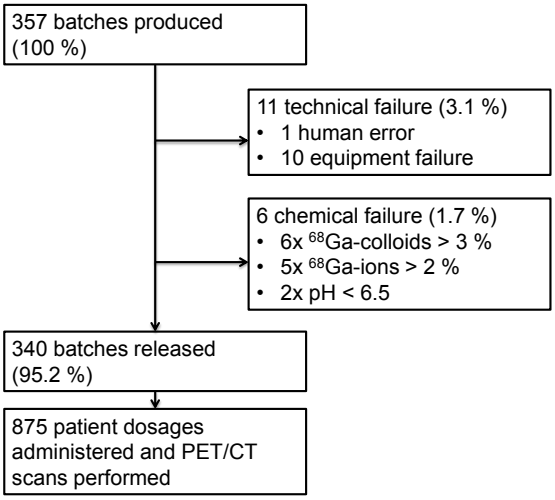

Figure 1. Flow chart of produced, failed, and released batches.

Figure 2 shows an ^{68}Ga-DOTATATE PET/CT scan without evidence of disease. Physiological uptake can be seen in the liver and spleen. ^{68}Ga-DOTATATE is excreted by the kidneys and is therefore visible in the urinary tract. Figure 3 shows a patient with a primary tumor in the pancreas.

In spite of careful preparations, not all acquired PET images are of optimal quality, of which two examples are given. Figure 4A shows an example of a patient with a lower dose ^{68}Ga-DOTATATE, due to a delay in the production of ^{68}Ga-DOTATATE which lead to less activity being present in the patient. This leads to more noisy images. Figure 4B shows an image with a motion artifact.

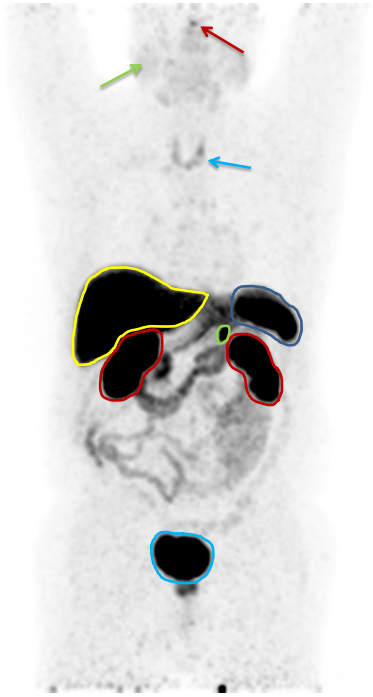

Arrows
Red: Pituitary gland
Blue: Thyroid gland
Green: Salivary glands

Delineations
Red: Kidneys
Dark blue: Spleen
Green: Adrenal gland
Yellow: Liver
Light Blue: Bladder

Figure 2. Maximum intensity projection of a representative ^{68}Ga-DOTATATE of a patient with no evidence of disease**.** High physiological uptake of ^{68}Ga-DOTATATE is seen in the liver (yellow delineation), spleen (dark blue delineation), and adrenal gland (green delineation). Uptake is the kidneys (red delineation) is due to both physiological uptake and excretion, while the uptake in the bladder (light blue) is due to excretion only. Moderate to low physiological uptake of ^{68}Ga-DOTATATE is seen in the pituitary gland (red arrow), thyroid gland (blue arrow), and salivary glands (green arrow).

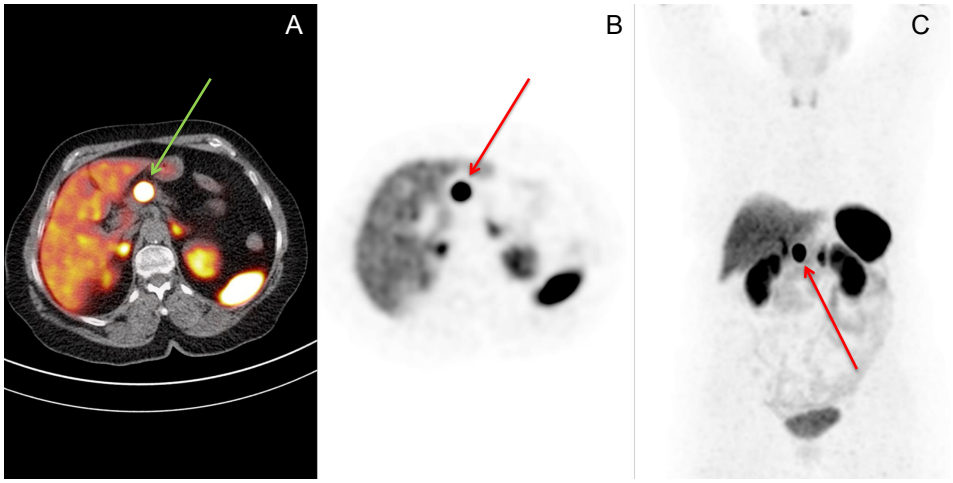

Figure 3. ^{68}Ga-DOTATATE PET/CT of a patient with a primary pancreatic neuroendocrine tumor. (A) Fused axial PET/CT image visualizing the primary pancreatic NET (green arrow). (B) Axial PET image visualizing the primary pancreatic NET (red arrow). (C) Coronal maximum intensity projection of the PET visualizing the primary pancreatic NET (red arrow).

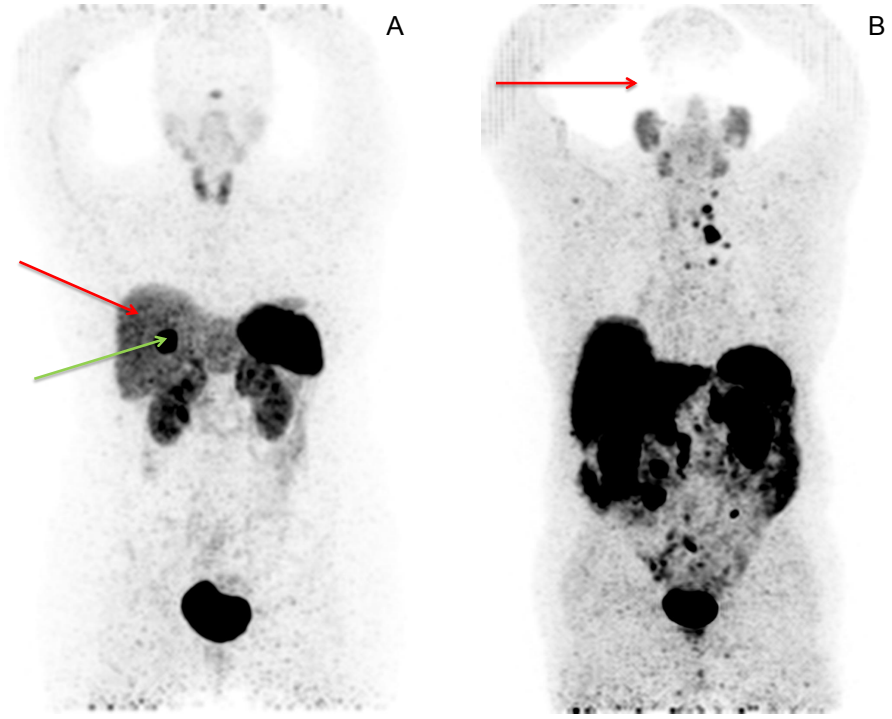

Figure 4. Examples of suboptimal ^{68}Ga-DOTATATE PET images. (A) Coronal maximum intensity projection a ^{68}Ga-DOTATATE PET in a patient that received only 42 MBq of ^{68}Ga-DOTATATE. More noise can be seen in the image, especially in the liver (red arrow). A liver metastases is still visible (green arrow). (B) Coronal maximum intensity projection a ^{68}Ga-DOTATATE PET with a motion artifact. Due to movement of the head between the PET and CT acquisitions, reconstruction of the PET images leads to this artifact.

DISCUSSION

This protocol describes production and subsequent PET/CT imaging of ^{68}Ga-DOTATATE. In order for efficient use of each produced batch of ^{68}Ga-DOTATATE, an optimal workflow with strict timing is required. Since the half-life of ^{68}Ga is 68 minutes, a relatively small time-delay of 15 minutes leads to a 15% loss of radioactivity. This requires active communication between the production facility, the personnel administrating the dose to the patient and the PET/CT technician. Also patients should be instructed that it is critical to meet the appointment time. Furthermore the number of patient dosages per batch is dependent on the ^{68}Ge/^{68}Ga generator size and age and will therefore decrease over time. A cost-benefit analysis can be performed to determine when the generator should be replaced.

Although the sensitivity and specificity of ^{68}Ga-DOTATATE for the detection of neuroendocrine tumors is high, several limitations should be considered. Firstly, when NET dedifferentiates and becomes more aggressive (grade 3 NET or neuroendocrine carcinoma) somatostatin receptor expression is often lost. Tumor lesions will therefore not be detected with ^{68}Ga-DOTATATE PET/CT. In these cases ^{18}F-FDG PET/CT, which visualizes glucose metabolism, is indicated. Secondly, ^{68}Ga-DOTATATE shows physiological uptake in the liver, which is also the organ in which metastases of NET are the most common. Liver uptake is peptide dependent, but the differences between peptides are small and not clinically relevant.[15-16] Visualization of smaller liver lesions with moderate somatostatin receptor expression will not be possible in all cases. When a clinical suspicion of liver lesions does exist with negative findings on ^{68}Ga-DOTATATE, dedicated CT or MR imaging of the liver is recommended. Thirdly, ^{68}Ga-DOTATATE imaging is limited by the resolution of the PET system which lies around 5 mm. Lesions smaller than 5 mm will only be detected if there is high uptake of ^{68}Ga-DOTATATE.

The use of long-acting somatostatin analogues prior to ^{68}Ga-SRS imaging has been controversial. The current guideline recommends discontinuation of long-acting somatostatin analogues 4-6 weeks prior to imaging for concerns of reduced uptake in tumor lesions.[13] However, a recent prospective intra-patient comparison demonstrated that the long-acting somatostatin analogue Lanreotide did not reduce tumor uptake of ^{68}Ga-DOTATATE but led to a slight increase in tumor-to-background ratios.[17] Serial ^{68}Ga-SRS PET/CT imaging performed under the same conditions, either with or without long-acting somatostatin analogues, will produce the most stable results.

^{68}Ga-somatostatin receptor imaging as described in this paper is performed with ^{68}Ga-DOTATATE, but other peptides such as ^{68}Ga-DOTATOC and ^{68}Ga-DOTANOC are also suitable. The three peptides show small differences in their affinity for the five different subtypes of the somatostatin receptor, but all have high specificity and sensitivity for NET. The choice of peptide should be made according to regulatory approval, cost, and availability.

In conclusion, ^{68}Ga-DOTATATE PET/CT imaging of neuroendocrine tumors has become standard of care. This protocol describes the production, quality control, and PET/CT imaging of ^{68}Ga-DOTATATE.

SUPPLEMENTAL DATA

Name of Material/ Equipment	Company	Catalog Number	Comments/Description
Acetonitrile	Biosolve	012007	> 99.9 %
Ammonium acetate	Merck	101116	≥ 98 %
Aqua / Water for injections	Braun		
Automated labeling system	Scintomics		GRP 3V
C-18 cartridge	Waters	WAT023501	Sep-Pak C18 Plus Light
Dose calibrator	Veenstra Instruments		
HA-DOTATATE	Scintomics	GRPC/R-000095	
EDTA	Merck	324503	
Ethanol	Sigma Aldrich	32221-M	≥ 99.8 %
Ga-68 labeling kit	ABX	SC-01	
Ge-68/Ga-68 generator	Eckert & Ziegler		
HCl 0.1M for elution	ABX	HCl-03	
HEPES	Sigma Aldrich	H3375	≥ 99.5 %
Iodine	Sigma Aldrich	207772	≥ 99.8 %, solid
ITLC-SG F254 plates	Merck	105735	TLC Silica gel 60 F254
ITLC-SG paper	Agilent	SGI0001	Glass fiber
Methanol	Sigma Aldrich	32213-M	≥ 99.8 %, Ph. Eur.
Millex-MP 0.22 um filter	Merck	SLMPL25SS	
PET/CT	Philips		Gemini TOF
pH indicator strips	Merck	109584	MColorpHast (pH2.0-9.0)
Tryptic soy broth medium	Biotrading	K111F010QK	
Well counter	Canberra		

Table S1. Materials and equipment used.

REFERENCES

1. Oronsky B, Ma P.C, Morgensztern D, Carter CA. Nothing but NET: a review of neuroendocrine tumors and carcinomas. *Neoplasia.* 2007;19:991-1002.
2. Dasari A, Shen C, Halperin D, et al. Trends in the incidence, prevalence, and survival outcomes in patients with neuroendocrine tumors in the United States. *JAMA Oncol*. 2017;3:1335-1342.
3. Krenning EP, Breeman W, Kooij P, et al. Localistion of endocrine-related tumours with radioiodinated analogue of somatostatin. *Lancet*. 1987;333:242-244.
4. Krenning EP, Kwekkeboom D, Bakker W, et al. Somatostatin receptor scintigraphy with [^{111}In-DTPA-D-Phe1]- and [^{123}I-Tyr3]-octreotide: the Rotterdam experience with more than 1000 patients. *Eur J Nucl Med*. 1993;20:716-731.
5. Balon HR, Goldsmith S, Siegel BA, et al. Procedure guideline for somatostatin receptor scintigraphy with (111)In-pentetreotide. *J Nucl Med*. 2001;42:1134-1138.
6. Kayani I, Bomanji JB, Groves A, et al. Functional imaging of neuroendocrine tumors with combined PET/CT using ^{68}Ga-DOTATATE (Dota-$_D$Phe^1,Tyr^3-octreotate) and ^{18}F-FDG. *Cancer*. 2008;112**:**2447-2455.
7. Hofman MS, Kong G, Neels OC, Hong E, Hicks RJ. High management impact of Ga-68 DOTATATE (GaTate) PET/CT for imaging neuroendocrine and other somatostatin expressing tumours. *J Med Imaging Radiat Oncol*. 2012;56:40-47.
8. Srirajaskanthan R, Kayani I, Quigley AM, Soh J, Caplin ME, Bomanji J. The role of ^{68}Ga-DOTATATE PET in patients with neuroendocrine tumors and negative or equivocal findings on ^{111}In-DTPA-octreotide scintigraphy. *J Nucl Med*. **51** (6), 875-882 (2010).
9. Deppen SA, Blume J, Bobbey AJ, et al. ^{68}Ga-DOTATATE compared with ^{111}In-DTPA-octreotide and conventional imaging for pulmonary and gastroenteropancreatic neuroendocrine tumors: a systematic review and meta-analysis. *J Nucl Med*. 2016;57:872-878.
10. Yang J, Kan Y, Ge BH, Yuan L, Li C, Zhao W. Diagnostic role of Gallium-68 DOTATOC and Gallium-68 DOTATATE PET in patients with neuroendocrine tumors: a meta-analysis. *Acta Radiol*. 2014;55:389-398.
11. Barrio M, Czernin J, Fanti S, et al. The impact of somatostatin receptor-directed PET/CT on the management of patients with neuroendocrine tumor: a systematic review and meta-analysis. *J Nucl Med.* 2017;58:756-761.
12. Strosberg JR, Halfdanarson TR, Bellizzi AM, et al. The north American neuroendocrine tumor society consensus guidelines for surveillance and medical management of midgut neuroendocrine tumors. *Pancreas*. 2017;46:707-714.
13. Virgolini I, Ambrosini V, Bomanji JB, et al. Procedure guidelines for PET/CT tumour imaging with ^{68}Ga-DOTA-conjugated peptides: ^{68}Ga-DOTA-TOC, ^{68}Ga-DOTA-NOC, ^{68}Ga-DOTA-TATE. *Eur J Nucl Med Mol Imaging*. 2010;67:2004-2010.
14. European Pharmacopoeia, vol 9. Monograph 01/2013:2482 Gallium (^{68}Ga) edotreotide injection.
15. Brogsitter C, Zöphel K, Hartmann H, Schottelius M, Wester HJ, Kotzerke J. Twins in spirit part II: DOTATATE and high-affinity DOTATATE - the clinical experience. *Eur J Nucl Med Mol Imaging*. 2014;41:1158-1165.
16. Sandström M, Velikyan I, Garske-Román U, et al. Comparative biodistribution and radiation dosimetry of ^{68}Ga-DOTATOC and ^{68}Ga-DOTATATE in patients with neuroendocrine tumors. *J Nucl Med*. 2013;54**:**1755-1759.
17. Aalbersberg EA, de Wit-van der Veen BJ, Versleijen MWJ, et al. Influence of lanreotide on uptake of ^{68}Ga-DOTATATE in patients with neuroendocrine tumours: a prospective intra-patient evaluation. *Eur J Nucl Med Mol Imaging*. 2019;46:696-703.


195mPt
IT
68GA
B+

Chapter 6

Differences in uptake between ^{68}Ga-DOTATATE and ^{68}Ga-HA-DOTATATE: a retrospective study in 342 patients

Else A. Aalbersberg
Linda J. de Wit-van der Veen
Martine M. Geluk-Jonker
Lisanne R. Bonsen
Marcel PM. Stokkel

Submitted and under review.

ABSTRACT

Background: Neuroendocrine tumours (over)express the somatostatin receptor (SSTR). Somatostatin analogues are used for the detection of NETs with PET/CT when attached to a radioactive isotope. Different ^{68}Ga-conjugated peptides have been developed.

Aim: To retrospectively evaluate the distribution of ^{68}Ga-DOTATATE and ^{68}Ga-HA-DOTATATE in an independent patient population.

Methods: Patients with a ^{68}Ga-DOTATATE or ^{68}Ga-HA-DOTATATE PET/CT scan acquired were included. SUVmax and SUVpeak were determined in a volume of interest in both normal organ tissue (liver, spleen, kidney, aorta, and adrenal, pituitary, and thyroid glands) and tumour lesions.

Results: 342 scans were available, 110 with ^{68}Ga-DOTATATE and 232 with ^{68}Ga-HA-DOTATATE. SUVmax and SUVpeak were significantly increased in most normal organs after injection of ^{68}Ga-HA-DOTATATE compared to ^{68}Ga-DOTATATE. In tumour lesions the uptake of ^{68}Ga-HA-DOTATATE was increased in metastases in the liver, bone, and other organs, but not in the primary tumour or metastases in the abdomen or lymph nodes. Tumour-to-liver ratio remained the same.

Conclusion: ^{68}Ga-HA-DOTATATE and ^{68}Ga-DOTATATE have a different distribution in vivo in contrary to previously published reports. Uptake of ^{68}Ga-HA-DOTATATE is significantly increased in most organs, but only at some tumour sites. This difference should be taken into account when choosing a peptide for somatostatin imaging or treatment.

INTRODUCTION

Neuroendocrine tumours (NETs) is a group of tumours that arise from neuroendocrine cells. Primary tumours can originate almost anywhere in the body, but the most common sites are in the pancreas and gastrointestinal tract.[1] Although NETs is a heterogeneous group of tumours, one of the common characteristics shared in these tumours is the (over)expression of the somatostatin receptor (SSTR), especially subtype 2. The expression of SSTRs is higher in well-differentiated tumours than in poorly differentiated tumours.[2] This has led to the development of somatostatin analogues (SSAs) such as octreotide and lanreotide for the treatment of NETs.[3]

SSAs are not only used for symptom relief or treatment, they can be used for the detection of NETs when attached to a radioactive isotope. Due to the variability in anatomical location and small size of the tumours, it has proven to be difficult to localize lesions with traditional anatomical imaging such as computed tomography (CT) or magnetic resonance imaging (MRI). Therefore, molecular nuclear imaging has been used in NETs for decades. Originally SSAs were labelled with Indium-111 for detection with single photon emission computed tomography (SPECT). The use of Gallium-68 (^{68}Ga) and positron emission tomography (PET) has increased the sensitivity and specificity for the detection of NETs.[4] Different ^{68}Ga-conjugated peptides have been developed over the past years, the most common being DOTATATE, DOTATOC, and DOTANOC which all bind predominantly to the SSTR2.[5] Though differences in binding affinities to the SSTR are previously described, no evidence of a profound clinical impact has been reported.

Originally, ^{68}Ga-DOTATATE (^{68}Ga-DOTA-Tyr3-octreotate) was developed, but its use was restricted since 2012 by patents (Mallinckrodt Pharmaceuticals). Therefore, high affinity DOTATATE or ^{68}Ga-HA-DOTATATE (^{68}Ga-DOTA-3- iodo-Tyr3-octreotate) was designed.[6] In four related articles produced by the group of Wester, the similarities between ^{68}Ga-DOTATATE and ^{68}Ga-HA-DOTATATE were investigated. A preclinical study in cells and tumour-bearing mice demonstrated that receptor affinity for SSTR2 between the two agents was similar, but ^{68}Ga-HA-DOTATATE showed slightly higher uptake in background tissues and tumour in animals leading to comparable tumour-to-background ratios.[7] The first human pilot study in one patient showed somewhat better visual results of liver metastasis with ^{68}Ga-HA-DOTATATE.[6] In the following cohort of 23 consecutive patients the difference between ^{68}Ga-DOTATATE and ^{68}Ga-HA-DOTATATE was analysed retrospectively. Background uptake was similar in liver, kidney, and spleen, but in the pituitary gland the uptake of ^{68}Ga-HA-DOTATATE was somewhat higher. No differences were found in tumour uptake at different metastatic sites.[8] Finally, the dosimetry of ^{68}Ga-HA-DOTATATE was evaluated and it was comparable to other ^{68}Ga-labelled somatostatin analogues.[9]

Up to now, all data comparing ^{68}Ga-DOTATATE with ^{68}Ga-HA-DOTATATE have been produced by one group and is based on a small cohort. To provide a more substantiated comparison, we performed a retrospective evaluation of the distribution of ^{68}Ga-DOTATATE and ^{68}Ga-HA-DOTATATE in a larger independent patient population due to the clinical suspicion that the biodistribution might not be the same.

MATERIALS AND METHODS

Radiosynthesis and quality control

^{68}Ga-DOTATATE was prepared with an in-house designed semi-automatic labelling system. The ^{68}Ge/^{68}Ga generator (iThemba Labs, IDB Holland, the Netherlands) is eluted with hydrochloric acid (HCl) and purified for ^{68}Ga ions by anion exchange chromatography. The ^{68}Ga ions are eluted with water and added to 30 µg DOTATATE (Bachem, Switzerland) dissolved in HCl and acetate buffer solution in a reaction vial. The reaction vial is heated to 90°C for 5 minutes. After cooling, the solution in the vial is diluted with NaCl and filtered through a 0.2 µm filter in a sterile vial.

^{68}Ga-HA-DOTATATE was prepared with a fully automated labelling system (Scintomics GmbH, Germany) and a sterile single-use cassette (ABX GmbH, Germany) was used for each labelling. In short, the ^{68}Ge/^{68}Ga generator (iThemba Labs, IDB Holland, the Netherlands) is eluted and purified for ^{68}Ga ions by a cation exchange cartridge. The eluate is added to 20 µg HA-DOTATATE (ABX, Germany) and heated to 100°C for 10 minutes. The remaining ^{68}Ga (III) ions are removed by a C18 exchange cartridge and the final ^{68}Ga-DOTATATE is diluted in PBS and filtered to ensure sterility.

Before patient administration for both ^{68}Ga-HA-DOTATATE and ^{68}Ga-DOTATATE the radiochemical purity was determined by instant thin-layer chromatography and solid phase chromatography.

Patient selection

All whole-body ^{68}Ga-DOTATATE and ^{68}Ga-HA-DOTATATE PET/CT scans acquired between August 2011 and April 2016 were retrospectively evaluated. To rule out any bias due to protocol violations, scans that did not meet protocol standards of acquisition 45±10 minutes post-injection were excluded. Somatostatin analogues were discontinued prior the imaging according to the guidelines.[5]

Image acquisition and analysis

80-100 MBq of ^{68}Ga-HA-DOTATATE or ^{68}Ga -DOTATATE was administered intravenously. PET scans were acquired approximately 45 minutes post-injection from top to mid-thigh for 2-2.5 minutes per bed position on a Gemini TF PET/CT (Philips, the Netherlands). A low-dose CT scan was acquired for attenuation correction and anatomical correlation.

Image analysis was performed in Osirix v7.0.3 (Pixmeo Sarl, Switzerland). Body-weight corrected SUVmax and SUVpeak were determined in a volume of interest (VOI) placed in both normal organ- and tumour tissue. A spherical VOI with a diameter of 2 cm was placed

in the central part of the normal liver parenchyma, to minimize partial volume effects due to breathing. In the spleen, a spherical VOI with a diameter of 1 cm was placed in the centre. For the kidney, a spherical VOI was drawn around the caudal half of the left kidney. To measure the blood pool, a spherical VOI with a diameter of 1 cm was placed in the aortic arch. For the pituitary gland, left adrenal gland, thyroid gland, left parotid gland, a VOI was place over the entire organ based on fused PET/CT images. For tumour measurements, SUV was determined only in the lesion with the highest uptake in 7 categories: primary tumour or metastasis in liver, bone, lung, abdomen (including lymph nodes), lymph nodes (not in the abdomen), and other. Tumour-to-background ratios were calculated using the liver as background organ.[10]

Statistics

To determine the difference in uptake in healthy organ uptake between ^{68}Ga-DOTATATE and ^{68}Ga-HA-DOTATATE, two analyses were performed. For unpaired analysis of organ data (analysis 1), all selected scans were included. For paired analysis of organ data (analysis 2), all patients with both a ^{68}Ga-DOTATATE and ^{68}Ga-HA-DOTATATE PET/CT were included. To determine the difference in tumour uptake between ^{68}Ga-DOTATATE and ^{68}Ga-HA-DOTATATE only the first available scan of each unique patient was included to rule out skewing of the data due tumour treatment or progression. Unpaired analyses were performed for tumour uptake (analysis 3) and tumour-to-liver ratio (analysis 4).

An independent-samples T-test was used to determine the difference in uptake between the cohorts imaged with ^{68}Ga-HA-DOTATATE and ^{68}Ga-DOTATATE (analysis 1, 3 and 4). A paired-samples T-test was used for the analysis of patients who had both ^{68}Ga-HA-DOTATATE and ^{68}Ga-DOTATATE PET/CT (analysis 2). Statistical analysis was performed in SPSS Statistic (v22, IBM, United States) and graphs were produced in Prism (v7.02, GraphPad Software Inc., United States).

RESULTS

Patient selection

444 ^{68}Ga-DOTATATE and ^{68}Ga-HA-DOTATATE PET/CT scans were performed between August 2011 and April 2016 (see figure 1). Ninety-nine scans did not meet the inclusion criteria of being acquired 45 ± 10 minutes post-injection, two scans were excluded for incorrect patient weight data, and one scan was excluded due to reconstruction errors. This resulted in 342 PET/CT scans available for the cohort-based normal organ tissue analysis, 110 scans after injection of ^{68}Ga-DOTATATE and 232 scans after injection of ^{68}Ga-HA-DOTATATE. Characteristics of both groups are shown in Table 1. 41 patients received both ^{68}Ga-DOTATATE and ^{68}Ga-HA-DOTATATE; these scans were available for a patient-based paired analysis of normal organ distribution of both radiopharmaceuticals.

For tumour measurements, 97 scans were follow-up scans of patients already in the dataset and subsequently excluded. Of the 245 remaining PET scans, 158 patients had at least one measurable neuroendocrine tumour lesion, 64 with ^{68}Ga-DOTATATE and 94 with ^{68}Ga-HA-DOTATATE.

Normal organ tissue in all patients (analysis 1)

SUVmax was significantly increased with ^{68}Ga-HA-DOTATATE compared to ^{68}Ga-DOTATATE in the liver (11.83 vs. 8.14 p=0.000), spleen (28.96 vs. 19.27 p=0.000), kidney (17.93 vs. 14.06 p=0.000), adrenal gland (17.45 vs. 12.19 p=0.000), pituitary gland (6.62 vs. 4.79 p=0.000), and thyroid gland (5.47 vs. 3.88 p=0.000). There was no difference in the SUVmax of the parotid gland (3.98 vs. 3.65 p=0.082). In the blood pool measured in the aorta, the SUVmax was lower with ^{68}Ga-HA-DOTATATE (1.34 vs. 1.73 p=0.000). The same pattern was seen for ^{68}Ga-HA-DOTATATE compared to ^{68}Ga-DOTATATE when measured as SUVpeak in all organs; liver (10.19 vs. 6.77 p=0.000), spleen (26.19 vs. 17.35 p=0.000), kidney (13.92 vs. 11.11 p=0.000), adrenal gland (11.80 vs. 8.37 p=0.000), pituitary gland (3.64 vs. 2.73 p=0.000), thyroid gland (3.93 vs. 2.82 p=0.000), parotid gland (3.12 vs. 2.84 p=0.0^{68}), and aorta (0.98 vs. 1.25 p=0.000). These results of SUVmax and SUVpeak can be seen in Figure 2A-B.

Paired normal organ tissue in 41 patients (analysis 2)

The median time between the HA-DOTATATE and DOTATATE PET/CT scans was 25 months (range 8-41 months). Uptake of ^{68}Ga-HA-DOTATATE was significantly higher than ^{68}Ga-DOTATATE in liver (SUVmax 11.61 vs. 8.08 p=0.000, SUVpeak 9.91 vs. 6.80 p=0.000), spleen (SUVmax 29.21 vs. 18.85 p=0.000, SUVpeak 26.51 vs. 16.76 p=0.000), kidney (SUVmax 17.80 vs. 13.60 p= 0.046, SUVpeak 13.96 vs. 10.^{68} p=0.092), adrenal gland (SUVmax 18.57 vs. 12.65 p=0.004, SUVpeak 12.24 vs. 8.57 p=0.004), pituitary gland (SUVmax 6.71 vs. 4.57 p=0.004, SUVpeak 3.79 vs. 2.62 p=0.002), and thyroid gland (SUVmax 5.62 vs. 3.80

p=0.000, SUVpeak 4.05 vs. 2.75 p=0.000). In the aorta the uptake of ^{68}Ga-HA-DOTATATE was significantly lower than ^{68}Ga-DOTATATE (SUVmax 1.48 vs. 1.69 p=0.009, SUVpeak 1.25 vs. 1.09 p=0.081). The results are shown in Figure 2C-D. An example of a patient with both scans is shown in Figure 3.

	^{68}Ga-DOTATATE (n=110)	^{68}Ga-HA-DOTATATE (n=232)
Sex		
Male	51 (46.4%)	110 (47.2%)
Female	59 (53.6%)	122
Age (years)	62.3	61.8
Location Primary NET		
Small bowel	42	99
Unknown primary	10	38
Pancreas	11	31
Lung	8	13
Appendix	7	2
Colon + rectum	5	20
Stomach	3	7
Other NET	2	6
Data not available	20	11
Other than NET	2	5
Grade NET		
1	53	98
2	17	72
3	0	1
Unknown / not NET	40	61
Injected activity (MBq)	89.2 ± 21.9	88.8 ± 13.4
Time post-injection (min)	44.5 ± 6.1	44.7 ± 5.6

Table 1. Patient characteristics of the 332 patients included for analysis. If applicable, data are shown as mean ± range. NET = Neuroendocrine tumour, MBq = Mega Becquerel.

Tumour tissue (analysis 3)

SUVmax was significantly higher with ^{68}Ga-HA-DOTATATE compared to ^{68}Ga-DOTATATE in the metastasis in the liver (34.71 vs. 24.59 p=0.006), bone (26.51 vs. 11.83 p=0.005), and other organs (19.36 vs. 10.59 p=0.018) but no difference was seen in the primary tumour (26.98 vs. 21.59 p=0.248) or in metastases in the abdomen (24.^{68} vs. 17.93 p=0.069) and lymph nodes (20.51 vs. 17.80 p=0.473). For SUVpeak, again a similar pattern was seen; ^{68}Ga-HA-DOTATATE uptake was higher in metastases in the liver (27.17 vs. 19.19 p=0.011), bone (10.^{68} vs. 6.60 p=0.003), abdomen (18.01 vs. 11.50 p=0.026) and other organs (13.06 vs. 6.56 p=0.022), but not in the primary tumour (18.27 vs. 15.86 p=0.454) or metastases in lymph nodes (13.76 vs. 12.35 p=0.616). Due to the presence of only seven lung lesions in total, these lesions were excluded from all analyses. The results can be seen in Figure 2E-F.

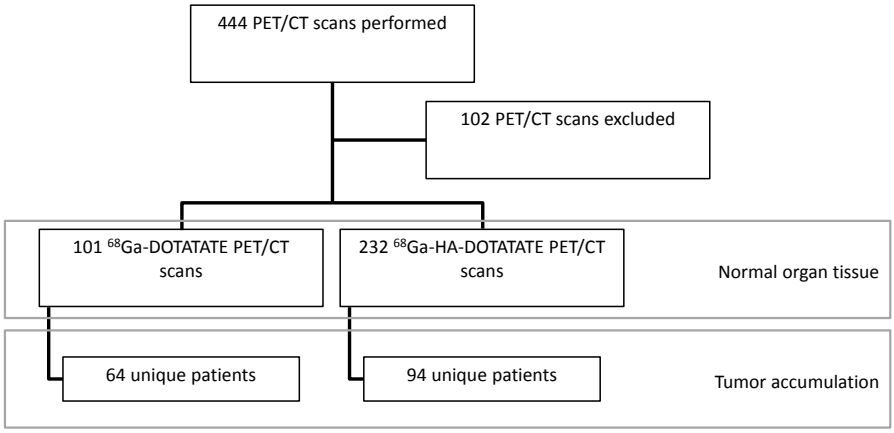

Figure 1. Flow chart of included scans and patients.

Tumour-to-liver ratio (analysis 4)

Tumour-to-liver ratio is shown in Figure 2. There is no significant difference in tumour-to-liver ratio of ^{68}Ga-HA-DOTATATE or ^{68}Ga-DOTATATE of the primary tumour (SUVmax 2.21 vs. 2.63 p=0.326, SUVpeak 1.72 vs. 2.37 p=0.098), or metastases in the liver (SUVmax 3.67 vs. 3.71 p=0.942, SUVpeak 3.30 vs. 3.47 p=0.747), abdomen (SUVmax 2.49 vs. 3.09 p=0.363, SUVpeak 2.04 vs. 2.42 p=0.461), lymph nodes (SUVmax 1.93 vs. 2.87 p=0.084, SUVpeak 1.50 vs. 2.37 p=0.069) or other organs (SUVmax 2.06 vs. 1.87 p=0.^{68}3, SUVpeak 1.63 vs. 1.33 p=0.456). Only the tumour-to-liver ratio of the SUVpeak of bone metastases was significantly higher for ^{68}Ga-HA-DOTATATE (SUVmax 2.63 vs. 1.71 p=0.153, SUVpeak 1.98 vs. 1.08 p=0.037). The results are shown in Figure 2G-H.

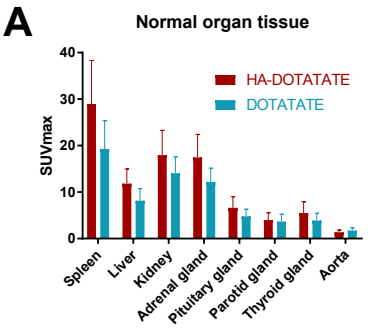
A
Normal organ tissue
HA-DOTATATE
DOTATATE
SUVmax
40
30
20
10
0
Spleen
Liver
Kidney
Adrenal gland
Pituitary gland
Parotid gland
Thyroid gland
Aorta

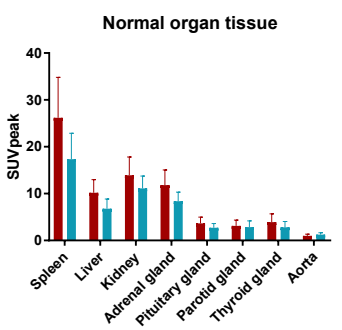
B
Normal organ tissue
SUVpeak
40
30
20
10
0
Spleen
Liver
Kidney
Adrenal gland
Pituitary gland
Parotid gland
Thyroid gland
Aorta

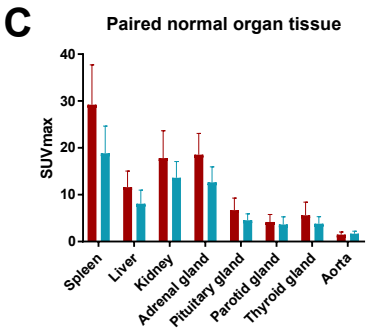
C
Paired normal organ tissue
SUVmax
40
30
20
10
0
Spleen
Liver
Kidney
Adrenal gland
Pituitary gland
Parotid gland
Thyroid gland
Aorta

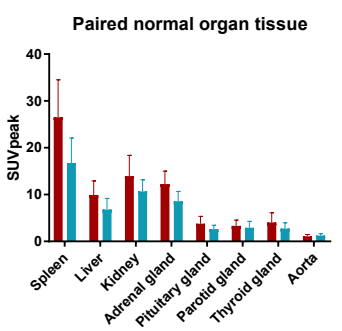
D
Paired normal organ tissue
SUVpeak
40
30
20
10
0
Spleen
Liver
Kidney
Adrenal gland
Pituitary gland
Parotid gland
Thyroid gland
Aorta

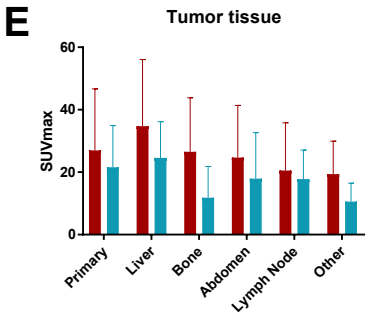
E
Tumor tissue
SUVmax
60
40
20
0
Primary
Liver
Bone
Abdomen
Lymph Node
Other

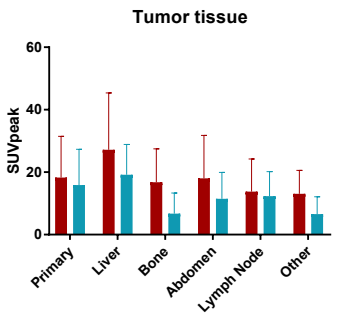
F
Tumor tissue
SUVpeak
60
40
20
0
Primary
Liver
Bone
Abdomen
Lymph Node
Other

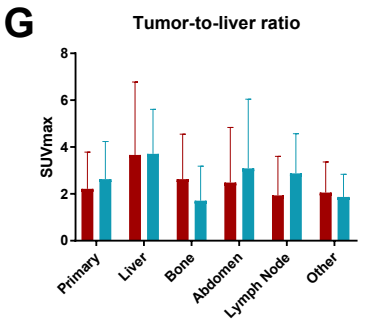
G
Tumor-to-liver ratio
SUVmax
8
6
4
2
0
Primary
Liver
Bone
Abdomen
Lymph Node
Other

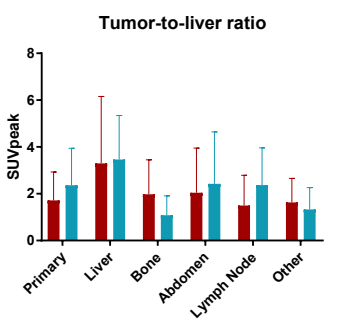
H
Tumor-to-liver ratio
SUVpeak
8
6
4
2
0
Primary
Liver
Bone
Abdomen
Lymph Node
Other

◂ **Figure 2**. Uptake of ^{68}Ga-HA-DOTATATE and ^{68}Ga-DOTATATE. (A-B) SUVmax and SUVpeak of normal organ tissue in all patients. (C-D) SUVmax and SUVpeak of normal organ tissue in the subgroup of patients in which paired analyses was possible. (E-F) SUVmax and SUVpeak of tumor tissue. (G-H) Tumor-to-liver ratio for the SUVmax and SUVpeak. ^{68}Ga-HA-DOTATATE = blue, ^{68}Ga-DOTATATE = red, SUV = standard uptake value.

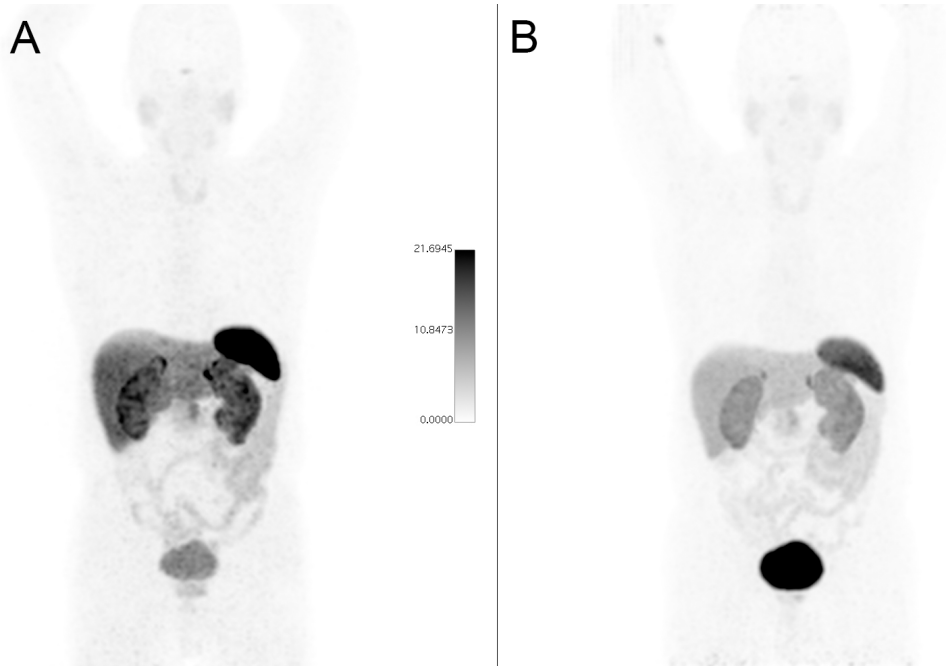

Figure 3. Image of the same patient with ^{68}Ga-HA-DOTATATE (A) and ^{68}Ga-DOTATATE (B). Uptake in the spleen, liver and kidneys is visibly lower with DOTATATE compared to HA-DOTATATE.

DISCUSSION

With the increasing use of ^{68}Ga-SRS imaging for neuroendocrine tumours, the choice of peptide has become a topic of discussion. In this debate, characteristics such as tumour uptake, normal tissue distribution, tumour-to-background ratio, and dosimetry play an important role although costs and availability should also be taken into account. The most commonly used peptides are DOTATOC, DOTANOC, DOTATATE, and HA-DOTATATE, while new peptides for NET imaging are being developed. Studies have been performed to compare these different peptides with each other[11-13], mostly as interpatient studies which are limited in the number of patients which can be included. To our knowledge, this is the largest study to be performed comparing two peptides, namely DOTATATE and HA-DOTATATE.

Normal tissue and tumour uptake

This study demonstrates that HA-DOTATATE has a significantly higher uptake in normal tissue when compared to DOTATATE, but that the tumour-to-background ratio remains the same. The uptake pattern and SUVmax values of DOTATATE in this study are comparable to previously published reports on the distribution of DOTATATE.[14-15] When comparing this study to the previously published studies by the group of Wester comparing DOTATATE and HA-DOTATATE[8-9], our results do show a significant difference in background uptake of HA-DOTATATE compared to DOTATATE. This could be due to the number of patients needed to find a significant difference, which could in part be due to the range within the normal distribution pattern.[14-15] When looking at the number of lesions detected, Brogsitter et al. reported that HA-DOTATATE detected 95.3% of all lesions and DOTATATE 96.4% of lesions. This was not measured in this study, but although the tumour-to-background ratio remains the same on average, it could be possible to miss lesions when the background uptake is higher with HA-DOTATATE.

The question remains which peptide is optimal for NET imaging. Sensitivity, specificity, and dosimetry have been determined for multiple peptides (DOTATOC, DOTANOC, DOTATATE, HA-DOTATATE) and all lie in within the same range and have been reviewed by Johnbeck et al. In summary, DOTATOC has a higher uptake in normal organs compared to DOTATATE and DOTANOC, the sensitivity of DOTATATE might be slightly lower, and all peptides have a specificity close to 100%.[16] Peptide choice will therefore probably depend on experience, personal preference, cost and availability.

Consequences for ^{177}Lu-SRS treatment

Although a similar tumour-to-background ratio might not have a large effect on imaging studies, this does not apply to ^{177}Lu-SRS treatments where a higher uptake in the background could lead to measurable side effects. Previous clinical studies have been performed with both

^{177}Lu-DOTATATE and ^{177}Lu-DOTATOC.[17] However only ^{177}Lu-DOTATATE has been studied and in a phase 3 trial that showed a benefit for PRRT over standard of care (including octreotide) in both overall- and progression free survival.[18] Therefore ^{177}Lu-DOTATATE is probably the most commonly used radiopharmaceutical for PRRT.

Conflicting reports have been published on the differences between DOTATATE and HA-DOTATATE when bound to ^{177}Lu.[19-20] Since the binding to the somatostatin receptor is dictated by the DOTA-peptide and not the ion binding to it, the findings of this study could also hold true for labelling with ^{177}Lu, which might make DOTATATE the more suitable peptide for peptide receptor radionuclide therapy.

Limitations

This study has several limitations. Firstly, no visual comparison on the number of detected lesions could be performed due to the time between follow-up scans in the same patients. However, since the tumour-to-background ratio remained the same between the two peptides, it could be expected that both peptides would detect the same lesions. Secondly, most analyses performed were cohort-based while only 41 patients were available for patient-based analysis. However both analyses showed similar results. Thirdly peptide amount has not been taken into account in this study or any other published studies to our knowledge. Mass-dependent differences of DOTATATE uptake with 111In have been demonstrated in rats.[21] In our study 20 µg of HA-DOTATATE or 30 µg of DOTATATE was labelled, but this amount is divided among 2-5 patients, depending on the decay of the generator. Which implies that patients generally received between 4-10 µg of HA-DOTATATE or 6-15 µg of DOTATATE. This will be general practice in most centres performing ^{68}Ga imaging in order to make efficient use of each radiopharmaceutical production. Due to the time frame of this study (~5 years), many generator cycles are included in this study and we believe this effect will be the same in each group of patients. Lastly, for the paired study of normal organ uptake in 41 patients, there was 25 months between the two scans. Since treatment with somatostatin analogues may alter the biodistribution of radiolabeled somatostatin analogues, these were discontinued prior to acquisition of the PET/CT scan. Although there is no evidence that other treatment such as chemotherapy alter the biodistribution of radiolabeled somatostatin analogues, this cannot be verified.

CONCLUSION

^{68}Ga-HA-DOTATATE and ^{68}Ga-DOTATATE have a different distribution pattern in vivo as demonstrated in these 342 patients, which is in contrast to previously reported studies. Uptake of ^{68}Ga-HA-DOTATATE is significantly increased in most organs, but only at some tumour sites. This difference should be taken into account when choosing a peptide for somatostatin imaging or treatment.

REFERENCES

1. Oberg K, Castellano D. Current knowledge on diagnosis and staging of neuroendocrine tumors. *Cancer Metastasis Rev*. 2011;30 Suppl 1:3-7.
2. Gatto F, Hofland LJ. The role of somatostatin and dopamine D2 receptors in endocrine tumors. *Endocr Relat Cancer*. 2011;18:R233-51.
3. Cakir M, Dworakowska D, Grossman A. Somatostatin receptor biology in neuroendocrine and pituitary tumors: part 2–clinical implications. *J Cell Mol Med*. 2010;14:2585-2591.
4. Geijer H, Breimer LH. Somatostatin receptor PET/CT in neuroendocrine tumors: update on systematic review and meta-analysis. *Eur J Nucl Med Mol Imaging*. 2013;40:1770-1780.
5. Virgolini I, Ambrosini V, Bomanji JB, et al. Procedure guidelines for PET/CT tumour imaging with 68Ga-DOTA-conjugated peptides: 68Ga-DOTA-TOC, 68Ga-DOTA-NOC, 68Ga-DOTA-TATE. *Eur J Nucl Med Mol Imaging*. 2010;67:2004-2010.
6. Brogsitter C, Schottelius M, Zöphel K, Kotzerke J, Wester H.J. Twins in spirit: DOTATATE and high-affinity DOTATATE. *Eur J Nucl Med Mol Imaging*. 2013;40:1789-1798.
7. Schottelius M, Simecek J, Hoffman F, Willibald M, Schwaiger M, Wester HJ. Twins in spirit - episode I: comparative preclinical evaluation of [^{68}Ga]DOTATATE and [^{68}Ga]HA-DOTATATE. *EJNMMI Res*. 2015;5:22-32.
8. Brogsitter C, Zöphel K, Hartmann H, Schottelius M, Wester HJ, Kotzerke J. Twins in spirit part II: DOTATATE and high-affinity DOTATATE - the clinical experience. *Eur J Nucl Med Mol Imaging*. 2014;41:1158-1165.
9. Hartmann H, Freudenberg R, Oehme L, et al. Dosimetric measurements of ^{68}Ga-High Affinity DOTATATE: Twins in spirit - part III. *Nuklearmedizin*. 2014;53:211-216.
10. Kwekkeboom DJ, Teunissen JJ, Bakker WH, et al. Radiolabeled somatostatin analog [^{177}Lu-DOTA0, Tyr3]octreotate in patients with endocrine gastroenteropancreatic tumors. *J Clin Oncol*. 2005;23:2754-2762.
11. Kabasakal L, Demirci E, Ocak M, et al. Comparison of ^{68}Ga-DOTATATE and ^{68}Ga-DOTANOC PET/CT imaging in the same patient group with neuroendocrine tumors. *Eur J Nucl Med Mol Imaging*. 2012;39:1271-1277.
12. Sandström M, Velikyan I, Garske-Román U, et al. Comparative biodistribution and radiation dosimetry of ^{68}Ga-DOTATOC and ^{68}Ga-DOTATATE in patients with neuroendocrine tumors. *J Nucl Med*. 2013;54:4-8.
13. Poeppel TD, Binse I, Petersenn S, et al. ^{68}Ga-DOTATOC versus ^{68}Ga-DOTATATE PET/CT in functional imaging of neuroendocrine tumors. *J Nucl Med*. 2011;52:1864-1870.
14. Kuyumcu S, Özkan ZG, Sanli Y, et al. Physiological and tumoral uptake of ^{68}Ga-DOTATATE: standardized uptake values and challenges in interpretation. *Ann Nucl Med*. 2013;27:538-45.
15. Kunikowska J, Krolicki L, Pawlak D, Zerizer I, Mikolajczak R. Semiquantitative analysis and characterization of physiological biodistribution of ^{68}Ga-DOTA-TATE PET/CT. *Clin Nucl Med*. 2012;37:1052-1057.
16. Johnbeck CB, Knigge U, Kjaer A. PET tracers for somatostatin receptor imaging of neuroendocrine tumors: current status and review of the literature. *Futur Oncol*. 2014;10:2259-2277.
17. Ambrosini V, Fani M, Fanti S, Forrer F, Maecke HR. Radiopeptide imaging and therapy in Europe. *J Nucl Med*. 2011;52:42S-55S.
18. Strosberg J, El-Haddad G, Wolin E, et al. Phase 3 trial of ^{177} Lu-Dotatate for midgut neuroendocrine tumors. *N Engl J Med*. 2017;376:125-135.

19. Brogsitter C, Hartmann H, Wunderlich G, Schottelius M, Wester HJ, Kotzerke J. Twins in spirit part IV- [^{177}Lu] high affinity DOTATATE. A promising new tracer for peptide receptor radiotherapy? *Nuklearmedizin*. 2017;56:1-8.
20. Schuchardt C, Kulkarni HR, Wiessalla, et al. Dosimetry using Lu-177 DOTATATE, Lu-177 HA-DOTATATE and Lu-177 DOTATOC: Comparative results in patients undergoing peptide receptor radionuclide therapy (PRRT). *Eur J Nucl Med Mol Imaging*. 2014;41:S224-S225.
21. de Jong M, Breeman WA, Bernard BF, et al. Tumor uptake of the radiolabeled somatostatin analog [DOTA0,Tyr3] octreotide is dependent on the peptide amount. *Eur J Nucl Med*. 1999;26:693-8.


195mPt
IT
68GA
B+

Chapter 7

Influence of Lanreotide on Uptake of ^{68}Ga-DOTATATE in Patients with Neuroendocrine Tumours: a Prospective Intra-Patient Evaluation

Else A. Aalbersberg
Linda J. de Wit-van der Veen
Michelle W.J. Versleijen
Lisette J. Saveur
Gerlof D. Valk
Margot E.T. Tesselaar
Marcel P.M. Stokkel

Eur J Nucl Med Mol Imaging. 2019;46(3):696-703.

ABSTRACT

Introduction: Somatostatin receptor imaging with PET is standard of care for patients with a neuroendocrine tumour (NET). Since therapy and imaging with somatostatin analogues utilize the same receptor, current guidelines recommend withdrawing long-acting somatostatin analogues for 3-4 weeks prior to somatostatin receptor PET imaging. The aim of this study is to prospectively assess the effect of lanreotide use on the uptake of ^{68}Ga-DOTATATE intra-individually one day prior to and one day post injection of lanreotide.

Methods: Thirty-four patients with metastatic and/or unresectable NET and currently on lanreotide therapy for at least 4 months were included in the study. A ^{68}Ga-DOTATATE PET/CT scan was performed on the day before and the day after lanreotide injection. In each patient ^{68}Ga-DOTATATE uptake ($SUV_{max, mean, peak}$) was assessed in both tumour lesions and normal tissue. All scans were assessed by two blinded nuclear medicine physicians for visual analysis. Paired T-tests were performed to determine the differences between the scans.

Results: Of the 34 patients included, 31 were available for analyses in which 190 tumour lesions were measured. Uptake of ^{68}Ga-DOTATATE in tumour lesions was increased significantly after lanreotide, but decreased significantly in the liver, spleen, and thyroid gland resulting in a higher tumour-to-liver ratio.

Conclusion: Lanreotide injection prior to ^{68}Ga-DOTATATE PET/CT does not result in decreased tumour uptake. In contrast, tumour uptake was increased whereas the uptake in normal organs is decreased, leading to an increased tumour-to-liver ratio. However, these differences were small and not deemed clinically relevant. These results strongly suggest that discontinuation of lanreotide injections in the weeks prior to ^{68}Ga-DOTATATE PET examinations is unnecessary and does not compromise nuclear medicine imaging results.

INTRODUCTION

Neuroendocrine tumours (NET) are a heterogeneous group of rare cancers that represent only 2% of all malignancies.[1] Over the last decades the incidence of a NET has increased from 1.09 per 100000 people in 1973 to 6.98 per 100000 in 2012 in the United States.[2] NET arise from neuroendocrine cells anywhere throughout the body but the most common location is in the gastroenteropancreatic tract.[3] Although heterogeneous, almost all NET are characterized by an (over)expression of the somatostatin receptor (SSTR) of which five subtypes are known. Of these subtypes, $SSTR_2$ and $SSTR_5$ are most often expressed in NET.[4] The SSTR is utilized as a target for first-line therapy for the treatment of symptoms and tumour control of NET with somatostatin analogues (SSA) such as octreotide and lanreotide, which have a high affinity for $SSTR_2$ and $SSTR_5$ in metastatic midgut NET.[5-6]

The SSTR can also be used for diagnostic imaging. In that case, a somatostatin analogue is coupled to ^{111}In for SPECT imaging or ^{68}Ga for PET imaging.[7] The three main radiopharmaceuticals used for SSTR imaging by PET are ^{68}Ga-DOTATATE, ^{68}Ga-DOTANOC, and ^{68}Ga-DOTATOC. A meta-analysis on the performance of SSA PET/CT in NET, showed a sensitivity of 93% and a specificity of 96%.[8]

Since both therapy with non-radiolabelled SSA and PET imaging with labelled ^{68}Ga-SSA involve binding to the same receptors, it is assumed that the uptake of ^{68}Ga-SSA is decreased due to receptor internalization and/or saturation from high-dose non radiolabelled SSA therapy.[9-10] This assumption has even led to the recommendation that long-acting SSA treatment should be withdrawn 3-4 weeks prior to acquiring a ^{68}Ga-SSA PET scan in order to ensure tumour uptake.[11]

Up to now, only two studies with octreotide evaluated the effect of SSA administration on the uptake of ^{68}Ga-DOTATATE. Both studies demonstrated that octreotide does not diminish tumour uptake of ^{68}Ga-DOTATATE. However, in one study the intra-individual comparison was only possible in a small subgroup of patients (9/105) and in the other study the time interval between the scan prior to- and after octreotide was 9.6±7.2 months as they compared a scan of treatment naïve patients to a scan after start of therapy. Therefore tumour response or progression could not be excluded.[12-13]

The aim of the present study, therefore, was to prospectively assess the effect of lanreotide on the uptake of ^{68}Ga-DOTATATE intra-individually by comparing the scan 1 day prior to lanreotide injection to the scan 1 day after lanreotide injection.

MATERIALS AND METHODS

Patients

This prospective clinical study was performed at the Netherlands Cancer Institute in Amsterdam, The Netherlands. The study was approved by the Medical Ethics Committee (NL45948.031.13) and all patients provided written informed consent. Eligible patients were aged 18 years or older, had histologically confirmed well differentiated NET (grade I-II) that was treated with lanreotide (Ipsen, France) for at least 4 months, measurable disease ≥ 1 cm on ^{68}Ga-DOTATATE PET/CT, WHO performance status ≤ 2, and a life expectancy of at least 3 months. Patients were excluded in case of pregnancy or claustrophobia.

Study protocol

^{68}Ga-DOTATATE PET/CT imaging was performed 1 day prior and 1 day after lanreotide administration. The lanreotide injection was given at the regular dose (standard clinical dosages of 60, 90, or 120 mg) and time (every 3-4 weeks) for the individual patients and was administered by the family physician or home care nurse per regular protocol. A study team member contacted the family physician or home care nurse prior the administration of lanreotide to ensure that the injection was given on the day between the PET scans.

Sample size calculation

The day-to-day variation in the tumour uptake of ^{68}Ga DOTATATE is unknown, but assumed to be in the range of 0-10%, which is considered normal for other PET tracers. In a smaller similar study, Janson *et al*. compared the uptake of ^{111}In-octreotide before and after 12 months of treatment with lanreotide in a small group of patients (n=8). The tumour-to background ratio increased on average 50% (range -79 to 1087%).[14] Based on this concept, a power-analysis was performed for the current study with a non-inferiority design. To measure an effect size of 0.5 in tumour-to-background ratio (80% power; two-sided alpha of 0.05), 34 patients were required for this study.

^{68}Ga-DOTATATE preparation

Fully automated labelling of ^{68}Ga-DOTATATE was performed using a labelling system (Scintomics GmbH, Germany) and sterile single-use cassettes (ABX GmbH, Germany). The peptide used was GMP grade DOTA-3-iodo-Tyr3-octreotate (ABX GmbH, Germany) with counterion acetate salt, purity > 96%, and the packaged quantity was within 20% of the required quantity of peptide. In short, ^{68}Ga was eluted from a ^{68}Ge/^{68}Ga generator (iThemba Labs, IDB Holland, the Netherlands; Galliapharm, Eckert & Ziegler, Germany; ITG, Germany) with hydrochloric acid. The eluate was added to 20-50 µg peptide and heated for 10 minutes at 100°C. Quality control was performed with instant thin-layer chromatography and solid phase chromatography, which was validated with the quality

control method provided by the European Pharmacopoeia for ^{68}Ga-Edotreotide. Batches were released for clinical usage if ^{68}Ga ions were < 2% and ^{68}Ga colloids < 3% of the final product. Peptide amount per patient was calculated with the amount of peptide at the start of production, the total amount of radiolabeled peptide produced and the individual patient activity administered.

PET/CT imaging

PET/CT scans were performed approximately 45 minutes post injection of 100 MBq ^{68}Ga-DOTATATE from base of skull to mid-thigh; the sequential scans were performed at initial uptake time +/- 5 minutes. Acquisitions were obtained on a Gemini ToF PET/CT (Philips, the Netherlands) with 2-2.5 minutes per bed position. A low-dose CT scan was acquired for attenuation correction and anatomical correlation.

Visual analysis

Visual analysis was performed by two Nuclear Medicine physicians with extensive experience with ^{68}Ga-DOTATATE PET/CT. Both physicians were blinded to which scans were pre- and post lanreotide injection. A consensus was reached on which scan was preferred visually (scan 1, scan 2, or no preference). Furthermore, the number of lesions that were only visible on either one of the scans were determined.

Image quantification

SUV_{max}, SUV_{peak}, and $SUV_{mean50\%}$ were quantified in tumour lesions and normal organ tissue using the Metavol software (University of California, USA). Tumour lesions were categorized according to anatomical site as: primary, abdominal (including lymph nodes), lymph nodes (not in the abdomen), liver, lung, bone, other. The three visually most intense lesions in each category were quantified in each patient when available. Normal organ uptake was measured in liver, spleen, kidney, bone marrow, adrenal-, pituitary, parotid-, and thyroid gland. When possible the organ was automatically segmented using $SUV_{50\%max}$. If auto segmentation could not be performed a spherical VOI of 1 cm^3 was placed in the organ. In those cases SUV_{peak} was not determined as it would be equal to SUV_{mean}. In case of diffuse liver metastases, no uptake in normal parenchyma was measured since these measurements were considered unreliable. Tumour-to-liver ratio was calculated as this was deemed the most clinically relevant due to the physiological high uptake of ^{68}Ga-DOTATATE and the frequent presence of NET metastases in the liver. This was calculated by dividing the SUV_{max} or SUV_{mean} of the tumour by the corresponding SUV_{max} or SUV_{mean} of the liver.

Statistical analysis

For image quantification paired T-tests were performed to determine whether or not there were significant differences in uptake of ^{68}Ga-DOTATATE between the two scans. Data is expressed as mean ± standard deviation (SD), with a p-value of <0.05 considered significant. When less than ten measurements were available no statistical analysis was done. Analyses were performed in SPSS v22 (IBM, USA) and graphs were produced in GraphPad Prism v7.03 (GraphPad Software Inc., USA).

RESULTS

Patients and PET imaging

Thirty-four patients were included in this study. Patient demographics are shown in Table 1. Three patients did not undergo the second scan; in one instance the radiopharmaceutical did not pass quality control, 1 patient was reported to be treated with lanreotide but this was not the case, and 1 patient failed to appear at the second appointment. The average injected activity and time between scan and injection were not significantly different between scan 1 (89.59 MBq, 47.8 minutes) and scan 2 (91.98 MBq, 48.9 minutes) and are shown in Figure 1. Peptide mass was identical between scan 1 and scan 2 (7.39±4.10 µg vs 7.65±4.34 µg, p=0.649). ^{68}Ga ions (mean±SD 0.73±0.41%) and ^{68}Ga colloids (mean±SD 1.47±0.56%) were within limits.

Gender	Male	21 (61.8%)
	Female	13 (38.2%)
Age (years)		64.2 (45-78)
Primary tumour site	Small bowel	24 (70.6%)
	Pancreas	4 (11.8%)
	Caecum	2 (5.9%)
	Rectum	1 (2.9%)
	Unknown primary	3 (8.8%)
Grade	I	22 (64.7%)
	II	12 (35.3%)
Lanreotide dose (mg)*	60	2 (5.9%)
	90	13 (38.2%)
	120	18 (52.9%)

Table 1. Demographics of the 34 patients included in this study. Data is shown as absolute number (percentage) or as mean (range). *for 33 patients, 1 patient was excluded for not receiving lanreotide.

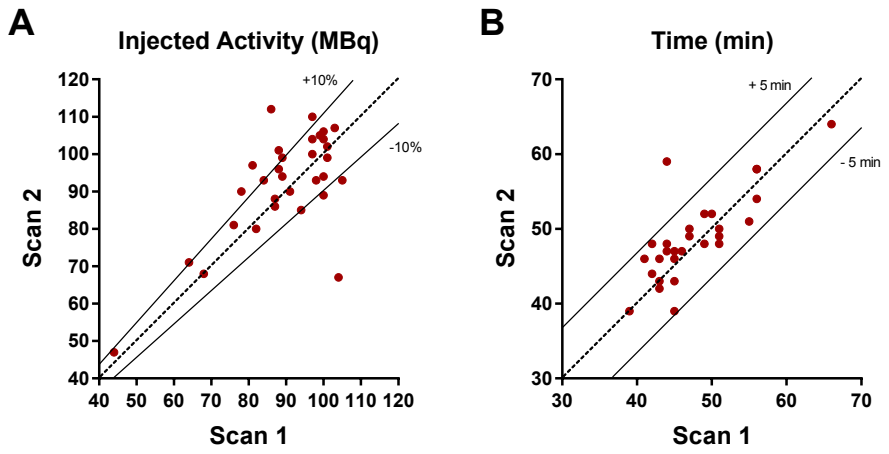

Figure 1. Injected activity and time post injection for each patient. Scan 1 is prior to lanreotide injection and scan 2 after lanreotide injection. The dotted diagonal line represents equal parameters for both scans. The solid lines are the optimal range of deviation between the two scans; ±10% for injected activity and ±5 minutes for time post-injection.

Visual analysis

Visually, the preferred scan was pre-lanreotide in 2 cases (6%) and post-lanreotide in 13 cases (42%) while in 16 cases (52%) it was ambiguous. Preference was most often caused by lower liver uptake leading to better visibility of tumour lesions in the liver. On the scans performed before lanreotide injection 16 lesions were not identified, 14 in the liver and 2 in the bone. On the scans performed after lanreotide injection 6 lesions were not identified, equally divided between liver and bone. The visualisation of the additional lesions on either scan did not have a clinical impact in any of the patients.

Tumour uptake

One hundred ninety tumour lesions were quantified in 31 patients. In general, SUV_{max} significantly increased in tumour lesions after lanreotide injection (20.96 vs. 21.64 (prior vs. post lanreotide), p=0.034) while SUV_{peak} (16.45 vs. 16.86, p=NS) and SUV_{mean} (14.77 vs. 15.03, p=NS) remained relatively unchanged. Although uptake significantly increased, this difference is not deemed clinically relevant. Subgroup analyses could be performed for metastatic lesions in the abdomen, liver, lymph nodes, bone, and other. Only the SUV_{peak} (16.96 vs. 18.06, p=0.047) and SUV_{mean} (15.38 vs. 16.55, p=0.025) in abdominal lesions was significantly higher after lanreotide. No other significant differences were found. All data is shown in Table 2 and Figure 2A shows the SUV_{max} on the second scan as percentage of the first scan.

Tumour		Scan 1 Before lanreotide	Scan 2 After lanreotide	Paired difference	p-value
All lesions	SUV_{max}	20.96 ± 12.37	21.64 ± 12.63	-0.67 ± 4.35	0.034 *
n=190	SUV_{peak}	16.45 ± 10.92	16.86 ± 11.22	-0.41 ± 2.99	0.076
	SUV_{mean}	14.77 ± 8.57	15.03 ± 8.69	-0.25 ± 2.86	0.254
Primary	SUV_{max}	28.87 ± 13.98	32.66 ± 16.19	nd	nd
n=4	SUV_{peak}	24.05 ± 12.73	26.63 ± 13.32	nd	nd
	SUV_{mean}	19.20 ± 9.72	21.12 ± 10.29	nd	nd
Abdominal	SUV_{max}	22.61 ± 13.11	24.49 ± 13.52	-1.88 ± 4.87	0.052
n=28	SUV_{peak}	16.96 ± 10.57	18.06 ± 10.72	-1.10 ± 2.44	0.047 *
	SUV_{mean}	15.38 ± 8.78	16.55 ± 8.73	-1.17 ± 2.97	0.025 *
Liver	SUV_{max}	26.20 ± 10.66	26.77 ± 11.14	-0.57 ± 4.95	0.356
n=64	SUV_{peak}	24.28 ± 9.00	24.58 ± 10.03	-0.30 ± 4.23	0.671
	SUV_{mean}	19.80 ± 6.83	19.59 ± 7.59	0.21 ± 3.36	0.633
Lymph nodes	SUV_{max}	18.13 ± 12.80	18.85 ± 12.17	-0.72 ± 3.95	0.223
n=46	SUV_{peak}	13.99 ± 10.65	14.43 ± 10.32	-0.45 ± 2.55	0.208
	SUV_{mean}	13.05 ± 8.82	13.58 ± 8.45	-0.53 ± 2.65	0.271
Bone	SUV_{max}	16.79 ± 11.05	15.92 ± 10.67	0.88 ± 3.29	0.142
n=32	SUV_{peak}	11.33 ± 8.40	10.76 ± 8.08	0.57 ± 1.91	0.098
	SUV_{mean}	11.79 ± 7.74	11.09 ± 7.38	0.71 ± 2.34	0.103
Lung	SUV_{max}	11.50 ± 11.34	11.13 ± 10.23	nd	nd
n=6	SUV_{peak}	7.62 ± 8.42	7.81 ± 8.44	nd	nd
	SUV_{mean}	7.69 ± 7.35	7.65 ± 7.11	nd	nd
Other	SUV_{max}	11.76 ± 6.27	13.84 ± 9.57	-2.08 ± 3.59	0.100
n=10	SUV_{peak}	7.70 ± 4.65	8.98 ± 6.64	-1.28 ± 2.30	0.109
	SUV_{mean}	8.08 ± 4.28	9.40 ± 6.40	-1.32 ± 2.34	0.112

Table 2. SUV_{max}, SUV_{peak}, and SUV_{mean} for tumour lesions (mean ± SD). Paired differences for scan 1 - scan 2 (mean ± SD). nd = not determined. * = significant (p<0.05).

Normal tissue uptake

Contrary to tumour uptake, SUV_{max} in normal tissue significantly decreased after lanreotide injection; in the liver (10.15 vs. 9.08 (prior vs. post lanreotide), p<0.001), spleen (25.77 vs. 22.35, p<0.001), and thyroid gland (4.13 vs. 3.14, p<0.001). The same held true for the SUV_{mean} in the liver (8.80 vs. 7.87, p<0.001), spleen (23.07 vs. 20.11, p<0.001), and thyroid gland (3.15 vs. 2.47, p<0.001). In the kidney, bone marrow, adrenal-, pituitary-, and parotid gland no significant differences were seen in either SUV_{max}, SUV_{peak}, or SUV_{mean}. All data is shown in Table 3 and Figure 2B shows the SUV_{max} on the second scan as percentage of the first scan.

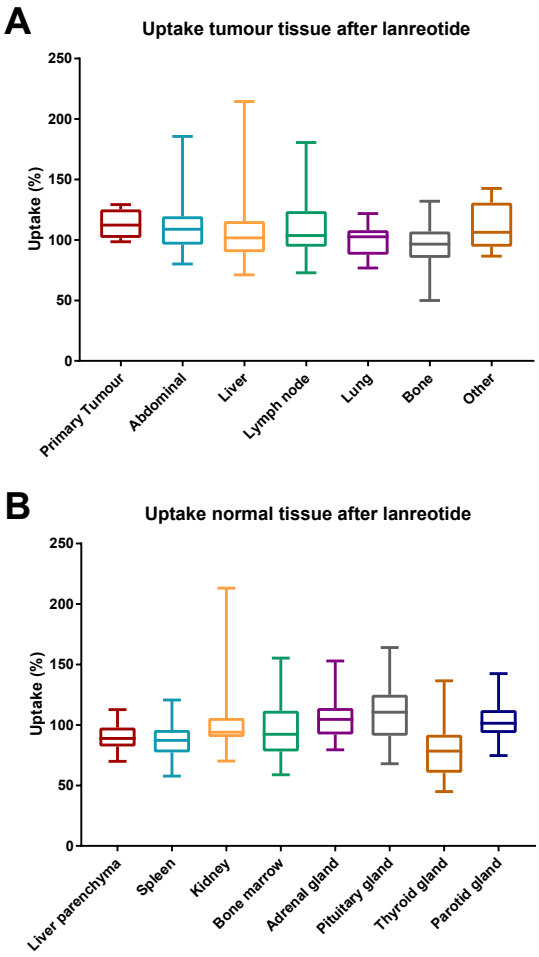

Figure 2. Percentage of uptake of ^{68}Ga-DOTATATE after lanreotide compared to before lanreotide in (A) tumour lesions and (B) normal organ tissue. Box plots indicate the median, 25th and 75th percentile, and minimum and maximum values.

Tumour-to-liver ratio

The tumour-to-liver ratio for SUV_{max} increased after lanreotide injection in all lesions (2.21 vs. 2.59 (prior vs. post lanreotide), p<0.001), in abdominal (2.58 vs. 3.09, p=0.002), liver (2.80 vs. 3.18, p<0.001), lymph node (1.77 vs. 2.16, p<0.001), as well as in bone (1.89 vs. 2.18, p=0.012) lesions. The tumour-to-liver ratio of SUV_{mean} increased after lanreotide injection in all lesions (1.83 vs. 2.11, p<0.001); abdominal (2.02 vs. 2.40, p=0.001), lymph node (1.4 vs. 2.77, p<0.001), as well as in bone (1.51 vs. 1.77, p=0.003) lesions. All data is shown in Table 4.

Normal tissue		Scan 1 Before lanreotide	Scan 2 After lanreotide	Paired difference	p-value
Liver parenchyma n=27	SUV_{max}	10.15 ± 2.26	9.08 ± 2.34	1.07 ± 1.06	<0.001 *
	SUV_{peak}	nd	nd	nd	nd
	SUV_{mean}	8.80 ± 2.04	7.81 ± 1.93	1.0 ± 0.95	<0.001 *
Spleen n=31	SUV_{max}	25.77 ± 7.60	22.35 ± 7.34	3.42 ± 3.57	<0.001 *
	SUV_{peak}	nd	nd	nd	nd
	SUV_{mean}	23.07 ± 6.90	20.11 ± 6.64	2.96 ± 3.27	<0.001 *
Adrenal gland n=29	SUV_{max}	19.20 ± 4.50	20.55 ± 6.49	-1.35 ± 3.62	0.054
	SUV_{peak}	14.53 ± 3.07	15.13 ± 4.18	-0.60 ± 2.41	0.236
	SUV_{mean}	13.23 ± 3.03	13.89 ± 4.24	-0.66 ± 2.42	0.153
Pituitary gland n=27	SUV_{max}	6.57 ± 2.38	7.07 ± 2.47	-0.50 ± 1.34	0.062
	SUV_{peak}	3.99 ± 1.40	4.17 ± 1.39	-0.18 ± 0.77	0.230
	SUV_{mean}	4.64 ± 1.72	4.98 ± 1.71	-0.34 ± 0.91	0.067
Parotid gland n=29	SUV_{max}	3.99 ± 1.58	4.18 ± 2.05	-0.20 ± 0.83	0.213
	SUV_{peak}	3.74 ± 1.37	4.05 ± 2.09	-0.31 ± 0.93	0.257
	SUV_{mean}	3.03 ± 1.18	3.18 ± 1.52	-0.16 ± 0.66	0.205
Thyroid gland n=26	SUV_{max}	4.13 ± 2.17	3.14 ± 1.71	0.99 ± 1.01	<0.001 *
	SUV_{peak}	nd	nd	nd	nd
	SUV_{mean}	3.15 ± 1.71	2.47 ± 1.41	0.68 ± 0.73	<0.001 *
Kidney n=31	SUV_{max}	19.75 ± 5.18	20.66 ± 9.75	-0.91 ± 7.32	0.493
	SUV_{peak}	nd	nd	nd	nd
	SUV_{mean}	12.95 ± 3.43	13.72 ± 5.24	-0.77 ± 3.45	0.222
Bone marrow n=31	SUV_{max}	2.39 ± 0.62	2.23 ± 0.58	0.16 ± 0.53	0.092
	SUV_{peak}	nd	nd	nd	nd
	SUV_{mean}	1.48 ± 0.42	1.84 ± 2.12	-0.36 ± 2.15	0.356

Table 3. SUV_{max}, SUV_{peak}, and SUV_{mean} for normal tissue (mean ± SD). Paired differences for scan 1 - scan 2 (mean ± SD). nd = not determined. * = significant (p<0.05).

Tumour		Scan 1 Before lanreotide	Scan 2 After lanreotide	p-value
All lesions n=165	Ratio SUV_{max}	2.21	2.59	<0.001 *
	Ratio SUV_{mean}	1.83	2.11	<0.001 *
Primary n=3	Ratio SUV_{max}	2.76	3.10	nd
	Ratio SUV_{mean}	2.26	2.49	nd
Abdominal n=26	Ratio SUV_{max}	2.58	3.09	0.002 *
	Ratio SUV_{mean}	2.02	2.40	0.001 *
Liver n=52	Ratio SUV_{max}	2.80	3.18	<0.001 *
	Ratio SUV_{mean}	2.66	2.86	0.093
Lymph nodes n=41	Ratio SUV_{max}	1.77	2.16	<0.001 *
	Ratio SUV_{mean}	1.44	1.77	<0.001 *
Bone n=27	Ratio SUV_{max}	1.89	2.18	0.012 *
	Ratio SUV_{mean}	1.51	1.77	0.003 *
Lung n=6	Ratio SUV_{max}	1.22	1.25	nd
	Ratio SUV_{mean}	0.88	1.01	nd
Other n=10	Ratio SUV_{max}	1.24	1.75	0.080
	Ratio SUV_{mean}	0.97	1.31	0.091

Table 4. Tumour-to-liver ratio. nd = not determined. * = significant ($p<0.05$).

DISCUSSION

This study evaluates the effect of lanreotide on the uptake of ^{68}Ga-DOTATATE. It is the first prospective intra-individual comparison study in which both the time interval between the injection of the somatostatin analogue and ^{68}Ga-DOTATATE (1 day) and the interval between the pre- and post lanreotide scans (2 days) remained were standardized.

Due to utilization of the SSTR by SSAs for both therapy and imaging, it is currently recommended to discontinue long-acting SSAs prior to imaging.[11] Although the older guideline from 2010 explains that this issue is still up to debate but not standard clinical protocol in all centres, in the current guideline uncertainties are omitted and recommendations are based solely on one published clinical study.[15-16] In that study, ^{68}Ga-DOTATOC uptake is measured after intravenous injection of different dosages of octreotide (0, 50, 250, 500 µg) in nine patients. Interestingly, they conclude that tumour-to-background ratio is highest after pre-administration of 50 µg of octreotide in 5/6 patients.[16]

As long ago as 1993, clinical studies have been published that investigate whether or not non-radiolabelled SSAs influence the uptake of radiolabelled SSAs. Dörr *et al.* showed in two small trials (n=5 and n=10, resp.) that tumour visualization with ^{111}In-pentetreotide scintigraphy improved during treatment with SSAs and that tumour detection, including liver metastases, might be improved during SSA therapy. Based on these small cohorts it was also concluded that the biodistribution changed significantly during SSAs treatment, with decreased spleen (25-63%), hepatic (50-84%) and renal (72-88%) accumulation.[17-18] In 1999, Janson *et al.* investigated 8 NET patients with ^{111}In-pentetreotide scintigraphy prior and during lanreotide treatment, and showed an average increase of tumour-to-background uptake of 50% (-79% to +1087%) during SSA treatment.[14]

These three studies have very small patient numbers with large standard deviations and were performed before the introduction of ^{68}Ga-SSA PET/CT. More recently, 2 reports on the effect of octreotide on the uptake of ^{68}Ga-DOTATATE were published.[12-13] The first study compared the ^{68}Ga-DOTATATE PET/CT scans in 35 patients under treatment with octreotide to 70 patients without octreotide and performed an intra-individual comparison in 9 patients. They found no significant difference in SUV_{max} or SUV_{mean} of both the primary tumour or any metastases between the two groups, but a decrease in average uptake in the liver (6.6 ± 1.9 vs. 4.9 ± 1.4, $p<0.001$) and spleen (18.2 ± 5.0 vs. 12.8 ± 4.4, $p<0.001$) after octreotide treatment.[12] The main drawback of this study are its retrospective nature, the variety in time between octreotide administration and PET/CT (14.5 ± 11.4 days), and the small sample with an intra-individual comparison in which the time between the 2 scans was 13.8 ± 15.6 weeks. The latest report performed an intra-individual comparison of ^{68}Ga-DOTATATE PET/CT in 30 patients

prior to- and during octreotide treatment. Again, it was shown that octreotide decreased the uptake in normal tissues (liver, spleen, thyroid), but not in primary tumours or metastatic lesions.[13] This study however also had a retrospective design in which the time between the two PET/CT scans was 9.6 ± 7.2 months and the time between octreotide injection and PET/CT was 25.1 ± 14.8 days. Therefore, progression or response might have occurred in between and octreotide concentration was variable between patients. Furthermore, a small study in five patients compared uptake of ^{68}Ga-DOTATOC before and directly after ^{177}Lu-DOTATATE administration found no evidence of receptor saturation in tumours.[19]

In our prospective, well standardized study only a few lesions were visible on either one PET/CT (prior to or after lanreotide administration), though in none of the patients this had impact on clinical staging or decision making. Additionally, no clinically relevant changes in tumour SUVs were observed between ^{68}Ga-PET/CT 1 day prior and 1 day after lanreotide injection (20.96 vs. 21.64, p=0.034). The uptake in normal liver parenchyma, spleen and thyroid gland did show significant decreases after lanreotide injection, as was also described in the previous studies. Consequently, the derived value tumour-to-liver ratio also increased after lanreotide injection in all lesions (2.21 vs 2.59, p<0.001). Given that the pharmacokinetic profile of lanreotide shows a maximal concentration within 1 day after injection with a gradual elimination phase, it has to be emphasized that present differences resemble the worst-case scenario.[20-21] Therefore, it can be concluded that the effect of lanreotide treatment on the diagnostic accuracy for the detection and quantification of NET lesions is very limited. However ,since a small change in tumour-to-liver ratio is demonstrated, clinicians need to be aware of this when using ^{68}Ga-DOTATATE PET/CT for response monitoring. Nevertheless, this study again underlines that the accuracy for the detection of liver lesions increases rather than decreases directly after lanreotide injection.

This study has several limitations and premises which will be addressed; the use of high affinity DOTATATE, the presence of a low dose of lanreotide in the control group, the timing of the scan after lanreotide, and that three patients that dropped out of the study. This study has been performed with high affinity DOTATATE whilst the most commonly used peptide is DOTATATE. We do not expect this to influence the results as the both peptides have been compared and the investigators concluded that there were no differences in uptake in mayor organs or tumour lesions.[22] In this study the control group has a low plasma dose of lanreotide. The study was designed this way since this represents the clinical situation in which patients are under treatment with a somatostatin analogue and cannot be withheld until the plasma levels are undetectable, which is at least 90 days.[21] We do not expect this to influence the results since the concentration remaining is several times lower than the peak concentration. This study assumes that peak tissue concentration and receptor binding of lanreotide is reached within one day. Although the tissue binding profile of lanreotide is unknown, this premise is

based on two known parameters. The first is that the maximum concentration of lanreotide in plasma is reached within a day of intramuscular injection.[21] The second is that receptor binding occurs very fast after introduction of lanreotide in the blood. This is supported by data from studies with 177Lu-DOTATATE, which show that maximum tumour uptake is reached within several hours after intravenous administration and by pharmacokinetic modelling.[23-24] Since this study examines the maximum achievable difference in lanreotide plasma concentration, it is expected to be generalizable to all other time points. Finally, three patients dropped out of the study which led to the samples size not being reached. However, even with fewer patients (n=31 with 190 tumour lesions) a small difference was demonstrated. Therefore we do not expect a dropout rate of <10% to influence the results.

If long-acting somatostatin analogues such as lanreotide can be continued during ^{68}Ga-SSA PET/CT examinations, this is of major benefit for both the patient and the nuclear medicine department. Patients will no longer have to extend the duration between SSA administration and the PET/CT or switch to short-acting SSAs that have to be administered three times daily. For nuclear medicine departments this ensures that ^{68}Ga-SSA PET/CT patients can be clustered and examinations performed at any time without observing each patients' personal SSA administration schedule.

A question that remains unanswered is the effect of non-radiolabelled SSAs on the uptake of ^{177}Lu- or ^{90}Y-SSAs for peptide receptor radionuclide therapy (PRRT). Since the amount of peptide administered during PRRT is approximately 10x higher than for ^{68}Ga-SSA PET, the results of this study should not be extrapolated without further research to PRRT.

CONCLUSION

Whether somatostatin analogues should be discontinued prior to somatostatin receptor imaging has been debated for many years. The present study demonstrates that administration of lanreotide prior to ^{68}Ga-DOTATATE leads to similar or increased tumour uptake, decreased or equal normal tissue uptake, and an increased tumour-to-liver ratio. These results strongly suggest that discontinuation of SSAs prior to somatostatin receptor imaging is unnecessary and that therapy can be continued without compromising the outcomes of nuclear medicine imaging.

REFERENCES

1. Oronsky B, Ma PC, Morgensztern D, Carter CA. Nothing but NET: a review of neuroendocrine tumors and carcinomas. *Neoplasia.* 2017;19:991–1002.
2. Dasari A, Shen C, Halperin D, et al. Trends in the Incidence, prevalence, and survival outcomes in patients with neuroendocrine tumors in the United States. *JAMA Oncol.* 2017;77030:1335–42.
3. Oberg K, Castellano D. Current knowledge on diagnosis and staging of neuroendocrine tumors. *Cancer Metastasis Rev.* 2011;30 Suppl 1:3–7.
4. Cakir M, Dworakowska D, Grossman A. Somatostatin receptor biology in neuroendocrine and pituitary tumours: part 2–clinical implications. *J Cell Mol Med.* 2010;14:2585–91.
5. Rinke A, Müller HH, Schade-Brittinger C, et al. Placebo-controlled, double-blind, prospective, randomized study on the effect of octreotide LAR in the control of tumor growth in patients with metastatic neuroendocrine midgut tumors: A report from the PROMID study group. *J Clin Oncol.* 2009;27:4656–63.
6. Caplin ME, Pavel M, Cwikła JB, et al. Lanreotide in metastatic enteropancreatic neuroendocrine tumors. *N Engl J Med.* 2014;371:224–33.
7. Johnbeck CB, Knigge U, Kjaer A. PET tracers for somatostatin receptor imaging of neuroendocrine tumors: current status and review of the literature. *Futur Oncol.* 2014;10:2259–77.
8. Geijer H, Breimer LH. Somatostatin receptor PET/CT in neuroendocrine tumours: update on systematic review and meta-analysis. *Eur J Nucl Med Mol Imaging.* 2013;40:1770–80.
9. Cescato R, Schulz S, Waser B, et al. Internalization of sst2, sst3, and sst5 receptors: effects of somatostatin agonists and antagonists. *J Nucl Med.* 2006;47:502–11.
10. de Jong M, Breeman WA, Bernard BF, et al. Tumor uptake of the radiolabeled somatostatin analog [DOTA0,Tyr3] octreotide is dependent on the peptide amount. *Eur J Nucl Med*. 1999;26:693-8.
11. Bozkurt MF, Virgolini I, Balogova S, et al. Guideline for PET/CT imaging of neuroendocrine neoplasms with 68Ga-DOTA-conjugated somatostatin receptor targeting peptides and 18F–DOPA. *Eur J Nucl Med Mol Imaging.* 2017;44:1588–601.
12. Haug AR, Rominger A, Mustafa M, et al. Treatment with octreotide does not reduce tumor uptake of ^{68}Ga-DOTATATE as measured by PET/CT in patients with neuroendocrine tumors. *J Nucl Med.* 2011;52:1679–83.
13. Ayati N, Lee ST, Zakavi SR, et al. Long-acting Somatostatin analog therapy differentially alters ^{68}Ga-DOTATATE uptake in normal tissues compared to primary tumors and metastatic lesions. *J Nucl Med.* 2017;59:223-27.
14. Janson E, Kalkner K, Eriksson B, Westlin J, Oberg K. Somatostatin receptor scintigraphy during treatment with lanreotide in patients with neuroendocrine tumors. *Nucl Med Biol.* 1999;26:877–82.
15. Virgolini I, Ambrosini V, Bomanji JB, et al. Procedure guidelines for PET/CT tumour imaging with ^{68}Ga-DOTA-conjugated peptides: ^{68}Ga-DOTA-TOC, ^{68}Ga-DOTA-NOC, ^{68}Ga-DOTA-TATE. *Eur J Nucl Med Mol Imaging.* 2010;37:2004–10.
16. Velikyan I, Sundin A, Eriksson B, et al. In vivo binding of [68Ga]-DOTATOC to somatostatin receptors in neuroendocrine tumours-impact of peptide mass. *Nucl Med Biol.* 2010;37:265–75.
17. Dörr U, Wurm K, Höring E, Guzman G, Räth U, Bihl H. Diagnostic reliability of somatostatin receptor scintigraphy during continuous treatment with different somatostatin analogs. *Horm Metab Res Suppl.* 1993;27:36–43.

18. Dorr U, Rath U, Sautter-Bihl M, et al. Improved visualization of carcinoid liver metastases by indium-111 pentetreotide scintigraphy following treatment with cold somatostatin analogue. *Eur J Nucl Med.* 1993;20:431–3.
19. Sabet A, Nagarajah J, Dogan AS, et al. Does PRRT with standard activities of ^{177}Lu-octreotate really achieve relevant somatostatin receptor saturation in target tumor lesions?: insights from intra-therapeutic receptor imaging in patients with metastatic gastroenteropancreatic neuroendocrine tumors. *EJNMMI Research.* 2013;3:82-7.
20. SmPC Somatuline LA. Accessed Mar 5 2018. www.medicines.org.uk/emc/product/965/smpc
21. Astruc B, Marbach P, Bouterfa H, et al. Long-acting octreotide and prolonged-release lanreotide formulations have different pharmacokinetic profiles. *J Clin Pharmacol.* 2005;45:836–44.
22. Brogsitter C, Zöphel K, Hartmann H, Schottelius M, Wester HJ, Kotzerke J. Twins in spirit part II: DOTATATE and high-affinity DOTATATE- the clinical experience. *Eur J Nucl Med Mol Imaging.* 2014;41:1158-1165.
23. Schuchardt C, Kulkarni HR, Prasad V, Zachert C, Müller D, Baum RP. The Bad Berka dose protocol: comparative results of dosimetry in peptide receptor radionuclide therapy using ^{177}Lu-DOTATATE, ^{177}Lu-DOTANOC, and ^{177}Lu-DOTATOC. *Recent Results Cancer Res.* 2013;194:519-36.
24. Puszkiel A, Bauriaud-Mallet M, Bourgeois R, Dierickx L, Courbon F, Chatelut E. Evaluation of the interaction of amino acid infusion on ^{177}Lu-Dotatate pharmacokinetics in patients with gastroenteropancreatic neuroendocrine tumors. *Clin Pharmacokinet.* 2019;58:213-222.


195mPt
IT
68GA
B+

Chapter 8

Parameters to predict progression free and overall survival after peptide receptor radionuclide therapy: a multivariate analysis in 782 patients

Else A. Aalbersberg
Daphne M.V. Huizing
Iris Walraven
Linda J. de Wit-van der Veen
Harshad R. Kulkarni
Aviral Singh
Marcel P.M. Stokkel
Richard P. Baum

J Nucl Med. 2019 [e-pub ahead of print].

ABSTRACT

Introduction: Peptide receptor radionuclide therapy (PRRT) is an effective treatment for patients with neuroendocrine neoplasms. The aim of this study was to identify clinical and treatment parameters associated with progression free survival (PFS) and overall survival (OS).

Methods: All patients treated from October 2002 until March 2016 at the Zentralklinik Bad Berka with at least three administrations of PRRT (maximal interval six months between consecutive administrations) were included. Data were collected in five categories: general patient characteristics, tumor characteristics, prior treatments, radioisotope used for PRRT, and blood chemistry. Survival was analyzed using Kaplan-Meier curves. Univariate and multivariate Cox regression analyses were performed to identify parameters associated with PFS and OS.

Results: 782 patients were included with a median follow-up of 36 months. The median PFS and OS were 22 and 53 months, respectively. Parameters associated with lower PFS in the multivariate analysis were Ki-67 of more than 5%, previous treatment with interferon-α and chemotherapy, presence of diabetes, and chromogranin-A (CgA) levels higher than 336 µg/l. Parameters associated with lower OS were Ki-67 of more than 10%, performance status of at least 1, previous chemotherapy and ablation, and CgA levels higher than112 µg/l.

Conclusion: Higher Ki-67 values had a negative outcome on both PFS and OS, as well as higher CgA levels and previous chemotherapy. Furthermore, PFS was negatively associated with previous interferon-α treatment and diabetes, while lower OS was related to prior ablation and higher performance status.

INTRODUCTION

Well-differentiated neuroendocrine tumors (NETs) arise from neuroendocrine cells and although they can occur anywhere throughout the body, the most common locations are the gastrointestinal tract, pancreas, and lungs.[1] In the United States, NETs comprise 0.5% of new cancer diagnoses, with an incidence of approximately 6.98/100,000/year.[2] Most NETs are characterized by the expression of the somatostatin receptor (SSTR), which can be exploited for diagnostic imaging and (radionuclide) therapy. Treatment with radiolabeled somatostatin analogues (SSA) - called peptide receptor radionuclide therapy (PRRT) was introduced using ^{111}Indium-pentetreotide, followed by ^{90}Yttrium (^{90}Y)-octreotide and ^{177}Lutetium-octreotate (^{177}Lu-DOTATATE).[3-5] A randomized phase III PRRT clinical trial (NETTER-1) was concluded in 2017.[6] NETTER-1 randomized treatment for NET patients between four cycles of ^{177}Lu-DOTATATE (plus long-acting Sandostatin 30 mg/month) and a control group with high dose octreotide (long-acting 60 mg/month). The progression free survival (PFS) was 28.4 months in the ^{177}Lu-DOTATATE group and 8.4 months in the control group. Based on this trial, PRRT was approved in the United States and Europe for treatment of metastatic or irresectable NETs and is included now in the societal guidelines from ENETS, IAEA, EANM, and SNMMI.[7-8]

Patients eligibility for PRRT is primarily based on tumor lesion SSTR expression, visualized with ^{68}Gallium (^{68}Ga)-labeled SSA PET/CT. Treatment is effective when sufficient uptake is shown on ^{68}Ga-SSA PET/CT.[3,9] Several studies have investigated non-imaging parameters that affect outcome after PRRT. Ezziddin et al. demonstrated that a proliferation index (or Ki-67) of less than 20% resulted in good response after PRRT, while Ki-67 of more than 20% often led to progression within 3 months after treatment.[10] Ki-67 was also found to be a predictive factor for overall survival (OS) after PRRT in a multivariate analysis (74 patients). Other factors identified were hepatic tumor burden, performance status, and neuron-specific enolase level.[11] Brunner et al. found that SSTR type 2 expression is an independent prognostic marker for OS in 279 NET-patients. A subgroup analysis of 61 patients with pancreas NET (pNET) showed that SSTR expression is not a prognostic marker for OS in pNET.[12] Other non-histological parameters associated with survival after PRRT include gene cluster expression, primary tumor site, resection of the primary tumor, dominant liver metastases, and lesions' size.[13-15] A previous study to analyze multiple factors was an intention-to-treat analysis and included all patients that started PRRT - but not all received full treatment.[16] The aim of the current study was to identify clinical parameters that predict PFS and OS after PRRT in a large patient population.

MATERIALS AND METHODS

Patients

All patients treated with PRRT at Zentralklinik Bad Berka (Germany) from October 2002 to March 2016 were reviewed. Patients with histopathological proven NET were referred for PRRT in case of progressive metastatic or inoperable disease. Treatment was performed according to the local Bad Berka protocol, followed by the ENETS protocol and the IAEA/EANM/SNMMI protocol.[7-8,17] SSTR expression was confirmed and dedifferentiation excluded by pre-therapy ^{68}Ga-SSA PET/CT and ^{18}F-FDG PET/CT, respectively and scored as described.[18] Renal function was evaluated with ^{99m}Tc-MAG3 renography and tubular excretion rate evaluated.[8] An in-house produced amino acid infusion containing lysine and arginine was given during each administration for nephroprotection.[17] Patients were treated with ^{177}Lu, ^{90}Y, or both according to the previously described protocol.[17] Written informed consent was obtained from all patients prior to treatment, including data use for research and institutional review board approval was obtained. Inclusion criteria for this study were at least three administrations of PRRT and a maximum interval of six months between consecutive administrations. Patients previously treated with PRRT at a different center were excluded.

Data Collection

Data was collected in five categories: general patient characteristics, tumor characteristics, prior treatments, PRRT radionuclide, and laboratory parameters and tumor biomarkers. Progression was determined based on RECIST and/or PERCIST criteria.[19-20] Progression and survival were determined in January 2017. PFS was calculated from start of PRRT to progression or death from any cause. OS was calculated from start of PRRT to death from any cause.

Statistical Analysis

Statistical analyses were performed in SPSS v22.0 (IBM, United States). In case of non-normal distribution in a histogram, the variable was categorized in quartiles. Univariate cox regression was performed to determine the association between single parameters and PFS and OS. In order to be not too stringent, the multivariate Cox regression model included all parameters with a P value of less than 0.1 in the univariate analysis. Accordingly, after every iteration the parameter with the highest P value (above $P > 0.05$) was removed from the multivariate model (backward selection). The final model only contained variables significantly ($P < 0.05$) associated with survival. In addition, survival per primary tumor location and after primary tumor resection was evaluated.

RESULTS

Patient and PRRT Characteristics

A total of 1,425 patients were reviewed, of which 782 met the inclusion criteria. The median follow-up time was 36.0 months (range 4-155). The mean age prior to treatment was 60.3 years and 94.2% of the patients were in good health (WHO 0-1). Most tumors (92.4%) were G1/G2. Regarding other treatments, 33.2% of patients were treated with one, 24% with two, and 12.9% with three to five treatments before PRRT, while 29.7% of patients were treatment-naïve. PRRT consisted of three administrations (50.4%), four administrations (42.1%), or five to six administrations (7.5%). Half of the patients were treated with both ^{177}Lu and ^{90}Y (Table S1), whilst 37.7% received ^{177}Lu only and 12.3% ^{90}Y only. Most patients had NETs originating from the small intestine (28.3%) or pancreas (35.4%) and 50% of the patients had a functional tumor. All patient characteristics are shown in Table 1. Table 2 presents the PFS and OS per primary tumor location, showing that gastroenteropancreatic (GEP-) NETs have a higher PFS and OS.

Progression free survival

Progression was observed in 643 (82.2%) patients with a median PFS of 22 months (interquartile range (IQR) 14.0-31.3, Figure 1A). In univariate analyses, ten parameters were associated with lower PFS: primary tumor in the lung compared to primary tumor in the small intestine (HR 1.625 CI [1.186-2.226]), performance status WHO 1 (HR 1.352 CI [1.127-1.623]) and WHO 2/3 (HR 1.741 CI [1.262-2.402]) compared to WHO 0, prior treatments with chemotherapy (HR 1.362 CI [1.123-1652]), interferon-α (HR 1.487 CI [1.046-2.114]), and radiotherapy (HR 2.059 CI [1.420-2.984]). Furthermore, Ki-67 quartile 3 (Q3), Ki-67 5-10% (HR 1.466 CI [1.111-1.934]) and Q4, Ki-67 >10% (HR 1.631 CI [1.230-2.163]) resulted in lower PFS compared to Q1 (Ki-67 <2%). Finally, initial CgA levels Q3, 336-1168 µg/L (HR 1.580 CI [1.241-2.011]) and Q4, CgA >1,168 µg/L (HR 2.148 CI [1.679-2.747]) were associated with lower PFS compared to CgA Q1 (<112 µg/L). Only the combination of ^{177}Lu&^{90}Y was positively associated with PFS compared to ^{177}Lu alone (HR 0.797 CI [0.672-0.944]). Different treatment strategies concerning the isotopes resulted in median PFS for ^{177}Lu of 20mo, ^{90}Y 25mo and 23mo when patients were treated with both isotopes. Finally, G3 tumors showed lower PFS compared to G1 (HR 1.522 CI [1.062-2.180]): median 23mo for G1, 21mo for G2 and 18mo for G3.

The final multivariate model included: Ki-67 Q3 (HR 1.419 CI [1.041-1.935]) and Q4 (HR 1.493 CI [1.090-2.045]) compared to Q1, prior treatment with chemotherapy (HR 1.375 CI [1.039-1.820]), interferon-α (HR 2.054 CI [1.211-3.485]), presence of diabetes (HR 1.706 CI [1.117-2.605]), and CgA Q3 (HR 1.469 CI [1.084-1.992]) and Q4 (HR 2.039 CI [1.488-2.794]). All significant results regarding PFS are shown in Table 3, and the full results are in Supplemental Table 2.

Gender	Male	444	(56.8%)
	Female	338	(43.2%)
Age (years)		60.3±11.0	(22-83)
Location primary tumor	Small intestine	221	(28.3%)
(n=782)	Large intestine	42	(5.4%)
	Lung	60	(7.7%)
	Pancreas	277	(35.4%)
	Unknown primary	106	(13.6%)
	Other	76	(9.7%)
Tumor grade	Grade 1	182	(31.9%)
(n=570)	Grade 2	345	(60.5%)
	Grade 3	43	(7.5%)
Ki-67 (n=503)	Q1	≤2%	
	Q2	3-5%	
	Q3	6-10%	
	Q4	>10%	
Functional tumor	Yes	280	(50.5%)
(n=555)	No	275	(49.5%)
Performance status	WHO 0	547	(69.9%)
(n=782)	WHO 1	190	(24.3%)
	WHO 2-3	45	(5.8%)
Comorbidities	Hypertension (n=239)	99	(41.4%)
	Diabetes (n=782)	46	(5.9%)
Prior treatment	Interferon-a (n=727)	36	(5.0%)
	Chemotherapy (n=727)	159	(21.9%)
	Resection primary tumor (n=710)	336	(47.3%)
	Ablation (n=727)	100	(13.8%)
	Radiotherapy (n=727)	35	(4.8%)
	Somatostatin analogue (n=727)	297	(40.9%)
Isotope	^{177}Lutetium	295	(37.7%)
(n=782)	^{90}Yttrium	96	(12.3%)
	^{177}Lutetium & ^{90}Yttrium	391	(50.0%)
Number of PRRT administrations	3	395	(50.4%)
(n=782)	4	329	(42.1%)
	5-6	59	(7.5%)

Cumulative activity in GBq	^{177}Lutetium	21.7	[13.3-36.7]
(n=782)	^{90}Yttrium	11.5	[4.8-23.6]
	^{177}Lutetium & ^{90}Yttrium	18.2	[5.0-33.7]
Blood count (n=782)	Normal	546	(69.8%)
CgA (n=661)	Q1	<112	
	Q2	112-333	
	Q3	336-1168	
	Q4	>1168	
Serotonin (n=627)		273	[10-14200]
eGFR (n=778)		81.2	[30.56-259.08]
Creatinine (n=778)		75.0	[27-186]

Table 1. Patient, tumor, and treatment characteristics. Continuous data are mean ± SD followed by range. Categoric data are number followed by percentage. When variables are divided into quartiles, range of quartile is given. Percentages may not add up to 100% due to rounding.

	PFS (mo)		OS (mo)	
Primary tumor location	**Median**	**IQR**	**Median**	**IQR**
Small intestine	24	17 – 39	67	36 – 111
Large intestine	22	14 – 33	51'	24 – 68
Lung	18'	14 – 26	41'	30 – 67
Pancreas	23	16 – 35	50'	28 – 88
CUP	23	17 – 35	59	36 – 104
Other	19	14 – 31	52	96 – 22
Overall	22	16 – 35	53	30 – 98

Table 2. PFS and OS per primary tumor location. 'Significant in univariate analysis.

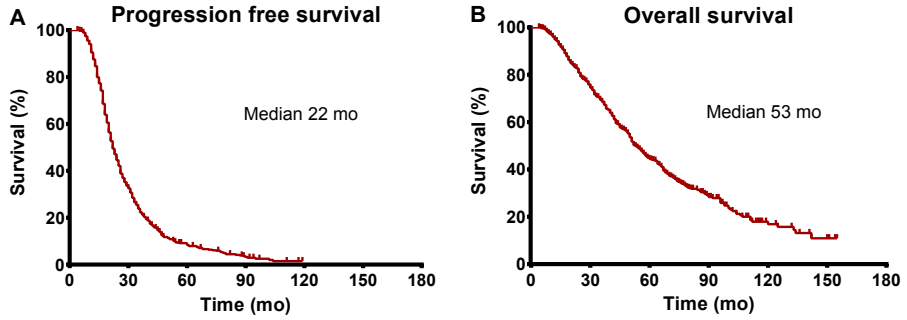

Figure 1. Kaplan-Meier curves of PFS (A) and OS (B).

Parameter	Group	Univariate			Multivariate		
		HR	95% CI	*P*	HR	95% CI	*P*
Ki-67	Q1: <2 %	1		0.002	1		0.044
	Q2: 2-5%	1.165	0.898-1.513		1.171	0.880-1.557	
	Q3: 5-10%	1.466	1.111-1.934		1.419	1.041-1.935	
	Q4: >10%	1.631	1.230-2.163		1.493	1.090-2.045	
Comorbidities	Diabetes	1.373	0.989-1.907	0.058[#]	1.706	1.117-2.605	0.013
Prior treatment	Chemotherapy	1.362	1.123-1.652	0.002[†]	1.375	1.039-1.820	0.026
	Interferon-a	1.487	1.046-2.114	0.027	2.054	1.211-3.485	0.008
CgA (µg/l)	Q1: <112	1		<0.001	1		<0.001
	Q2: 112-333	1.189	0.932-1.517		1.267	0.922-1.741	
	Q3: 336-1168	1.580	1.241-2.011		1.469	1.084-1.992	
	Q4: >1168	2.148	1.679-2.747		2.039	1.488-2.794	

Table 3. PFS analysis. HR > 1 indicates a greater risk for disease progression compared to the reference value (HR = 1).

Overall survival

Median OS was 53 months (IQR 18.0-57.0) and death of any cause was observed in 405 (51.8%) patients (Figure 1B). Eleven parameters were associated with lower OS in univariate analyses: primary tumor in the pancreas (HR 1.519 CI [1.184-1.948]), large intestine (HR 1.594 CI [1.003-2.533]), and lung (HR 1.716 CI [1.150-2.560]) compared to small intestine, performance status WHO 1 (HR 1.781 CI [1.432-2.214]) and WHO 2/3 (HR 2.817 CI [1.941-4.089]) compared to WHO 0, prior treatment with ablation (HR 1.458 CI [1.103-1.928]), interferon-α (HR 1.504 CI [1.002-2.256]), radiotherapy (HR 1.780 CI [1.120-2.829]), and chemotherapy (HR 1.792 CI [1.434-2.239]). Ki-67 Q3 (HR 1.519 CI [1.051-2.194]) and Q4 (HR 2.143 CI [1.488-3.087]) resulted in lower PFS compared to Q1. Furthermore, initial CgA levels Q2, 112-336 µg/l (HR 1.887 CI [1.354-2.631]), Q3 (HR 1.531 CI [1.100-2.131]) and Q4 (HR 3.357 CI [2.434 -4.631]) were associated with lower PFS

compared to CgA Q1. Both resection of the primary tumor (HR 0.715 CI [0.584 -0.877]) and the combination of ^{177}Lu&^{90}Y compared to ^{177}Lu alone (HR 0.792 CI [0.636-0.986]) were associated with improved OS. The median OS for patients only treated with ^{177}Lu was 48 months, 57mo for ^{90}Y only and 56mo when patients were treated with both isotopes. Finally, G2 tumors (HR 1.394 CI [1.065-1.826]) and G3 (HR 2.473 CI [1.621-3.772]) showed lower OS compared to G1: median 74mo for grade 1, 51mo for grade 2 and 26mo for grade 3. For selected results, Kaplan-Meier curves are shown in Fig. 2 and Fig. 3.

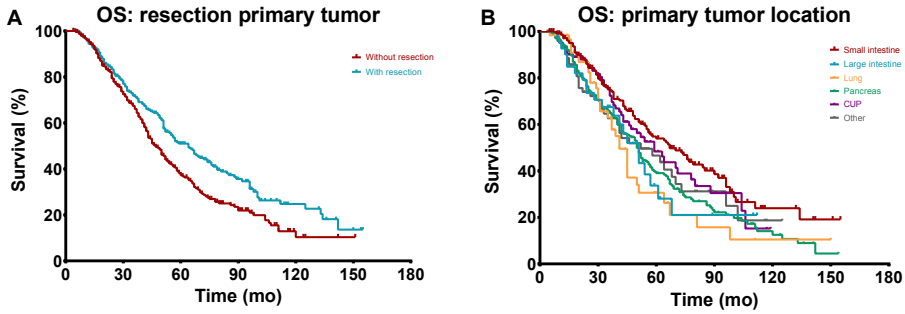

Figure 2. Kaplan-Meier curves of OS after resection of the primary tumor and OS per primary tumor location. Median OS is 43 and 65 mo without and with resection, respectively. Median OS is 67 months for small intestine NETs, 51 mo for large intestine, 41 mo for lung, 50 mo for pancreas, 59 mo for cancer of unknown primary (CUP) and 52 mo for other NETs.

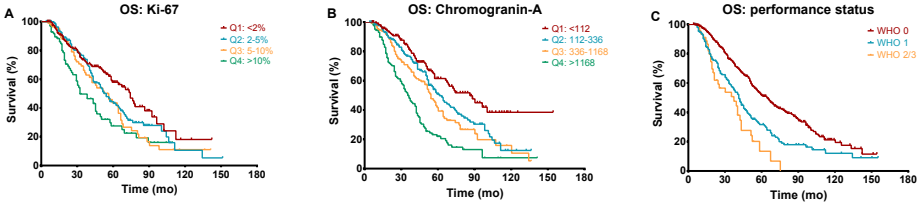

Figure 3. Kaplan-Meier curves of OS per Ki-67 and CgA quartiles and performance status classes. Median OS for Ki-67 < 2% is 74 mo, 2-5% 54 mo, 5-10% 56 mo and > 10% 32 mo. For CgA < 112, the median OS is 86 mo, 61 mo for 112-336, 54 mo for 336-1168 and 35mo for > 1,168. Median OS is 64 mo for WHO 0, 41 mo for WHO 1, and 37 mo for WHO 2/3.

In the multivariate analysis, the following parameters were associated with lower OS: Ki-67 Q4 (HR 1.930 CI [1.285-2.899]) compared to Q1, performance status WHO 1 (HR 1.551 CI [1.109-2.169]) and WHO 2/3 (HR 2.305 CI [1.432-3.713]) compared to WHO 0, ablation (HR 1.519 CI [1.041-2.215]), chemotherapy (HR 1.979 CI [1.412-2.773]), CgA Q2 (HR 1.690 CI [1.095-2.608]), Q3 (HR 1.816 CI [1.718-2.799]) and Q4 (HR 2.671 CI [1.717-4.155]) compared to Q1. The median

OS was 47 months (IQR 29-80) without and 64 months (IQR 32-112) with resection of the primary tumor, significantly different in primary pancreas or small intestine NETs after univariate Cox regression analysis (Table 4). All results with regard to OS are shown in Table 5 and in Supplemental Table 3.

	Median OS (mo)		Univariate cox regression analysis		
Primary tumor location	Resected	Unresected	HR	95% CI	*P*
Small intestine	77 (37-134)	48 (32-90)	0.649	0.423-0.995	0.047*
Large intestine	51 (28-∞)	45 (24-61)	0.625	0.257-1.522	0.301
Lung	51 (26-67)	41 (31-45)	0.755	0.374-1.522	0.432
Pancreas	65 (35-112)	43 (24-69)	0.595	0.426-0.832	0.002*
Overall	64 (32-112)	47 (29-80)	0.715	0.584-0.877	0.001*

Table 4. Resection of primary per tumor location. Data in parentheses are IQR. *significant

Parameter	Group	Univariate			Multivariate		
		HR	95% CI	*P*	HR	95% CI	*P*
Ki-67	Q1: <2 %	1		0.001	1		0.014
	Q2: 2-5%	1.340	0.960-1.871		1.363	0.946-1.965	
	Q3: 5-10%	1.519	1.051-2.194		1.203	0.798-1.814	
	Q4: >10%	2.143	1.488-3.087		1.930	1.285-2.899	
Performance status	WHO 0	1		<0.001	1		0.010
	WHO 1	1.781	1.432-2.214		1.551	1.109-2.169	
	WHO 2-3	2.817	1.941-4.089		2.305	1.432-3.713	
Prior treatment	Ablation	1.458	1.103-1.928	0.008	1.519	1.041-2.215	0.030
	Chemotherapy	1.792	1.434-2.239	<0.001	1.979	1.412-2.773	<0.001
CgA (µg/l)	Q1: <112	1		<0.001	1		<0.001
	Q2: 112-336	1.531	1.100-2.131		1.690	1.095-2.608	
	Q3: 336-1168	1.887	1.354-2.631		1.816	1.718-2.799	
	Q4: >1168	3.357	2.434-4.631		2.671	1.717-4.155	

Table 5. OS analysis. HR > 1 indicates a greater risk for death of any cause and HR < 1 a lower risk.

DISCUSSION

The reported PFS in other studies (32-41 mo) is higher than in the current study (22 mo). Meanwhile, the OS (43mo) of the current patient cohort is within the reported range in literature (38-82mo).[21-26] However, differences between the current study and literature exist. One study reported higher PFS and OS, yet only GEP-NET patients were included.[22] These patients are known to have a better survival than primary lung and colon NETs.[27] Another study included only patients with G1/G2 tumors, which are likely to have a longer OS compared to patients with G3 tumors.[24] In our study, high-risk patients with characteristics such as G3 tumors, WHO 2/3 and non GEP-NETs were also included.

Tumor grade is significantly associated in the univariate analysis for both PFS and OS. Differences in survival between G1/G2 tumors were previously shown, however in this study only observed in the univariate analysis.[28] As tumor grade and Ki-67 index are related, both indicate a more aggressive tumor, while the latter is generally associated with shorter OS.[29-30] Ezziddin et al. showed in 74 patients that patients with a Ki-67 of more than 10% have both lower PFS and OS.[11] In the current study, this was confirmed from a Ki-67 of more than 5% for PFS and more than 10% for OS in multivariate analysis. The performance status is a well-known factor that affects PFS and OS regardless of tumor type. The current study found that patients with WHO 1 and WHO 2/3 have decreased OS compared to patients with WHO 0, which was also confirmed by another study.[25]

Our data show reduction in PFS and OS in both univariate and multivariate analysis in patients pretreated with chemotherapy, which was also demonstrated in other studies.[23,25] Additional analysis in our dataset revealed out of the 43 patients with a G3 tumor, 19 (44%) were treated with chemotherapy while in patients with G1 and G2 tumors, only 12% and 23% were treated with chemotherapy. According to current ENETS guidelines, chemotherapy is indicated for G3 NEN.[31] Therefore the association between chemotherapy and survival might be the result of high-grade tumor patients receiving chemotherapy.

Resection of the primary tumor significantly improved OS (47 vs. 64mo), significantly different in primary pNETs or small intestine NETs after univariate Cox regression analysis (Table 4). Bertani et al. reported 112 months OS without- and 65 months with resection and that resection increased the median PFS (70 vs. 30mo). The longer OS reported could be explained by solely including G1/G2 pNET patients with liver metastases only.[15] Prolonged OS after resection of the primary tumor was also observed in pNET populations in a systematic review and meta-analysis.[32] According to current guidelines, resection of the primary tumor is indicated for G1/G2 tumors with curative intent and the presence of liver or lymph node metastases is not a contraindication for primary tumor resection.[31]

Resection of a primary pNET is hypothesized to improve survival due to underlying anatomical and biological mechanisms. First, part of the pancreatic venous blood flow drains into the portal vein, which directly flows into liver parenchyma which is therefore the first organ reached by metastatic pNET cells (seed-and-soil hypothesis). Second, the liver might be more susceptive to metastases due to its microenvironment with stromal build-up, growth factors, and immune cells (metastatic niche hypothesis).[33-34] Thus resection of the primary tumor, as the source of metastasizing cells, may improve survival even in the presence of metastases.

High levels of the biomarker CgA were associated with lower PFS and OS in the current patient population. CgA levels greater than 336 µg/l prior to PRRT were predictors for lower PFS, where for OS this level was greater than 112 µg/l. Previous studies showed that CgA levels greater than 600 µg/l were associated with shorter PFS and OS in smaller patient populations.[35-36] The current ENETS guidelines indicate that high CgA levels indicate poorer prognosis, probably associated with a high tumor load.[29,37]

In the current study, the choice of the radioisotope did not influence PFS and OS in the multivariate analysis. In the univariate analysis, however, the combination of ^{177}Lu&^{90}Y improved OS and PFS compared to ^{177}Lu alone. This is a different result compared to a German cohort study, where treatment with only ^{90}Y was associated with decreased OS compared ^{177}Lu only or tandem PRRT (^{177}Lu&^{90}Y concurrently).[21] Nevertheless, it is known that ^{90}Y implies a risk for nephrotoxicity compared to ^{177}Lu alone.[38] However, a bias in radionuclide selection exists in the current study as patients with large tumor burden often receive tandem PRRT.[17]

Besides the disadvantages inherent with a retrospective analysis, this study has other limitations. First, information about the extent of the disease (tumor burden and hepatic involvement) was not included as the goal was to define non-imaging related parameters. Second, patients could have received other treatments after PRRT, which could have extended their survival but this was beyond the scope of this research. Also toxicity was not covered in this study, which has been evaluated in another large multivariate analysis.[38] However, nephrological disease could decrease life expectancy, yet nephrotoxicity and related side effects due to medical interventions were not taken into consideration as a confounders for survival in this study.

The association of some parameters in this dataset with PFS and OS were already described in other papers.[12,23,25,28-30,32,35-36] However, to our knowledge, this is the first study that combines all parameters in a multivariate analysis. The fact that some patients have factors which are related to shorter PFS or OS does not indicate that PRRT is an unsuitable treatment for these

patients. Patients could still respond to treatment and have a longer PFS or OS compared to other treatments. This is especially true for patient with G3 tumors or SSTR-positive neuroendocrine carcinomas.[39] Furthermore, this study could assist physicians and patients to manage expectations from PRRT based on individual characteristics.

CONCLUSION

Higher Ki-67-values had a negative outcome on both PFS and OS, as well as higher CgA levels and previous chemotherapy. Furthermore, PFS was negatively associated with previous interferon-α treatment and diabetes, while lower OS was related to prior ablation and higher performance status.

REFERENCES

1. Oberg K, Castellano D. Current knowledge on diagnosis and staging of neuroendocrine tumors. *Cancer Metastasis Rev.* 2011;30:Suppl 1:3–7.
2. Oronsky B, Ma PC, Morgensztern D, Carter CA. Nothing but NET: a review of neuroendocrine tumors and carcinomas. *Neoplasia*. 2017;19:991–1002.
3. Cives M, Strosberg J. Radionuclide therapy for neuroendocrine tumors. *Curr Oncol Rep*. 2017;19:9.
4. Krenning EP, Kooij P, Bakker W, et al. Radiotherapy with a radiolabeled somatostatin analogue, [^{111}In-DTPA-D-Phe^{1}]-octreotide. A case history. *Ann NY Acad Sci*. 1994;15:496–506.
5. Bodei L, Kidd M, Baum RP, Modlin IM. PRRT: defining the paradigm shift to achieve standardization and individualization. *J Nucl Med*. 2016;1753–7.
6. Strosberg J, El-Haddad G, Wolin E, et al. Phase 3 trial of ^{177}Lu-Dotatate for midgut neuroendocrine tumors. *N Eng J Med*. 2017;376:125–35.
7. Kwekkeboom DJ, Krenning EP, Lebtahi R, et al. ENETS consensus guidelines for the standards of care in neuroendocrine tumors: peptide receptor radionuclide therapy with radiolabeled somatostatin analogs. *Neuroendocrinology*. 2009;90:220–6.
8. Zaknun JJ, Bodei L, Mueller-Brand J, et al. The joint IAEA, EANM, and SNMMI practical guidance on peptide receptor radionuclide therapy (PRRNT) in neuroendocrine tumours. *Eur J Nucl Med Mol Imaging*. 2013;40:800–16.
9. Johnbeck CB, Knigge U, Kjaer A. PET tracers for somatostatin receptor imaging of neuroendocrine tumors: current status and review of the literature. *Futur Oncol*. 2014;10:2259–77.
10. Ezziddin S, Opitz M, Attassi M, et al. Impact of the Ki-67 proliferation index on response to peptide receptor radionuclide therapy. *Eur J Nucl Med Mol Imaging*. 2011;38:459–66.
11. Ezziddin S, Attassi M, Yong-Hing CJ, et al. Predictors of long-term outcome in patients with well-differentiated gastroenteropancreatic neuroendocrine tumors after peptide receptor radionuclide therapy with ^{177}Lu-octreotate. *Journal Nucl Med*. 2014;55:183–90.
12. Brunner P, Jörg AC, Glatz K, et al. The prognostic and predictive value of sstr2-immunohistochemistry and sstr2-targeted imaging in neuroendocrine tumors. *Eur J Nucl Med Mol Imaging*. 2017;44:468–75.
13. Bodei L, Kidd M, Modlin IM, et al. Measurement of circulating transcripts and gene cluster analysis predicts and defines therapeutic efficacy of peptide receptor radionuclide therapy (PRRT) in neuroendocrine tumors. *Eur J Nucl Med Mol Imaging*. 2016;43:839–51.
14. Kong G, Thompson M, Collins M, et al. Assessment of predictors of response and long-term survival of patients with neuroendocrine tumour treated with peptide receptor chemoradionuclide therapy (PRCRT). *Eur J Nucl Med Mol Imaging*. 2014;41:1831–44.
15. Bertani E, Fazio N, Radice D, et al. Resection of the primary tumor followed by peptide receptor radionuclide therapy as upfront strategy for the treatment of G1–G2 pancreatic neuroendocrine tumors with unresectable liver metastases. *Ann Surg Oncol*. 2016;23:981–9.
16. Baum RP, Kulkarni HR, Singh A, et al. Results and adverse events of personalized peptide receptor radionuclide therapy with ^{90}Yttrium and ^{177}Lutetium in 1048 patients with neuroendocrine neoplasms. *Oncotarget*. 2018;9:16932–50.
17. Baum RP, Kulkarni HR. Theranositcs: From molecular imaging using Ga-68 labeled tracers and PET/CT to personalized radionuclide therapy-the Bad Berka Experience. *Theranostics*. 2012;2:437-47.
18. Chan DL, Pavlakis N, Schembri GP, et al. Dual somatostatin receptor/FDG PET/CT imaging in metastatic neuroendocrine tumours: proposal for a novel grading scheme with prognostic significane. *Theranostics*. 2017;7:1149-58.

19. Wahl RL, Jacene H, Kasamon Y, Lodge MA. From RECIST to PERCIST: evolving considerations for PET response criteria in solid tumors. *J Nucl Med*. 2009;50:122S–150S.
20. Eisenhauer E, Therasse P, Bogaers J. New response evaluation criteria in solid tumours: revised RECIST guideline (version1.1). *Eur J Cancer*. 2009;45:228–47.
21. Hörsch D, Ezziddin S, Haug A, et al. Effectiveness and side-effects of peptide receptor radionuclide therapy for neuroendocrine neoplasms in Germany: a multi-institutional registry study with prospective follow-up. *Eur J Cancer*. 2016;58:41–51.
22. Brabander T, Van Der Zwan WA, Teunissen JJM, et al. Long-term efficacy, survival, and safety of [^{177}Lu-DOTA^{0},Tyr^{3}]octreotate in patients with gastroenteropancreatic and bronchial neuroendocrine tumors. *Clin Cancer Res*. 2017;23:4617–24.
23. Mariniello A, Bodei L, Tinelli C, et al. Long-term results of PRRT in advanced bronchopulmonary carcinoid. *Eur J Nucl Med Mol Imaging*. 2016;43:441–52.
24. Kunikowska J, Pawlak D, Bąk MI, Kos-Kudła B, Mikołajczak R, Królicki L. Long-term results and tolerability of tandem peptide receptor radionuclide therapy with ^{90}Y/^{177}Lu-DOTATATE in neuroendocrine tumors with respect to the primary location: a 10-year study. *Ann Nucl Med*. 2017;31:347–56.
25. Katona BW, Roccaro GA, Soulen MC, et al. Efficacy of peptide receptor radionuclide therapy in a United States–based cohort of metastatic neuroendocrine tumor patients. *Pancreas*. 2017;46:1121–6.
26. Garske-Román U, Sandström M, Katarzyna, et al. Prospective observational study of ^{177}Lu-DOTA-octreotate therapy in 200 patients with advanced metastasized neuroendocrine tumours (NETs): feasibility and impact of a dosimetry-guided study protocol on outcome and toxicity. *Eur J Nucl Med Mol Imaging*. 2018;45:970-988.
27. Dasari A, Shen C, Halperin D, et al. Trends in the incidence, prevalence, and survival outcomes in patients with neuroendocrine tumors in the United States. *Jama Oncol*. 2017;3:1335–42.
28. Ezziddin S, Khalaf F, Vanezi M, et al. Outcome of peptide receptor radionuclide therapy with ^{177}Lu-octreotate in advanced grade 1/2 pancreatic neuroendocrine tumours. *Eur J Nucl Med Mol Imaging*. 2014;41:925–33.
29. Niederle B, Pape UF, Costa F, et al. ENETS consensus guidelines update for neuroendocrine neoplasms of the jejunum and ileum. *Neuroendocrinology*. 2016;103:125–38.
30. Khan MS, Luong TV, Watkins J, Toumpanakis C, Caplin ME, Meyer T. A comparison of Ki-67 and mitotic count as prognostic markers for metastatic pancreatic and midgut neuroendocrine neoplasms. *Br J Cancer*. 2013;108:1838–45.
31. Pavel M, O'Toole D, Costa F, et al. ENETS consensus guidelines update for the management of distant metastatic disease of intestinal, pancreatic, bronchial neuroendocrine neoplasms (NEN) and NEN of unknown primary site. *Neuroendocrinology*. 2016;103:172–85.
32. Zhou B, Zhan C, Ding Y, Yan S, Zheng S. Role of palliative resection of the primary pancreatic neuroendocrine tumor in patients with unresectable metastatic liver disease: a systematic review and meta-analysis. *Onco Targets Ther*. 2018;11:975–82.
33. Psaila B, Lyden D. The metastatic niche: adapting the foreign soil. *Nat Rev Cancer*. 2009;9:285–93.
34. Hann A, Sainz Jr B, Hermann PC. The metastatic niche in the liver: tilling the soil for pancreatic cancer progression. *Transl Cancer Res*. 2017;6:S217–20.
35. Sabet A, Haug AR, Eiden C, et al. Efficacy of peptide receptor radionuclide therapy with ^{177}Lu-octreotate in metastatic pulmonary neuroendocrine tumors: a dual-centre analysis. *Am J Nucl Med Mol Imaging*. 2017;7:74–83.
36. Sabet A, Dautzenberg K, Haslerud T, et al. Specific efficacy of peptide receptor radionuclide therapy with ^{177}Lu-octreotate in advanced neuroendocrine tumours of the small intestine. *Eur J Nucl Med Mol Imaging*. 2015;42:1238–46.

37. Korse CM, Bonfrer JMG, Aaronson NK, Hart AAM, Taal BG. ChromograninA as an alternative to 5-hydroxyindoleacetic acid in the evaluation of symptoms during treatment of patients with neuroendocrine tumors. *Neuroendocrinology*. 2009;89:296–301.
38. Bodei L, Kidd M, Paganelli G, et al. Long-term tolerability of PRRT in 807 patients with neuroendocrine tumours: the value and limitations of clinical factors. *Eur J Nucl Med Mol Imaging*. 2014;42:5–19.
39. Thang SP, Lung MS, Kong G, et al. Peptide receptor radionuclide therapy (PRRT) in European Neuroendocrine Tumour Society (ENETS) grade 3 (G3) neuroendocrine neoplasia (NEN)- a single-institution retrospective analysis. *Eur J Nucl Med Mol Imaging*. 2018;45:262-77.

SUPPLEMENTAL DATA

Number of cycles		^{90}Y				
		1	**2**	**3**	**4**	**5**
^{177}Lu	**1**	0	78	37	8	1
	2	78	71	4	0	0
	3	77	13	1	0	0
	4	6	0	0	0	0
	5	0	0	0	0	0

Table S1. Overview of the number of patients that received both ^{177}Lu and ^{90}Y. *22 patients were excluded from this table, these patients received both ^{177}Lu and ^{90}Y within one cycle

Parameter	Group	Univariate			Multivariate		
		HR	95% CI	p-value	HR	95% CI	p-value
Location primary tumor	Small intestine	1		0.062*	-		
	CUP	1.155	0.890-1.497				
	Pancreas	1.162	0.954-1.415				
	Other	1.289	0.958-1.735				
	Large intestine	1.292	0.908-1.837				
	Lung	1.625	1.186-2.226				
Tumor grade	Grade 1	1		0.036*	-		
	Grade 2	1.224	0.999-1.500				
	Grade 3	1.522	1.062-2.180				
Ki-67	Q1: <2 %	1		0.002*	1		0.044
	Q2: 2-5%	1.165	0.898-1.513		1.171	0.880-1.557	
	Q3: 5-10%	1.466	1.111-1.934		1.419	1.041-1.935	
	Q4: >10%	1.631	1.230-2.163		1.493	1.090-2.045	
Functional tumor	Yes	1.052	0.873-1.269	0.595	-		
Performance status	WHO 0	1		<0.001*	-		
	WHO 1	1.352	1.127-1.623				
	WHO 2-3	1.741	1.262-2.402				
Comorbidities	Hypertension	0.842	0.624-1.135	0.258			
	Diabetes	1.373	0.989-1.907	0.058*	1.706	1.117-2.605	0.013
Prior treatment	Resection primary tumor	0.997	0.849-1.172	0.972	-		
	Somatostatin analogue	1.162	0.989-1.367	0.069*	-		
	Chemotherapy	1.362	1.123-1.652	0.002*	1.375	1.039-1.820	0.026
	Ablation	1.090	0.864-1.374	0.467	-		
	Interferon-a	1.487	1.046-2.114	0.027*	2.054	1.211-3.485	0.008
	Radiotherapy	2.059	1.420-2.984	<0.001*	-		
Isotope	^{177}Lutetium	1		0.028*	-		
	^{177}Lu & ^{90}Y	0.797	0.672-0.944				
	^{90}Yttrium	0.823	0.642-1.055				
Blood count	Normal	0.927	0.783-1.098	0.381	-		
CgA (µg/l)	Q1: <112	1		<0.001*	1		<0.001
	Q2: 112-333	1.189	0.932-1.517		1.267	0.922-1.741	
	Q3: 336-1168	1.580	1.241-2.011		1.469	1.084-1.992	
	Q4: >1168	2.148	1.679-2.747		2.039	1.488-2.794	
Serotonin		1	1.000-1.000	0.493	-		
eGFR		0.999	0.996-1.003	0.690	-		
Creatinine		1.002	0.998-1.006	0.270	-		

Table S2. Other parameters evaluated for progression free survival. HR > 1 indicates a greater risk for progression and HR < 1 a lower risk.HR = Hazard Ratio, CI = Confidence Interval, *p<0.01 parameter used as input for multivariate analysis

Parameter	Group	Univariate			Multivariate		
		HR	95% CI	p-value	HR	95% CI	p-value
Location primary tumor	Small intestine	1		0.014†	-		
	CUP	1.197	0.848-1.691				
	Other	1.413	0.968-2.062				
	Pancreas	1.519	1.184-1.948				
	Large intestine	1.594	1.003-2.533				
	Lung	1.716	1.150-2.560				
Tumor grade	Grade 1	1		<0.001†	-		
	Grade 2	1.394	1.065-1.826				
	Grade 3	2.473	1.621-3.772				
Ki-67	Q1: <2 %	1		0.001†	1		0.014
	Q2: 2-5%	1.340	0.960-1.871		1.363	0.946-1.965	
	Q3: 5-10%	1.519	1.051-2.194		1.203	0.798-1.814	
	Q4: >10%	2.143	1.488-3.087		1.930	1.285-2.899	
Performance status	WHO 0	1		<0.001†	1		0.010
	WHO 1	1.781	1.432-2.214		1.551	1.109-2.169	
	WHO 2-3	2.817	1.941-4.089		2.305	1.432-3.713	
Functional	Yes	0.865	0.675-1.108	0.251	-		
Comorbidities	Hypertension	0.927	0.616-1.396	0.716	-		
	Diabetes	1.184	0.777-1.805	0.431	-		
Prior treatment	Resection primary tumor	0.715	0.584-0.877	0.001†	-		
	Somatostatin analogue	1.159	0.949-1.417	0.148	-		
	Ablation	1.458	1.103-1.928	0.008†	1.519	1.041-2.215	0.030
	Interferon-a	1.504	1.002-2.256	0.049†			
	Radiotherapy	1.780	1.120-2.829	0.015†	-		
	Chemotherapy	1.792	1.434-2.239	<0.001†	1.979	1.412-2.773	<0.001
Isotope	^{177}Lutetium	1		0.110	-		
	^{90}Yttrium	0.843	0.627-1.133				
	^{177}Lu & ^{90}Y	0.792	0.636-0.986				
Blood count	Normal	0.732	0.593-0.903	0.004†	-		
CgA (µg/l)	Q1: <112	1		<0.001†	1		<0.001
	Q2: 112-336	1.531	1.100-2.131		1.690	1.095-2.608	
	Q3: 336-1168	1.887	1.354-2.631		1.816	1.718-2.799	
	Q4: >1168	3.357	2.434-4.631		2.671	1.717-4.155	
Serotonin		1.000	1.000-1.000	0.567	-		
eGFR		1.002	0.998-1.006	0.236	-		
Creatinine		0.998	0.994-1.003	0.510	-		

Table S3. Other parameters evaluated for overall survival. HR > 1 indicates a greater risk for death of any cause and HR < 1 a lower risk. HR = Hazard Ratio, CI = Confidence Interval, †p<0.01 parameter used as input for multivariate analysis


195mPt
IT
68GA
B+

Chapter 9

General discussion

GENERAL DISCUSSION

Biomarkers in general, and imaging biomarkers specifically, have a widespread use in oncology. With the increasing availability into (expensive) targeted therapies, the need for predictive and/or safety biomarkers is increasing. Predictive biomarkers aim at discriminating patients that will experience a favorable response to therapy from those with an unfavorable response, while safety biomarkers identify patients at risk for adverse events or toxicity.[1] Aside from treatment selection, predictive- and safety biomarkers can expedite clinical trials through enrichment designs. However, before biomarkers are implemented in clinical decision making, validation of the biomarker is imperative. This thesis aims at predictive imaging biomarker validation and optimization in nuclear medicine. Therefore, the validation of imaging biomarkers will be discussed and further explored regarding radiolabeled cisplatin and somatostatin receptor PET/CT which are the focus of this thesis. The lessons learned and advices for daily practice are summarized including a perspective on steps for further optimizing already existing and treatments.

Imaging biomarker development and validation

Biomarker validation is composed of two principle components, firstly technical validation and secondly clinical validation and utility. The technical validation roughly answers the following question 'Does the biomarker accurately and consistently measure that what it should measure?' and includes amongst others repeatability, reliability, and bias. Clinical validation and utility answers the questions 'Does the biomarker correlate to a clinical variable?' and 'Does the biomarker correlate with outcome such as response to treatment?' and includes, but is not limited to, sensitivity, specificity, and consistency.[2] Parallel to technical and clinical validation, several additional steps are necessary, such as a safety assessment (in case of novel radiopharmaceuticals) and development of a standardized protocol.

Step 1: Technical validation and protocol development

Technical validation for biomarkers in nuclear medicine encompasses two parts; preparation of the required radiopharmaceutical and development of an acquisition and reconstruction protocol.

Developing a synthesis protocol for clinical radiopharmaceuticals can be challenging and time-consuming. For all radiopharmaceuticals, prerequisites exist for personnel, the facility and equipment, quality assurance and documentation, and control of the process, the laboratory, and the finished product.[3] Within these conditions, a product can be developed with high radiochemical purity. Furthermore, quality control of the final product should be performed within a time frame that is compatible with the half-life of the radioactive decay. Once a protocol has been developed, this is ideally transferred to either a kit formulation and/or automated labeling system, for which protocols are standardized and can easily be transferred to other centers for multi-center research and broad clinical availability.

Image acquisition and reconstruction is the second part of the technical validation of a biomarker. For every pair of system and isotope, the sensitivity, resolution, limits of detection, and bias can be determined. These images can subsequently be quantified; measuring the radioactivity within different parts of an image. Quantification of radiopharmaceuticals is highly dependent on scanner system, acquisition- and reconstruction settings, and quantification of acquired image data depends on signal calibration and tumor segmentation methods. More advanced analysis of images is even more challenging, with repeatability and reproducibility being essential.[4–6] Understanding the limits for each isotope and radiopharmaceutical, and development of imaging protocols that consider these limits, is necessary for quantifiable imaging biomarkers.

Step 2: Clinical validation and protocol development: Biodistribution, safety, and dosimetry
For nuclear medicine imaging there is a narrow relationship between the biodistribution of a tracer, dosimetry, and safety. The effective dose is in turn correlated to administered activity, which determines count statistics, image quality, and scan duration. These steps should be investigated for each radiopharmaceutical, but do not have to be repeated when using existing radiopharmaceuticals for which this data is already available.

Quantification of the biodistribution is also essential for diagnostic-therapeutic radiopharmaceutical pairs. High therapeutic doses of radiopharmaceuticals are administered after verification of uptake of a similar diagnostic radiopharmaceutical. For example, thyroid ablation with Iodine-131 is often preceded by Iodine-123 and peptide receptor radionuclide therapy of neuroendocrine tumors with Lutetium-177-DOTATATE is preceded by Gallium-68-DOTATATE. In these cases the biodistribution of each individual radiopharmaceutical should be known, but also whether the distribution of the diagnostic tracer accurately represents the distribution of the therapeutic radiopharmaceutical given at a later stage.

Step 3: Clinical correlation
The most challenging and time-consuming step in imaging biomarker development is clinical correlation, in which the imaging parameter is correlated to a clinical meaningful outcome such as response to treatment, survival, or toxicity. This involves using either available retrospective data or performing a prospective clinical trial with adequate follow-up time. Several guidelines and roadmaps are available for the design and execution of such trials.[2,7]

Step 4: External influences
Biomarkers are often studied and validated in a controlled set of patients. Once introduced in the clinic however, the circumstances are less controlled and external factors might influence the performance of a biomarker. If these external factors change the quantification

of imaging biomarkers, cut-off values might not be accurate in circumstances different from the original research situation. Clarifying such effects and interpreting aberrant results is essential for continued clinical use and evolvement of the biomarker.

In this thesis the four steps for imaging biomarker development were further explored for ^{195m}Pt-cisplatin and ^{68}Ga-DOTATATE in preclinical as well as in the clinical context.

Radiolabeled cisplatin

Cisplatin is one of the most common anticancer drugs worldwide and the dates of both the discovery of its antitumor effect by Rosenberg in 1965 and FDA approval for treatment of testicular, ovarian, and bladder cancer in 1978 are well-known.[8] Much more inconspicuous is the first report of radiolabeled cisplatin in 1971 to study cisplatin distribution in rabbits *in vivo* with gamma-camera imaging and in mice *ex vivo* with scintillation counting.[9] The first human administration soon followed in 1972, with planar gamma camera imaging of a patient with lymphoma and a patient with carcinoma of the cervix.[10] Despite the parallel development of radiolabeled cisplatin and cisplatin as an anticancer drug, and several reports on the use of radiolabeled cisplatin throughout the years, radiolabeled cisplatin is still far away from clinical implementation as an imaging biomarker. Hence the need for further validation for its clinical use.

Step 1: Technical validation and protocol development

Cisplatin, or cis-diamminedichloroplatinum(II), is a small inorganic compound and therefore has limited options for radiolabeling while retaining its pharmacokinetic and pharmacodynamics properties. Synthesis of cisplatin utilizing a radioactive isotope for the central platinum element in cisplatin meets this requirement. Three isotopes of platinum have been used for radiolabeled cisplatin (^{191}Pt, ^{193m}Pt, and ^{195m}Pt), each with its own advantages and drawbacks. Of the three isotopes, ^{195m}Pt has been used the most; the half-life of roughly 4 days provides ample opportunity for the synthesis of cisplatin and the emitted photons suitable for gamma camera imaging. The synthesis of radiolabeled cisplatin has been described and recently automated according to Good Manufacturing Practice regulations allowing for human use.[9,11,12]

Early studies with radiolabeled cisplatin relied on imaging for visual analysis, but for quantitative purposes *ex vivo* measurements of organs post mortem from animals or of blood and/or urine samples from patients were required.[10,13] With increasing resolution and sensitivity, quantitative imaging of radiolabeled cisplatin became available over two decades later with ^{191}Pt-cisplatin and this was used for dose calculations of ^{191}Pt-, ^{193m}Pt-, and ^{195m}Pt-cisplatin.[14] The first in-depth technical evaluation of ^{195m}Pt with SPECT was published in 2006, which measured sensitivity and spatial resolution in a Jaszczak phantom. In the chosen set-up, the sensitivity was 20 cps/MBq, immediately identifying an important issue in platinum imaging; low count statistics. The

consequence of this is that increased imaging times are needed to obtain suitable images. Visual resolution in the phantom was borderline 12 mm for hot spheres in which the activity concentration was approximately ten times higher than the background.[15]

With the development of high-resolution and high-sensitivity small-animal SPECT/CT equipment, the current limits of platinum imaging in mice were examined in **chapter 2**, demonstrating that quantifiable *in vivo* animal experiments with ^{195m}Pt-cisplatin have become possible. In mice, the smallest structures that could be visually distinguished were 0.85 mm after injection of 3-4 MBq of ^{195m}Pt with a scan time of 30 minutes. Although this resolution will not be reached in a clinical setting, it demonstrates that images with ^{195m}Pt can be acquired within a timeframe suitable for patient imaging. Furthermore, the amount of ^{195m}Pt in tissues could be accurately quantified and was highly correlated with *ex vivo* measurements of the same tissues. When extrapolated to patients, this implies that tissue and tumor uptake of cisplatin could be determined with ^{195m}Pt-cisplatin, and hopefully correlated with toxicity or treatment response.

Step 2: Clinical validation and protocol development: Biodistribution, safety, and dosimetry
The distribution and dosimetry of ^{195m}Pt-cisplatin has been studied twice in humans; calculated based on a ^{191}Pt-cisplatin imaging study[16] and recently in a dosimetry study with healthy volunteers.[17] The effective dose appears to lie around 20 mSv/MBq, resulting in 20 mSv after administration of 100 MBq which provides adequate image quality. The organs receiving the highest dose are the kidneys, spleen, and liver. Since the kidneys are the organs at risk during cisplatin therapy, additional damage from a diagnostic exam with ^{195m}Pt-cisplatin is highly undesirable. Toxicity from traditional diagnostic isotopes, such as ^{99m}Tc, is virtually non-existent, since these isotopes are almost exclusively gamma emitters. Platinum-195m, however, is not only a gamma-emitting isotope but also emits 36 auger electrons per disintegration.[18] Auger electron release a large amount of energy within a very short range, and are especially toxic (or effective) in the cell nucleus, causing DNA double strand breaks. When ^{195m}Pt is incorporated into cisplatin, which in itself binds to DNA, additional cell death might be expected.

Previous human studies did not study the effect of ^{195m}Pt-cisplatin on the kidneys in detail. This was subsequently studied in mice and described in **chapter 3**. In this study a therapeutic dosage of ^{195m}Pt-cisplatin was compared to a therapeutic dose of non-radiolabeled cisplatin. Although this is different from the situation of diagnostic imaging in patients, in which both the dose of cisplatin and activity of ^{195m}Pt will be much lower in comparison, critical monitoring of kidney dosimetry and function remains essential. However, patients suitable for diagnostic imaging with ^{195m}Pt-cisplatin are scheduled for high-dose cisplatin therapy. The extremely low risk of toxicity due to ^{195m}Pt-cisplatin imaging outweighs the benefits of being able to identify the group of patients at risk for nephrotoxicity due to cisplatin therapy, which is approximately one third of all treated patients.[19] In these cases, alternative treatments such as carboplatin should be considered.

Step 3: Clinical correlation

As an imaging biomarker, radiolabeled cisplatin has two objectives: response prediction and toxicity prediction. Clinical studies examining the use of radiolabeled cisplatin as an imaging biomarker in either of these areas do not yet exist. There is, however, data available from studies measuring platinum concentration after cisplatin-based chemo(radio)therapy in biopsies, surgical specimens, or post-mortem samples. The three largest studies have been performed in non-small cell lung cancer (NSCLC) and head and neck squamous cell carcinoma (HNSCC). Kim et al. showed that tumor tissue platinum in surgical specimens was correlated with time-to-recurrence, progression free-, and overall survival, with a higher platinum concentration leading to better prognosis.[20] Cisplatin-DNA adduct formation appeared predictive for survival in tumor samples of HNSCC and in buccal cells in NSCLC patients.[21,22] In smaller studies, tumor platinum concentration was correlated to response in gastric cancer, but not in bladder cancer.[23,24] Although the hypothesis that cisplatin tumor concentration correlates with outcome, this does not necessarily hold true, due to differences in cellular resistance to the damage caused by cisplatin. Clinical trials for validation of cisplatin as a predictive imaging biomarker should take this into account, for example through mutation analysis of genes involved in DNA double strand break repair.

Although there is a clear relationship between cisplatin dose and subsequent toxicity, very limited data is available on cisplatin tissue concentration and toxicity, since biopsy- or surgical samples are unavailable for normal organs.[25–27] From autopsy tissues, a relationship between platinum accumulation and clinical neurotoxicity has been demonstrated.[28] The organs of interest, however, are the kidneys since nephrotoxicity is often the dose limiting toxicity in patients with cisplatin-based chemotherapy.[19] Although quantification of cisplatin uptake in the kidneys with radiolabeled cisplatin can be challenging at early time points due to renal clearance of cisplatin, delayed imaging might provide valuable information on cisplatin retention in the kidneys.

Although several clinical studies with ^{195m}Pt-cisplatin have been described, the clinical correlation and validation of ^{195m}Pt-cisplatin as a biomarker has yet to be performed. In such a clinical trial, patients scheduled for cisplatin-based treatment will receive ^{195m}Pt-cisplatin prior to treatment. ^{195m}Pt-cisplatin uptake in the tumor will then be correlated to treatment outcome (response, stable disease, or progression) and ^{195m}Pt-cisplatin uptake in the kidneys will be correlated to the development of toxicity in these patients. Ideally cut-off values for nephrotoxicity and response can be determined and validated in a second group of patients. Ideally, with time, this could lead to treatment decisions being based on ^{195m}Pt-cisplatin imaging.

Step 4: External influences

Radiolabeled cisplatin might not only be useful as an imaging biomarker, but could also aid with (fundamental) research of cisplatin, its pharmacokinetics, alternative administration routes, and external factors that might influence the biodistribution of cisplatin. In daily clinical practice, patients undergoing treatment with cisplatin are pre- and post-hydrated with high volumes of intravenous saline to protect them for kidney damage. **Chapter 4** examines the effect of pre-hydration as one of the major external influences possibly decreasing the biodistribution of cisplatin and therefore its anti-tumor effect. This study demonstrates that pre-hydration indeed significantly decreases the tumor platinum concentration in mice. In our retrospective cohort with NSCLC patients receiving daily low-dose cisplatin chemoradiotherapy, this did not affect survival. However, in this chemoradiotherapy regimen, cisplatin is given as a radiosensitizer to the radiotherapy with low-volume pre-hydration. Administration of high-dose cisplatin therapy is however accompanied with high-volume pre-hydration and post-hydration. Based on the outcomes of the study described in chapter 4, it can be argued that in these patients a lower dose of cisplatin without hydration could accomplish the same effect as a higher dose with hydration. The willingness to do such a trial, however, is low amongst clinicians due to fear of high risks: an increase of nephrotoxicity and/or a decrease in efficacy. To gather more evidence on the effect of hydration on cisplatin biodistribution, a study into the pharmacokinetics of low-dose cisplatin with- and without pre-hydration is currently ongoing.

Many factors can influence the distribution of cisplatin, but these are not often studied. This can be due to a lack of funding, time-consuming clinical trials, or a lack of knowledge that seemingly unrelated changes might alter cisplatin pharmacokinetics. The use of radiolabeled cisplatin could increase the efficacy of these types of studies, requiring less animals and/or being able to study tumor cisplatin concentration fast and non-invasively in patients. Prior to changing treatment regimens, radiolabeled cisplatin could be used to determine the effects of such changes and prevent suboptimal treatment plans.

Neuroendocrine tumors

Nuclear imaging biomarkers for neuroendocrine tumors have been used clinically for over a quarter of a century, mostly as diagnostic biomarkers to examine the absence or presence of disease and as a prerequisite for peptide receptor radionuclide therapy.[29] The need for predictive biomarkers derived from these diagnostic scans is paramount in an era with an increasing number of treatment options in general and increasing costs of both existing and novel therapies. Although some steps in the development of predictive biomarkers can be copied from these diagnostic biomarkers, the need for clinical correlation between imaging outcome and patient outcome needs to be established. This part will focus on ^{68}Ga-somatostatin receptor PET/CT imaging for neuroendocrine tumors.

Step 1: Technical validation and protocol development
Gallium-68 is a positron emitting isotope that can be coupled to a somatostatin analogue and imaged with PET/CT (^{68}Ga-SSA PET/CT). The minimum detectable lesion size is 10 mm, while accurate quantification depends on lesion size and the tumor-to-background ratio.[30,31]

Multiple somatostatin analogues are available for clinical radiolabeling with ^{68}Ga, the most common being DOTATATE, HA-DOTATATE, DOTATOC, and DOTANOC. **Chapter 5** describes an automated production protocol with subsequent quality control for labeling of DOTATATE or HA-DOTATATE with ^{68}Ga. Such automated protocols make it possible to produce ^{68}Ga-DOTATATE of high quality multiple times a day while keeping the radiation dose to personnel low. Furthermore, standardization of protocols makes multi-center studies into imaging biomarkers possible. However, standardization of radiopharmaceutical production protocols remains challenging. Although the criteria which the final radiolabeled somatostatin analogue should meet are regulated and standardized, the choice of somatostatin analogue is not as clear-cut.[32] The choice for somatostatin analogue depends on cost, patent restrictions, national- and international regulations, availability and marketing approval in different countries, and local circumstances regarding available personnel and equipment. In the end it might come down to finding biomarker specific cut-off values for each peptide individually.

Step 2: Clinical validation and protocol development: Biodistribution, safety, and dosimetry
The biodistribution of each of the different ^{68}Ga-SSAs available is similar but not identical. In **chapter 6** the differences in distribution between ^{68}Ga-DOTATATE and ^{68}Ga-high affinity-DOTATATE (or ^{68}Ga-HA-DOTATATE) are studied. In ^{68}Ga-HA-DOTATATE, one amino acid in the receptor binding domain of ^{68}Ga-DOTATATE is replaced by an artificial amino acid. Our research demonstrated that this leads to higher uptake of ^{68}Ga-HA-DOTATATE in most normal organs and in several metastatic tumor sites. Quantification and subsequent treatment decisions based on cut-off values for uptake are therefore different between the two peptides. These differences should be considered during quantification and development of imaging biomarkers based on ^{68}Ga-SSA PET/CT.

Although these differences between ^{68}Ga-DOTATATE and ^{68}Ga-HA-DOTATATE were found, it is argued in literature that the peptides are similar and interchangeable. Preclinical studies showed that ^{68}Ga-HA-DOTATATE has a higher affinity than ^{68}Ga-DOTATATE for some subtypes of the somatostatin receptor *in vitro* and that this translates to higher uptake in the tumor, pancreas, and adrenal glands *in vivo*.[33] Clinical studies of ^{68}Ga-HA-DOTATATE preceded the preclinical work and the similarities between peptides were emphasized in a single case report and retrospective comparison study.[34,35] In the retrospective study, 23 patients were scanned with both ^{68}Ga-DOTATATE and ^{68}Ga-HA-DOTATATE and uptake in the normal organs and tumor lesions were compared. The main problem with this design, and retrospective

studies in general, is the lack of standardization; firstly the time between the two scans was 1-88 days and secondly the time between radiopharmaceutical injection and acquisition was 33-73 minutes. Variety in the time between the two scans gives an biased comparison of tumor lesions, since uptake of the ^{68}Ga-SSA can be influenced by treatment or progression between the two scans. Healthy tissue uptake will not be influenced by this parameter. Variety in time between injection and acquisition leads to variety in uptake of ^{68}Ga-SSA in both tumor and healthy tissues due to physiological dynamic changes at different time points, especially in the first 60 minutes. The conclusions of this retrospective might therefore not be valid; the claim that ^{68}Ga-DOTATATE and ^{68}Ga-HA-DOTATATE show very good concordance may have been too hastily reached.[35]

Although the difference between DOTATATE and HA-DOTATATE make quantifiable biomarkers challenging, it does not have an effect on patient safety or dose. This might not be the case when these peptides are coupled to ^{177}Lu for peptide receptor radionuclide therapy, in which toxicities are described in the kidneys and bone marrow due to physiological uptake of the radiopharmaceutical. In a retrospective analysis showed that ^{177}Lu-HA-DOTATATE leads to higher doses in normal organs.[36] The relationship between peptide used and toxicity, however, has not been studied.

Step 3: Clinical correlation

Although the value of ^{68}Ga-SSA PET/CT for diagnosis and follow-up of neuroendocrine tumors has been well established, the predictive value has proven more challenging.[37] The predictive value of radiolabeled somatostatin analogues for outcome prediction after peptide receptor radionuclide therapy (PRRT) has received the most attention, hypothesizing that logically there should be a relationship between uptake of radiolabeled somatostatin analogues for imaging and ^{177}Lu- or ^{90}Y-labeled somatostatin analogues for treatment. Indeed overall uptake on pre-therapeutic imaging categorized as being below-, equal to-, or higher than physiological liver uptake correlates to survival, and consequently sufficient uptake somatostatin analogues on imaging is mandatory for treatment with PRRT.[38,39]

The relationship between quantitative measures, typically based on the standardized uptake value (SUV), and outcome measures such as dose or survival does not appear to be as straightforward. The relationship between SUVmax and either maximum voxel dose or dose after PRRT has been examined in small studies and appears to lie around 0.7.[40,41] Other studies have reported cut-off values for SUVmax on pre-therapy imaging to distinguish responders from non-responders.[42,43] The draw-back of these values is that they are dependent on the peptide, acquisition protocol, and reconstruction protocol used and therefore often not translatable to other centers.

Very recently other tumor features have been examined in relationship with survival. Werner *et al.* demonstrated that entropy was prognostic for survival after PRRT in 31 patients.[44] In a rare prospective study in a larger group of patient (n=184), Tirosh *et al*. elucidated the relationship between somatostatin analogue avid tumor volume and progression free survival.[45]

Step 4: External influences

Many different factors can alter the biodistribution of radiopharmaceuticals. For ^{68}Ga-SSA PET the most well-known factor is the simultaneous treatment with non-radioactive somatostatin analogues for tumor control and symptomatic management. Since the administered dose is much higher in treatment than in diagnostic imaging, this might influence the uptake of ^{68}Ga-SSAs. **Chapter 7** studies the effect of one such SSA, namely lanreotide, on the uptake of ^{68}Ga-DOTATATE in NET patients. Contrary to previous hypotheses, lanreotide did not decrease the tumor uptake of ^{68}Ga-DOTATATE but did decrease uptake in normal tissues, thereby slightly increasing the tumor-to-background ratio. For tumor visualization, long-acting SSAs do not have to be continued prior to ^{68}Ga-DOTATATE PET/CT imaging. However, the use- and timing of SSAs should be noted as to not interpret an increased tumor-to-background ratio due to SSAs as tumor progression. It could even be argued that when patients are being treated with SSAs, they should be administered prior to scanning for optimal tumor visualization. Although unverified, if SSAs have the same effect on ^{177}Lu-DOTATATE as they do on ^{68}Ga-DOTATATE, administration of SSAs prior to ^{177}Lu-DOTATATE might increase tumor dose and decrease uptake and therefore dose to normal organs.

Co-administration of non-radioactive SSAs with ^{68}Ga-SSAs is not the only factor to be considered. Other known factors are the peptide mass administered, and amino acid infusions for renal protection has been shown to alter the pharmacokinetics of ^{177}Lu-DOTATATE.[46,47]

Conclusion and future perspectives

With the increasing call for personalized medicine in oncology, nuclear imaging biomarkers can provide valuable information for treatment selection and thus improve patient outcome. For general application of these biomarkers in different centers and accurate quantification, standardization of protocols regarding all aspects of nuclear medicine is required. In this thesis such a protocol is presented, but the effects of minor changes on these protocols are also highlighted.

The development of an imaging biomarker is a challenging process, in which different steps are performed parallel to each other and requires a multi-disciplinary approach. Once a biomarker has been introduced into clinical care, research is not completed as external factors influencing the biomarker are often discovered later when applied in large cohorts of patients. Therefore, although standardization is key to the clinical implementation of imaging

biomarkers, established imaging biomarker protocols are not absolute. New insights into external factors that affect these biomarkers should lead to revised protocols. This thesis underlines the effects that such external influences can have on the biodistribution of both ^{68}Ga-DOTATATE and cisplatin.

Radiolabeled cisplatin is being developed as an imaging biomarker for response- and toxicity prediction. Early studies were often hampered by technical limitations, while the recent state-of-the-art gamma camera's and SPECT/CT scanners provide adequate images with quantification. However, using ^{195m}Pt-cisplatin as a biomarker for outcome- or toxicity prediction after cisplatin-based therapy still has a long way to go. Initially biodistribution, dosimetry, safety, and image quality should be assessed in cancer patients with modern-day SPECT/CT systems. The relationship between tumor uptake of ^{195m}Pt-cisplatin and tumor response and between kidney uptake of ^{195m}Pt-cisplatin and nephrotoxicity should then be established. Ideally, this should be performed in patients with lung cancer and/or head-and-neck cancer; cancers in which the tumor is at a distant from organs with a high physiological uptake (liver, kidneys), and in which scatter and attenuation is minimized. If a correlation between uptake and outcome is found, cut-off values could be determined to distinguish patients at a high risk for toxicity or with a low chance of tumor response. These cut-off values should then be validated in a second independent cohort. Ultimately, a clinical trial is designed to prove the survival-benefit of pre-treatment ^{195m}Pt-cisplatin imaging, ideally a randomized controlled trial.

For future studies it is important to bear in mind that the intrinsic properties of cisplatin will remain to be the limiting factor for imaging due to high (~90%) binding of cisplatin to serum albumin. A second challenge is the supply chain of ^{195m}Pt, which is a reactor product, and the production of GMP-grade cisplatin for large scale clinical trials. These facilities are uniquely available in the Netherlands, making it the ideal country for such trials.

What distinguishes the implementation of ^{68}Ga-DOTATATE from ^{195m}Pt-cisplatin as a predictive imaging biomarker is that ^{68}Ga-DOTATATE PET/CT imaging is already used for diagnostic purposes. This leads to both opportunities and challenges for biomarker development. The large number of diagnostic scans that have been performed provide an enormous dataset in which follow-up data of these patients is also available. This dataset is- and can be used for exploratory studies into novel imaging biomarkers. The first challenge, however, lies in the retrospective and diagnostic nature of this dataset; finding data that has been acquired under the same circumstances in a group of patients similar in nature. If this challenge is not overcome, true imaging biomarkers may be lost due to the heterogeneity and therefore noise in the data. The second challenge is validation of biomarkers. Since exploratory studies are performed retrospectively, this can be done at low cost and with limited effort. Validation, however, ideally involves a different center with identical (or very similar) retrospective data

or even prospective data collection. This requires significantly higher costs and effort. Since uptake of ^{68}Ga-DOTATATE is a prerequisite for PRRT, ^{68}Ga-DOTATATE for optimization of said therapy. Further studies are necessary to elucidate the relationship between ^{68}Ga-DOTATATE uptake, ^{177}Lu-DOTATATE uptake, and treatment outcome in both per-lesion and per-patient analyses.

This thesis describes the importance of validation and critical assessment of imaging biomarkers in the context of ^{195m}Pt-cisplatin and ^{68}Ga-DOTATATE. When this is performed properly, predictive imaging biomarkers could provide a substantial contribution to the treatment selection of oncological patients.

REFERENCES

1. FDG-NIH Biomarker Working Group. *BEST (Biomarkers, EndpointS , and Other Tools) Resource*. 2018.
2. O'Connor J, Aboagye E, Adams J, et al. Imaging biomarker roadmap for cancer studies. *Nat Rev Clin Oncol*. 2016;14:169-186.
3. Elsinga P, Todde S, Penuelas I, et al. Guidance on current good radiopharmacy practice (cGRPP) for the small-scale preparation of radiopharmaceuticals. *Eur J Nucl Med Mol Imaging*. 2010;37:1049-1062.
4. Boellaard R, Delgado-Bolton R, Oyen WJG, et al. FDG PET/CT: EANM procedure guidelines for tumour imaging: version 2.0. *Eur J Nucl Med Mol Imaging*. 2014;42:328-354.
5. Aide N, Lasnon C, Veit-Haibach P, Sera T, Sattler B, Boellaard R. EANM/EARL harmonization strategies in PET quantification: from daily practice to multicentre oncological studies. *Eur J Nucl Med Mol Imaging*. 2017;44:17-31.
6. Pfaehler E, Beukinga R, de Jong J, et al. Repeatability of 18 F-FDG PET radiomic features: A phantom study to explore sensitivity to image reconstruction settings, noise, and delineation method. *Med Phys*. 2016;46:665-678.
7. Sauerbrei W, Taube SE, McShane LM, Cavenagh MM, Altman DG. Reporting recommendations for tumor marker prognostic studies (REMARK): an abridged explanation and elaboration. *J Natl Cancer Inst*. 2018;110:803-811.
8. Rosenberg B, Vancamp L, Krigas T. Inhibition of cell division in escherichia coli by electrolysis products from a platinum electrode. *Nature*. 1965;13:698-699.
9. Lange RC, Spencer RP, Harder HC. Synthesis and distribution of a radiolabeled antitumor agent: cis-diamminedichloroplatinum (II). *J Nucl Med*. 1971;13:328-330.
10. Lange RC, Spencer RP, Harder HC. The antitumor agent cis-Pt(NH3)2Cl2: distribution and dose calculations for ^{193m}Pt and ^{195m}Pt. *J Nucl Med*. 1972;14:191-195.
11. Zeevaart JR, Wagener J, Marjanovic-Painter B, et al. Production of high specific activity (195m) Pt-cisplatinum at South African Nuclear Energy Corporation for Phase 0 clinical trials in healthy individual subjects. *J Labelled Comp Radiopharm*. 2013;56:495-503.
12. Codee-van der Schilden K, Zwaagstra O, van der Born D. Automated synthesis of Pt-195m cisplatin for GMP production. *Eur J Nucl Med Mol Imaging*. 2017;44:S276.
13. Deconti RC, Toftness BR, Lange RC, Creasey WA. Clinical and pharmacological studies with cis-Diamminedichloroplatinum (II). *Cancer Res*. 1973;33:1310-1315.
14. Areberg J, Björkman S, Einarsson L, et al. Gamma camera imaging of platinum in tumours and tissues of patients after administration of ^{191}Pt-cisplatin. *Acta Oncol*. 1999;38:221-228.
15. Buckley SE, Ali PA, Evans CJ, El-Sharkawi AM. Gamma camera scintigraphy of tumours using (195m) Pt-cisplatin. *Phys Med Biol*. 2006;51:1325-1332.
16. Areberg J, Norrgren K, Mattsson È. Absorbed doses to patients from ^{191}Pt-, ^{193m}Pt- and ^{195m}Pt-cisplatin. *Appl Radiat Isot*. 1999;51:581-586.
17. Sathekge M, Wagener J, Smith S, et al. Biodistribution and dosimetry of ^{195m}Pt-cisplatin in normal volunteers. *Nuklearmedizin*. 2013;52:222-227.
18. Knapp F, Dash A. *Radiopharmaceuticals for Therapy*. 2016.
19. Crona DJ, Faso A, Nishijima TF, McGraw KA, Galsky MD, Milowsky MI. A Systematic Review of Strategies to Prevent Cisplatin-Induced Nephrotoxicity. *Oncologist*. 2017;22:609-619.
20. Kim ES, Lee JJ, He G, et al. Tissue platinum concentration and tumor response in non-small-cell lung cancer. *J Clin Oncol*. 2012;30:3345-3352.

21. Hoebers FJP, Pluim D, Verheij M, et al. Prediction of treatment outcome by cisplatin-DNA adduct formation in patients with stage III/IV head and neck squamous cell carcinoma, treated by concurrent cisplatin-radiation (RADPLAT). *Int J cancer*. 2006;119:750-756.
22. van de Vaart PJ, Belderbos J, de Jong D, et al. DNA-adduct levels as a predictor of outcome for NSCLC patients receiving daily cisplatin and radiotherapy. *Int J cancer*. 2000;89:160-166.
23. Cao Y, Chang Q, Cabanero M, et al. Tumor platinum concentrations and pathological responses following cisplatin-containing chemotherapy in gastric cancer patients. *J Gastrointest Cancer*. 2018 [e-pub ahead of print].
24. Guancial EA, Kilari D, Xiao GQ, et al. Platinum concentration and pathologic response to cisplatin-based neoadjuvant chemotherapy in muscle-invasive bladder cancer. *PLoS One*. 2016;11:1-10.
25. Miller RP, Tadagavadi RK, Ramesh G, Reeves WB. Mechanisms of cisplatin nephrotoxicity. *Toxins (Basel)*. 2010;2:2490-2518.
26. Stewart DJ, Mikhael NZ, Nanji AA, et al. Renal and hepatic concentrations of platinum: relationship to cisplatin time, dose, and nephrotoxicity. *J Clin Oncol*. 1985;3:1251-1256.
27. Rademaker-Lakhai JM, Crul M, Zuur L, et al. Relationship between cisplatin administration and the development of ototoxicity. *J Clin Oncol*. 2006;24:918-924.
28. Gregg RW, Molepo JM, Monpetit VJA, et al. Cisplatin neurotoxicity: the relationship between dosage, time, and platinum concentration in neurologic tissues, and morphologic evidence of toxicity. *J Clin Oncol*. 1992;10:795-803.
29. Johnbeck CB, Knigge U, Kjær A. PET tracers for somatostatin receptor imaging of neuroendocrine tumors: Current status and review of the literature. *Futur Oncol*. 2014;10:2259-2277.
30. Jönsson L, Stenvall A, Mattsson E, et al. Quantitative analysis of phantom studies of ^{111}In and ^{68}Ga imaging of neuroendocrine tumours. *EJNMMI Phys*. 2018;5:5.
31. Preylowski V, Schlögl S, Schoenahl F, et al. Is the image quality of I-124-PET impaired by an automatic correction of prompt gammas? *PLoS One*. 2013;8:1-8.
32. Gallium (68Ga) edotreotide injection. *European Pharmacopoeia 9.0*. 2016:1150-1152.
33. Schottelius M, Šimeček J, Hoffmann F, Willibald M, Schwaiger M, Wester HJ. Twins in spirit -episode I: comparative preclinical evaluation of [(68)Ga]DOTATATE and [(68)Ga]HA-DOTATATE. *EJNMMI Res*. 2015;5:22.
34. Brogsitter C, Schottelius M, Zöphel K, Kotzerke J, Wester HJ. Twins in spirit: DOTATATE and high-affinity DOTATATE. *Eur J Nucl Med Mol Imaging*. 2013;40:1789.
35. Brogsitter C, Zöphel K, Hartmann H, Schottelius M, Wester HJ, Kotzerke J. Twins in spirit part II: DOTATATE and high-affinity DOTATATE - The clinical experience. *Eur J Nucl Med Mol Imaging*. 2014;41:1158-1165.
36. Schuchardt C, Kulkarni HR, Wiessalla S, et al. Dosimetry using Lu-177 DOTATATE, Lu-177 HA-DOTATATE and Lu-177 DOTATOC: Comparative results in patients undergoing peptide receptor radionuclide therapy (PRRT). Eur J Nucl Med Mol Imaging. 2014;41:S224-S225.
37. Barrio M, Czernin J, Fanti S, et al. The impact of somatostatin receptor–directed PET/CT on the management of patients with neuroendocrine tumor: a systematic review and meta-analysis. *J Nucl Med*. 2017;58:756-761.
38. Imhof A, Brunner P, Marincek N, et al. Response, survival, and long-term toxicity after therapy with the radiolabeled somatostatin analogue [90Y-DOTA]-TOC in metastasized neuroendocrine cancers. *J Clin Oncol*. 2011;29:2416-2423.
39. Zaknun JJ, Bodei L, Mueller-Brand J, et al. The joint IAEA, EANM, and SNMMI practical guidance on peptide receptor radionuclide therapy (PRRNT) in neuroendocrine tumours. *Eur J Nucl Med Mol Imaging*. 2013;40:800-816.

40. Ezziddin S, Lohmar J, Yong-Hing CJ, et al. Does the pretherapeutic tumor SUV in ^{68}Ga DOTATOC PET predict the absorbed dose of ^{177}Lu Octreotate? *Clin Nucl Med*. 2012;37:e141-e147.
41. Hanscheid H, Sweeney RA, Flentje M, et al. PET SUV correlates with radionuclide uptake in peptide receptor therapy in meningioma. *Eur J Nucl Med Mol Imaging*. 2012;39:1284-1288.
42. Öksüz M, Winter L, Pfannenberg C, et al. Peptide receptor radionuclide therapy of neuroendocrine tumors with (90)Y-DOTATOC: is treatment response predictable by pre-therapeutic uptake of (68) Ga-DOTATOC? *Diagn Interv Imaging*. 2014;95:289-300.
43. Kratochwil C, Stefanova M, Mavriopoulou E, et al. SUV of [68Ga]DOTATOC-PET/CT Predicts Response Probability of PRRT in Neuroendocrine Tumors. *Mol Imaging Biol*. 2015;17:313-318.
44. Werner RA, Ilhan H, Lehner S, et al. Pre-therapy somatostatin receptor-based heterogeneity predicts overall survival in pancreatic neuroendocrine tumor patients undergoing peptide receptor radionuclide therapy. *Mol Imaging Biol*. 2019;21:582-590.
45. Tirosh A, Papadakis GZ, Millo C, et al. Prognostic utility of total ^{68}Ga-DOTATATE-avid tumor volume in patients with neuroendocrine tumors. *Gastroenterology*. 2018;154:998-1008.
46. de Jong M, Breeman WAP, Bernard BF, et al. Tumour uptake of the radiolabelled somatostatin analogue [DOTA0,TYR3] octreotide is dependent on the peptide amount. *Eur J Nucl Med*. 1999;26:693-698.
47. Puszkiel A, Bauriaud-Mallet M, Bourgeois R, Dierickx L, Courbon F, Chatelut E. Evaluation of the interaction of amino acid infusion on ^{177} Lu-Dotatate pharmacokinetics in patients with gastroenteropancreatic neuroendocrine tumors. *Clin Pharmacokinet*. 2019;58:213-222.


195mPt
IT
68GA
B+

Addendum

Nederlandse samenvatting

NEDERLANDSE SAMENVATTING

Kanker is de meest voorkomende doodsoorzaak bij zowel mannen als vrouwen in Nederland; 31% van alle sterfgevallen in 2017 werd hierdoor veroorzaakt. Hoewel nog steeds veel mensen overlijden aan kanker, wordt de overleving van kankerpatiënten steeds beter. Het percentage patiënten dat 10 jaar na een kankerdiagnose nog in leven is, steeg van 32% in de periode 1961-1970 naar 54% in de periode 2006-2010. Deze stijging in overleving wordt enerzijds veroorzaakt door vroegere detectie van kanker alsmede door verbeterde behandelmogelijkheden. Met de huidige grote keuze aan behandelopties, kan de behandeling voor elke patiënt in zekere zin 'op maat' gemaakt worden. De behandeling van kanker is in de loop der jaren echter ook complexer geworden door het grotere aanbod aan (dure) behandelingen, waarbij niet altijd zeker is op welke behandeling een patiënt het zal beste reageren zonder dat er teveel bijwerkingen optreden. Moleculaire beeldvorming kan een belangrijke rol spelen bij het selecteren van de juiste behandeling voor iedere specifieke patiënt.

De meeste methoden van diagnostische beeldvorming (bijvoorbeeld met een röntgenfoto, echo, CT scan of MRI scan) richten zich op het afbeelden van de anatomie, maar dit geeft vaak niet alle benodigde informatie. Bij moleculaire of functionele beeldvorming worden afbeeldingen gemaakt van fysiologische processen in het lichaam (met een gamma camera of PET/CT scan). Veelal wordt een kleine hoeveelheid radioactieve stof intraveneus toegediend, welke specifiek is ontworpen om een bepaald fysiologisch proces non-invasief middels een scan te visualiseren. De scan laat de verdeling van deze stof in het lichaam zien en biedt de mogelijkheid om de hoeveelheid stof die aanwezig is op een relevante lokalisatie te kwantificeren. Binnen de nucleaire geneeskunde worden met deze technieken onder andere tumoren in beeld gebracht, geneesmiddelen door het lichaam gevolgd, de expressie van specifieke eiwitten en receptoren gevisualiseerd of het functioneren van organen beoordeeld. Kanker heeft de eigenschap zich anders te gedragen dan normale weefsels en is daarom bijzonder geschikt om met moleculaire beeldvorming te diagnosticeren, te karakteriseren en te vervolgende gedurende en na een behandeling.

In dit proefschrift worden twee verschillende vormen van moleculaire beeldvorming beschreven die er op gericht zijn de juiste therapie voor een specifieke kankerpatiënt te selecteren. Echter voordat een moleculaire beeldvormingstechniek getest kan worden op voorspellende waarde, is het van belang dat dit technisch en klinisch wordt gevalideerd. Daarnaast worden factoren onderzocht die de moleculaire beeldvorming (onbedoeld) kunnen beïnvloeden. In het eerste deel wordt de ontwikkeling van radioactief cisplatin beschreven, wat gebruikt kan worden om te voorspellen welke patiënten baat hebben bij chemotherapie met cisplatin. In het tweede deel worden ontwikkelingen in de moleculaire beeldvorming van neuroendocriene tumoren beschreven.

Radioactief cisplatin

Cisplatin is een chemotherapeuticum welke wordt gebruikt voor de behandeling van verschillende typen kanker, waaronder longkanker en hoofd-hals kanker. Vaak wordt cisplatin gecombineerd met radiotherapie, wat volgens meerdere onderzoeken resulteert in een beter behandelresultaat dan een van deze behandelingen afzonderlijk. Ondanks de in opzet curatieve behandeling met cisplatin blijft de 2- en 5-jaars overleving van vergevorderde stadia van long- en hoofd-hals kanker laag. Daarnaast is therapie met cisplatin niet zonder toxiciteit; cisplatin is niet selectief toxisch in kankercellen maar ook in andere cellen waar het opgenomen wordt. Cisplatin wordt uitgescheiden door de nieren, maar tijdens dit proces komt er ook een verhoogde concentratie cisplatin in niercellen. Hierdoor is met name ernstige nierschade is een veelvoorkomende bijwerking.

Om voorafgaand aan de behandeling met cisplatin te voorspellen welke patiënt goed zal reageren op therapie en welke patiënt een grote kans op bijwerkingen heeft, is radioactief cisplatin (platina-195m-cisplatin) ontwikkeld. Chemisch is ^{195m}Pt-cisplatin identiek aan cisplatin; het centrale platina element is vervangen door het radioactieve platina isotoop ^{195m}Pt. De distributie van ^{195m}Pt-cisplatin in het menselijk lichaam zal dus identiek zijn aan dat van cisplatin. Na toediening van ^{195m}Pt-cisplatin kan met behulp van een gamma camera bekeken worden hoe cisplatin zich in het lichaam verdeelt; oftewel komt er voldoende cisplatin in de tumor (wenselijk) of komt er veel cisplatin in gezonde organen zoals de nieren (onwenselijk). In **hoofdstuk 2** worden de technische eigenschappen van beeldvorming met het isotoop ^{195m}Pt onderzocht. Hierin wordt aangetoond dat de resolutie en sensitiviteit voldoende is voor kwalitatief goede beelden. Daarnaast wordt een goede correlatie beschreven tussen *in vivo* metingen met beeldvorming en *ex vivo* metingen. **Hoofdstuk 3** beschrijft de veiligheid van *in vivo* beeldvorming met ^{195m}Pt-cisplatin in muizen. Dit hoofdstuk toont aan dat er weinig verschil is in toxiciteit tussen cisplatin en ^{195m}Pt-cisplatin, maar dat er wel een grote variatie is tussen verschillende dieren. In **hoofdstuk 4** wordt het effect van pre-hydratie op de distributie van cisplatin bestudeerd. Het geven van extra vocht voorafgaand aan cisplatin therapie beschermt de nieren door snellere uitscheiding van de chemotherapie, maar het leidt ook tot een lagere concentratie cisplatin in tumoren (en organen) bij muizen. Vooralsnog lijkt pre-hydratie bij patiënten met longkanker die dagelijks behandeld worden met radiotherapie en cisplatin, geen effect te hebben op de overleving. Het effect van pre-hydratie op de farmacokinetiek bij patiënten wordt momenteel nog onderzocht.

Concluderend uit de drie genoemde hoofdstukken kan worden gezegd dat ^{195m}Pt-cisplatin geschikt is voor beeldvorming van de cisplatin distributie, en dat dit kan helpen om relevante vragen voor de dagelijkse praktijk te beantwoorden. Voor de relatie tussen beeldvorming voorafgaand aan therapie en overleving na therapie zijn echter grotere patiënten studies nodig.

Neuroendocriene tumoren

Neuroendocriene tumoren (NET) zijn zeldzame tumoren die bijna op elke plaats in het lichaam kunnen ontstaan. Ondanks dat er een grote variatie is in kenmerken en beloop tussen de verschillende NETs, hebben zij één kenmerk gemeen: een sterke neiging tot overexpressie van de somatostatine receptor op het membraan van de tumorcellen. Moleculaire beeldvorming maakt gebruik van deze eigenschap om de tumoren in beeld te brengen door een somatostatine analoog (SSA) te labelen met het radioactieve isotoop Gallium-68 (^{68}Ga-SSA). Met behulp van een PET scan kunnen de NETs vervolgens in beeld gebracht worden.

Beeldvorming van NETs met behulp van ^{68}Ga-SSA PET/CT wordt al enkele jaren gebruikt voor het stellen van een diagnose of voor het volgen van het ziektebeloop. Het voorspellen van response op therapie met behulp van ^{68}Ga-SSA PET/CT is echter ingewikkeld. Eén van de complicerende factoren hierin is het gebrek aan een gestandaardiseerde werkwijze in verschillende ziekenhuizen. Hierdoor zijn onderzoeksresultaten naar de voorspellende waarde van ^{68}Ga-SSA PET/CT vaak niet toepasbaar in een ander ziekenhuis. In **hoofdstuk 5** wordt daarom een protocol beschreven voor het produceren van ^{68}Ga-DOTATATE (een specifieke ^{68}Ga-SSA) en het maken van een ^{68}Ga-DOTATATE PET/CT scan. **Hoofdstuk 6** onderzoekt de verschillen en overeenkomsten tussen twee verschillende ^{68}Ga-SSAs, namelijk ^{68}Ga-DOTATATE en ^{68}Ga-HA-DOTATATE. Het verschil tussen deze twee peptiden is slechts 1 aminozuur. Als deze peptiden toegediend worden aan patiënten, dan resulteert dit in een verschillende mate van binding aan de somatostatine receptor als de PET beelden gekwantificeerd worden. In **hoofdstuk 7** wordt onderzocht of behandeling met niet-radioactieve somatostatine analoga van invloed is op een ^{68}Ga-SSA PET/CT scan. Hierin wordt aangetoond dat deze therapie een kleine invloed heeft op ^{68}Ga-SSA kwantificatie van zowel tumoren als gezonde organen, maar dat tumoren beter te onderscheiden zijn als niet-radioactieve somatostatine analoga gegeven worden voorafgaand aan de ^{68}Ga-SSA PET/CT scan. Dit betekent dat de behandeling met somatostatine analoga niet gestaakt hoeft te worden voorafgaand aan een ^{68}Ga-SSA PET/CT scan, hetgeen patiëntvriendelijker is. Voor het maken van een keuze voor behandeling is het belangrijk om te kunnen voorspellen hoe de respons op behandeling met ^{68}Ga-SSA PET/CT zal zijn. In **hoofdstuk 8** wordt de voorspellende waarde van verschillende klinische factoren onderzocht voor overleving na therapie met radioactief SSA, echter er werd geen factor gevonden die sterk voorspellend is. Onderzoek naar andere voorspellende factoren, zoals beeldvorming, blijven daarom nodig om therapie van patiënten met een NET te verbeteren.

CONCLUSIE

Moleculaire beeldvorming voor het voorspellen van therapierespons of bijwerkingen bij kanker patiënten is volop in ontwikkeling. In dit proefschrift worden verschillende stappen in het onderzoek naar radioactief cisplatin en beeldvorming van neuroendocriene tumoren beschreven. Twee hiaten worden met name omschreven: het gebrek aan gestandaardiseerde protocollen en het gebrek aan kennis over verschillende factoren (e.g. pre-hydratie, andere therapieën) die van invloed zijn op de kwantificatie van beeldvorming.

De grote variatie tussen individuele kanker patiënten vraagt om een persoonlijke behandeling voor elke afzonderlijke patiënt. Om deze variatie te meten, zijn echter zijn echter gestandaardiseerde diagnostische protocollen nodig die getest en gevalideerd worden in een grote groepen patiënten. Alleen dan is het mogelijk om de relatie tussen diagnostiek en behandeling te meten en de beste behandeling aan iedere unieke patiënt te geven.

A


195mPt
IT
68GA
B+

Addendum

Dankwoord

DANKWOORD

Promotieonderzoek doen was vooral erg leuk werk; de vrijheid hebben om eigen onderzoeken op te zetten en praktische en creatief bezig zijn om deze onderzoeken ook daadwerkelijk uit te voeren. Maar wat het nog belangrijker is: een ontzettend leuke, gezellige, slimme collega's die elke dag weer de moeite waard maken!

Beste Wouter, zonder jou was ik niet bij de nucleaire geneeskunde gaan werken. Uit een lijstje met isotopen die te produceren waren had jij platinum-195m gekozen voor het maken van ^{195m}Pt-cisplatin en was je op zoek naar iemand die graag preklinisch onderzoek wilde doen. Bijna 7 jaar later zijn we nu bezig met het opzetten van een klinische studie met ^{195m}Pt-cisplatin, iets wat ik enkele jaren geleden niet meer had verwacht. Bedankt voor de samenwerking, je enthousiasme en de vele leuke (soms onmogelijke) ideeën!

Beste Marcel, bedankt dat ik mocht komen werken bij de nucleaire geneeskunde in het AVL! Het was jouw idee om mijn onderzoek uit te breiden met neuroendocriene tumoren. Bedankt voor het begeleiden en het blijven vragen 'wat betekent dit nu voor de patiënt?'.

Beste Gerlof, ik was al 5 jaar bezig met mijn promotieonderzoek toen jij mijn promotor werd. Het was erg fijn dat jij vanuit een breder perspectief naar mijn onderzoek keek en daar ook elke keer op wees. Bedankt voor het in goede banen leiden van de afrondende fase, ander was ik nu nog steeds niet gepromoveerd.

Lieve Linda, bedankt voor de gezelligheid, vriendschap, het theedrinken, beantwoorden van honderden vragen, wegwijs maken in de nucleaire geneeskunde, hulp bij experimenten (ondanks bijtende muizen en avonden), en nog veel meer. Bedankt dat je mijn paranimf wil zijn!

Lieve Martine, bedankt voor de gezellig en je enorme kennis over (radio)farmacie. Wat heb ik veel van je geleerd over het veilig bereiden van geneesmiddelen. Ik vond het erg leuk om met jouw op het lab te staan voor klinische bereidingen, test bereidingen, validatie bereidingen, studie bereidingen, etc.

Beste Erik, bedankt voor je hulp bij het ^{195m}Pt-cisplatin project, met name bij het muizen onderzoek. Fijn dat je een hele week 's avonds wilde helpen (en filmkijken) in het proefdiergebouw. Daarnaast weet ik zeker dat er geen taalfouten meer staan in de teksten die jij hebt gelezen. Veel plezier en succes met je nieuwe baan in Rotterdam!

Lieve mede-onderzoekers, zonder jullie was werken wel erg saai geweest. Bedankt voor de thee- en koffiepauzes, gezelligheid, kritische vragen, (werk)discussies, borrels, etc. Daphne, ik vond het erg leuk dat we aan gezamenlijke projecten konden werken, met als 'hoogtepunt' ons verblijf in Bad Berka; gezellig, erg koud, met een overvloed aan milka chocolade en wekelijks uit eten bij het Altes Brauhaus. Daan, bedankt voor je nuchtere blik op alles. Hopelijk is jouw proefschrift ook (bijna) af. Judith, bedankt voor je droge humor, de gezelligheid, je kritische en nuchtere vragen, en technische kennis (je bent in mijn ogen een held dat je zelf alles kan in Matlab). Hanna, ik vond het erg leuk om je te begeleiden tijdens je wetenschapsstage en fijn dat jij je onderzoek nu kan uitbreiden als onderzoeker. Bedankt voor de leuke gesprekken en de vele (soms extreem precieze) vragen. Lotte, bedankt voor het meedenken en werken op het gebied van radiofarmacie. Fijn dat je wilde helpen met de filmopnames en je kennis over promoveren in Utrecht. Bedankt aan de studenten die hebben meegeholpen met verschillende projecten: Aline, Lisanne, Marjolein, Jacobien.

In de afgelopen jaren is er veel veranderd op de nucleaire geneeskunde; mensen bijgekomen, mensen vertrokken. Gelukkig is de gezelligheid en de bereidheid om patiënten te helpen altijd gebleven. Administratie, bedankt voor jullie hulp met plannen en organiseren: Miena, Nancy, Lotte B, Sharon, Ingrid, Mijnie, Nicole. Dokterassistenten, bedankt voor het extra opletten bij studiepatiënten: Myriam, Marieke, Marijke, Maaike, Jonne, Esma. MNW'ers, bedankt voor jullie hulp op het lab en de camera's: Aafke, Arida, Bas H, Bert, Cas, Chelvi, Christel F, Colinda, Danielle, Elke, Esther, Hajar, Ilse, Jelmer, Jeroen E, Kirsten, Linda D, Lyandra, Marien, Martine, Mariette, Marintha, Marle, Minette, Natascha, Saskia B, Saskia H, Sophie, Ted, Weis. Nucleaire geneeskundigen, bedankt voor het meedenken met onderzoek en protocollen: Bernies, Christel B, Emilia, Erik, Ferida, Karen, Maarten, Marcel, Michelle, Philippe, Renato, Wouter en Zing. Apothekers, zonder jullie had er geen studie kunnen gebeuren: Martine en Jeroen.

Zonder faciliteiten is onderzoek doen onmogelijk. Desiree en Theo, bedankt voor alle hulp op het radionuclidecentrum (sorry voor de besmettingen). Niels, Natalie, Manon, Marieke en Sjoerd, bedankt voor jullie hulp en expertise bij het uitvoeren van muisexperimenten.

Onderzoek naar radioactief cisplatin was onmogelijk geweest zonder NRG in Petten. Karlijn en Sander (en vele anderen), heel erg bedankt voor de mooie samenwerking!

Het onderzoek naar hydratie en cisplatin had niet kunnen gebeuren zonder de afdeling radiotherapie: Iris bedankt voor al je hulp over statistische en methologische vragen, Jan-Jakob en Jose bedankt voor jullie interesse en begeleiden van het klinische onderzoek. Maddalena, bedankt voor al het werk dat je gedaan hebt en je inzet voor de lopende studie, zonder jouw zou het een chaos worden!

Daarnaast zijn er nog veel mensen die niet direct bijgedragen hebben aan dit onderzoek, maar indirect een grote bijdrage hebben geleverd; vier daarvan wil ik specifiek benoemen. Lotje, bedankt voor het begeleiden van mijn eerste en laatste stages en je grote interesse voor translationeel onderzoek. Ik vond het erg fijn om af en toe bij te kletsen en te brainstormen. Laurel, ik vond het erg leuk om tegelijk met jouw aan onze promoties en leven in Amsterdam te beginnen. Lieve Marjanne, bedankt voor je vriendschap! Ik ben blij dat jij mijn paranimf wil zijn en heel veel succes met je promotie overmorgen. Karianne, bedankt voor het oplossen van problemen, het zijn van een luisterend oor, gezelligheid, alles weten over- en in Amsterdam, en dat alles met een goed glas wijn!

Als laatste gaat mijn dank uit naar mijn familie. Papa en mama, bedankt voor alles wat jullie de afgelopen jaren (en alle jaren daarvoor) voor mij gedaan hebben! Ik vind het heel bijzonder dat jullie allebei heel geïnteresseerd zijn in mijn onderzoek en wetenschap in het algemeen en dat ik dit met jullie kan delen. Timon, ik had geen andere broer willen hebben. Het leven is nooit voorspelbaar met jou in de buurt. Opa en Oma, bedankt voor uw liefde en steun!


195mPt
IT
68GA
B+

Addendum

Affiliations

AFFILIATIONS

Else A. **Aalbersberg**	Department of Nuclear Medicine, Netherlands Cancer Institute (NKI-AVL)
Richard P. **Baum**	Theranostics Centre for Molecular Radiotherapy and Precision Oncology, Zentralklinik Bad Berka
Jose S. **Belderbos**	Department of Radiation Oncology, Netherlands Cancer Institute (NKI-AVL)
Lisanne **Bonsen**	Department of Nuclear Medicine, Netherlands Cancer Institute (NKI-AVL)
Karlijn **Codée-van der Schilden**	Nuclear Research and Consultancy Group (NRG)
Martine M. **Geluk-Jonker**	Department of Nuclear Medicine, Netherlands Cancer Institute (NKI-AVL)
Michel M. **van den Heuvel**	Department of Thoracic Oncology, Netherlands Cancer Institute (NKI-AVL)
Daphne M.V. **Huizing**	Department of Nuclear Medicine, Netherlands Cancer Institute (NKI-AVL)
Sjoerd **Klarenbeek**	Experimental Animal Pathology, Netherlands Cancer Institute (NKI-AVL)
Harshad R. **Kulkarni**	Theranostics Centre for Molecular Radiotherapy and Precision Oncology, Zentralklinik Bad Berka
Maddalena **Rossi**	Department of Radiation Oncology, Netherlands Cancer Institute (NKI-AVL)
Lisette J. **Saveur**	Department of Medical Oncology, Netherlands Cancer Institute (NKI-AVL)
Aviral **Singh**	Theranostics Centre for Molecular Radiotherapy and Precision Oncology, Zentralklinik Bad Berka
Jan-Jakob **Sonke**	Department of Radiation Oncology, Netherlands Cancer Institute (NKI-AVL)
Marcel P.M. **Stokkel**	Department of Nuclear Medicine, Netherlands Cancer Institute (NKI-AVL)
Margot E.T. **Tesselaar**	Department of Medical Oncology, Netherlands Cancer Institute (NKI-AVL)
Gerlof D. **Valk**	Department of Endocrine Oncology, University Medical Center Utrecht (UMCU)
Erik **Vegt**	Department of Nuclear Medicine, Netherlands Cancer Institute (NKI-AVL)
Michelle W.J. **Versleijen**	Department of Nuclear Medicine, Netherlands Cancer Institute (NKI-AVL)

Wouter V. **Vogel**	Department of Nuclear Medicine, Department of Radiation Oncology, Netherlands Cancer Institute (NKI-AVL)
Iris **Walraven**	Department of Radiation Oncology, Netherlands Cancer Institute (NKI-AVL)
Linda J. **de Wit-van der Veen**	Department of Nuclear Medicine, Netherlands Cancer Institute (NKI-AVL)
Thirumaraichelvi **Young-Mylvaganan**	Department of Nuclear Medicine, Netherlands Cancer Institute (NKI-AVL)
Oene **Zwaagstra**	Nuclear Research and Consultancy Group (NRG)

A


195mPt
IT
68GA
B+

Addendum

Publications

PUBLICATIONS

Saadani H, van der Hiel B, **Aalbersberg EA**, Zavrakidis I, Haanen JBAG, Hoekstra OS, Boellaard R, Stokkel MPM. Metabolic biomarker based BRAFV600 mutation association and prediction in melanoma. *J Nucl Med*. 2019 [e-pub ahead of print].

Aalbersberg EA, Geluk-Jonker MM, Young-Mylvaganan T, de Wit-van der Veen LJ, Stokkel MPM. A Practical Guide for the Production and PET/CT Imaging of ^{68}Ga-DOTATATE for Neuroendocrine Tumors in Daily Clinical Practice. *J Vis Exp*. 2019 (146), e59358.

Aalbersberg EA, Rossi MM, de Wit-van der Veen LJ, Walraven I, van den Heuvel MM, Sonke JJ, Belderbos JS, Vogel WV. Pre-hydration in cisplatin-based CCRT: Effects on tumour concentrations and treatment outcome. *Radiother Oncol*. 2019;134:30-36.

Aalbersberg EA, Huizing DMV, Walraven I, de Wit-van der Veen BJ, Kulkarni HR, Singh A, Stokkel MP, Baum RP. Parameters to predict progression free and overall survival after peptide receptor radionuclide therapy: a multivariate analysis in 782 patients. *J Nucl Med*. 2019 [e-pub ahead of print].

Aalbersberg EA, de Wit-van der Veen BJ, Versleijen MWJ, Saveur LJ, Valk GD, Tesselaar MET, Stokkel MPM. Influence of lanreotide on uptake of ^{68}Ga-DOTATATE in patients with neuroendocrine tumours: a prospective intra-patient evaluation. *Eur J Nucl Med Mol Imaging*. 2019;46:696-703.

Dohmen AJC, Sanders J, Canisius S, Jordanova ES, **Aalbersberg EA**, van den Brekel MWM, Neefjes J, Zuur CL. Sponge-supported cultures of primary head and neck tumors for an optimized preclinical model. *Oncotarget*. 2018;9:25034-25047.

Aalbersberg EA, de Wit-van der Veen BJ, Zwaagstra O, Codée-van der Schilden K, Vegt E, Vogel WV. Preclinical imaging characteristics and quantification of Platinum-195m SPECT. *Eur J Nucl Med Mol Imaging*. 2017;44:1347-1354.

Bonsen LR, **Aalbersberg EA**, Tesselaar M, Stokkel MPM. Cardiac neuroendocrine tumour metastases: case reports and review of the literature. *Nucl Med Commun*. 2016;37:461-465.


195mPt
IT
68GA
B+

Addendum

Curriculum Vitae

CURRICULUM VITAE

Else Aagje Aalbersberg was born on October 16, 1987 in Aalst-Waalre, the Netherlands. She graduated from high school in 2005 and went to Twente University in Enschede to study Technical Medicine the same year. After obtaining a bachelor's degree she continued her education with a master in Reconstructive Medicine. During her master studies she completed several internships in different hospital departments in the Netherlands (head and neck surgery and oncology, nephrology, trauma surgery, and orthopedic surgery). For her final internship she returned to the department of Head and Neck Surgery and Oncology and the department of Cell Biology at the Antoni van Leeuwenhoek Hospital / Netherlands Cancer Institute (NKI-AVL). Her research focused on predicting treatment response of individual patients through primary tissue cultures and prediction assays (in particular cisplatin response).

During her final year, she attended the conference Targeted Anticancer Therapies in Amsterdam. She attended a talk entitled 'Clinical imaging and drug development' and was fascinated by visualizing molecular and cellular processes in patients. After obtaining her master's degree in 2012, she therefore applied for a PhD-position at the department of Nuclear Medicine at the NKI-AVL, and started her research on cisplatin in the field of nuclear medicine. Her research was later extended to neuroendocrine tumors. This has resulted in several publications and oral presentations at international conferences. After obtaining her doctorate degree, she will continue to work at the department of Nuclear Medicine at the NKI-AVL as Technical Physician.